

**STRUCTURE AND DENSIFICATION OF THIN FILMS PREPARED
FROM SOLUBLE PRECURSOR POWDERS
BY SOL-GEL PROCESSING**

Dissertation

zur Erlangung des naturwissenschaftlichen Doktorgrades

der Julius-Maximilians-Universität Würzburg

vorgelegt von

Matthias Bockmeyer

aus Würzburg

Würzburg 2007

Eingereicht am:.....

Bei der Fakultät für Chemie und Pharmazie

1. Gutachter:

2. Gutachter:

der Dissertation.

1. Prüfer:

2. Prüfer:

3. Prüfer:

des öffentlichen Promotionskolloquiums.

Tag des öffentlichen Promotionskolloquiums:.....

Doktorurkunde ausgehändigt am:.....

**“I am still confused,
but on a higher level”**

Enrico Fermi

1	INTRODUCTION	1
2	STATE OF KNOWLEDGE	2
2.1	SOL-GEL PROCESSING	2
2.2	THIN FILM FORMATION	3
2.3	FILM DENSIFICATION	4
2.4	STRESS FORMATION IN THIN FILMS	5
2.5	CRACK FORMATION IN THIN FILMS	7
2.6	TITANIA	9
3	OBJECTIVES OF THESIS	10
4	EXPERIMENTAL	11
4.1	MATERIALS	11
4.2	PREPARATION	11
4.2.1	PRECURSOR POWDER PREPARATION.....	11
4.2.2	SOL PREPARATION	12
4.2.3	PREPARATION OF SOL POWDER AND FILM POWDER	12
4.2.3	THIN FILM PREPARATION	12
4.3	CHARACTERIZATION.....	13
4.3.1	ANALYTICAL ULTRACENTRIFUGATION	13
4.3.2	CHEMICAL ANALYSIS	13
4.3.3	DEFECT ANALYSIS	13
4.3.4	ELLIPSOMETRIC POROSIMETRY	13
4.3.5	FILM THICKNESS AND REFRACTIVE INDEX	14
4.3.6	INFRARED SPECTROMETRY	14
4.3.7	MICROSCOPY	14
4.3.8	NITROGEN SORPTION	14
4.3.9	PENCIL HARDNESS TEST	15
4.3.10	PHOTOCATALYTIC ACTIVITY	15
4.3.11	3-POINT BENDING TEST	15
4.3.12	REFRACTIVE INDEX OF POWDERS.....	15
4.3.13	SKELETAL DENSITY.....	15
4.3.14	STRESS MEASUREMENTS	15
4.3.15	THERMO ANALYSIS.....	16
4.3.16	VISCOSITY.....	16
4.3.17	X-RAY – DIFFRACTOMETRY	16
4.3.18	X-RAY – REFLEKTOMETRY	16

5	RESULTS AND DISCUSSION	18
5.1	SOLUBLE PRECURSOR POWDERS	18
5.2	ETHANOL BASED COATING SYSTEMS	22
5.2.1	SOLUBILITY AND STABILITY	22
5.2.2	CHANGES INDUCED BY THE SOLVENT COMPOSITION	24
5.2.3	DENSIFICATION OF ETHANOL BASED FILM POWDERS	30
5.2.3.1	GENERAL CONSEQUENCE OF LARGE SURFACE-TO-VOLUME RATIO AND AIR MOISTURE DURING FILM FORMATION	30
5.2.3.2	CHANGES INDUCED BY 1,5-PENTANEDIOL	36
5.2.4	MICROSTRUCTURE OF THIN FILMS	41
5.2.4.1	CONSTRAINT OF SHRINKAGE BY THE SUBSTRATE: GENERAL CONSEQUENCE	41
5.2.4.2	CHANGES INDUCED BY THE SOLVENT COMPOSITION.....	46
5.2.5	RESIDUAL STRESS AND CRACKING OF THIN FILMS	55
5.2.5.1	INFLUENCE OF SOLVENT COMPOSITION ON RESIDUAL STRESS OF THIN FILMS	55
5.2.5.2	CHARACTERIZATION AND ANALYSIS OF CRACKING IN THIN FILMS	57
5.2.5.3	INFLUENCE OF SOLVENT COMPOSITION ON CRACKING OF THIN FILMS	60
5.2.5.4	INFLUENCE OF AIR MOISTURE DURING COATING PROCEDURE	62
5.3	WATER BASED COATING SYSTEMS	66
5.3.1	SOLUBILITY AND STABILITY	66
5.3.2	GENERAL CONSEQUENCE OF WATER AS SOLVENT	69
5.3.3	CHANGES INDUCED BY THE SOLVENT COMPOSITION	74
5.3.4	DENSIFICATION OF WATER BASED FILM POWDERS	78
5.3.4.1	GENERAL CONSEQUENCE OF LARGE SURFACE-TO-VOLUME RATIO AND AIR MOISTURE DURING FILM FORMATION	78
5.3.4.2	CHANGES INDUCED BY 1,5-PENTANEDIOL IN THE SOLVENT.....	80
5.3.5	MICROSTRUCTURE AND CRACKING OF THIN FILMS	82
5.4	TRIETHANOLAMINE BASED PRECURSOR POWDERS	88
5.4.1	CHARACTERIZATION OF POWDERS ISOLATED FROM COATING SOLUTIONS	88
5.4.2	DENSIFICATION OF THIN FILMS.....	92
5.5	VALIDITY FOR OTHER SOL-GEL SYSTEMS (8YSZ)	98
5.6	FURTHER CONSEQUENCES OF THIN FILM DENSIFICATION	102
6	SUMMARY	104
7	ZUSAMMENFASSUNG	106
8	LITERATURE	109

1 INTRODUCTION

Besides mostly vacuum-based technologies such as physical or chemical vapor deposition (PVD, CVD) inorganic thin films can be prepared by sol-gel processing [BRI90]. Thin films can be fabricated on large areas with high quality from liquid precursors [GOM98,GOM00,TAK06]. From a commercial point of view this coating technology is especially advantageous even for small- and mid- sized companies, because only low investment and operating costs are required compared to vacuum-based technologies [LOE03b].

Most technological problems associated with the limited shelf-life of coating solutions can be solved by using soluble precursor powders [LOE00]. The amorphous precursor powders are indefinitely stable under ambient conditions and may be re-dissolved in different solvents and solvent mixtures [LOE05]. The resulting coating solutions can be applied on an industrial scale yielding high-quality films for optical applications [LOE03].

On a microscopic level thin film preparation by sol-gel processing is the result of complex interwoven sequences of interacting processes [SCH97a]. In a first step dispersions that contain amorphous particles are applied to substrates by various techniques such as dip-coating, spraying, doctor-blading, spin-coating or even pad-printing [MOU06,PUE04]. During thin film drying and aging further hydrolysis and condensation reactions occur [SCH97b]. As soon as the liquid film transforms to a gel, a rigid particulate network is formed. Upon further treatment decomposition of residual organic components occurs and the film is densified or even crystallized [BRI92, MAC00].

During the formation of sol-gel coatings, the film can only shrink perpendicularly to the substrate, because of the restricting effect of the substrate on film shrinkage [KOZ06]. Mainly, this causes tensile stresses in the coatings [BRI92]. When these forces exceed the inner cohesion of the coatings, cracking occurs either during drying, the aging processes or thermal annealing [CHO00].

In theory the processes during the coating process are well described and general strategies to avoid defects are proposed [LOE03b]. Though, on the stony way from the laboratory experiments to even large-scale industrial manufacturing often extensive experimental series and a lot of practical experience with the respective material system are needed, to avoid defects. Therefore, for all coating processes, it is crucial to understand the microstructural changes in the films in order to optimize the fabrication and to improve the film performance. However, the interrelationship between the densification and the microstructure of thin sol-gel films has been barely experimentally described, which even might be because of a lack off analytical accessibility.

In this context especially the analysis of defects and defect densities is rather vague, which often delays any optimization processes. Therefore, within the presented investigations, the formation of inorganic films, their drying and thermal densification was thoroughly investigated by using a new analytical approach. A method for the quantitative analysis of film defects was established. The results on thin sol-gel films can be related to the film densification and the microstructural changes associated with the processing.

2 STATE OF KNOWLEDGE

2.1 SOL-GEL PROCESSING

The sol-gel process is a method for producing non-metallic inorganic or hybrid materials by solution chemistry [BRI90]. It is a process that has, in the past years, gained much notoriety in the glass and ceramic fields [SCH06,TAK06]. First systematic investigations on sol-gel chemistry even reach back to the 18th century. The first real commercial application was the preparation of SiO₂/TiO₂ antireflective interference filters that was invented by Schroeder & Dislich at Schott Glasswerke 1958. [LOE03b]

Through this process, homogeneous inorganic oxide materials with desirable properties in respect to hardness, transparency, chemical durability, tailored porosity and thermal resistance, can be produced at lower temperatures, as opposed to temperatures required in conventional ceramic processing. Various material shapes are achievable, i.e. monoliths [LOE96,GEI98], films [BOC06], fibers [KRU04], and powders [GOE99,NIE06]. Many specific applications include microelectronics [WIJ01], protective [MAT04,MEH05] and porous films [BOS04,BU04,GRO06], optical coatings [GOM98,GOM00], dielectric and electronic coatings [KLU02,PET96], high temperature superconductors [AYT03,MCI92], reinforcement fibers [KRU06,KER02], fillers [RUE05,MAR03] and catalysts [NMA04].

The sol-gel process involves the evolution of inorganic networks through the formation of a colloidal suspension (sol) and gelation of the sol to form a network in a continuous liquid phase (gel) [KAL92,BRI85,SCH88c]. After drying and aging of the gel a xerogel is build that on sintering ceramizes (Figure 1). The precursors for synthesizing these colloids consist of a molecular-disperse metal surrounded by various reactive ligands [TAK00]. Metal alkoxides are most favored because they readily react with water [SAN88].

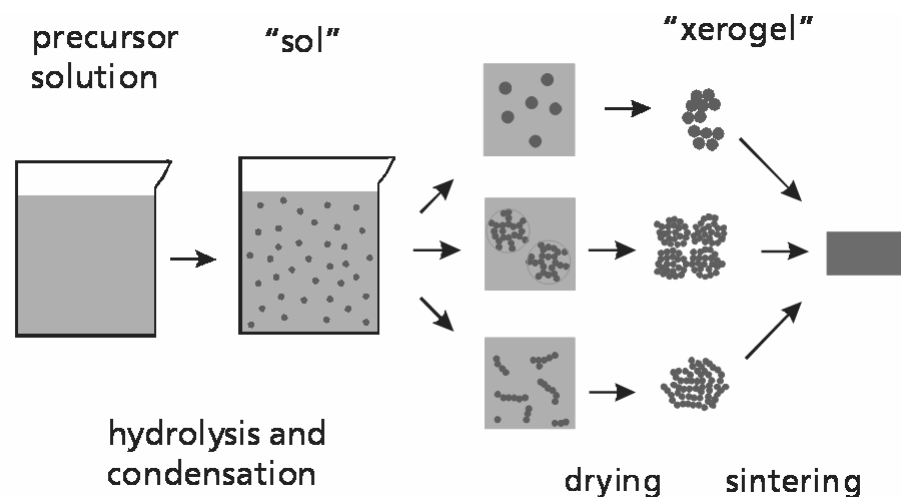


Figure 1. Schematic illustration of the sol-gel process, starting from molecular precursors which are finally transformed on processing to a ceramic product. (taken from [LOE03b])

At the molecular level, two reactions are generally describing the sol-gel process: hydrolysis and condensation [LIV89]. However, the characteristics and properties of a particular sol-gel inorganic

network are related to a number of factors that affect the rate of hydrolysis and condensation reactions, such as, pH, temperature and time of reaction, reagent concentrations, nature of catalyst, concentration, aging and drying conditions [FID03,DOE87].

Of the factors mentioned, pH, nature and ratio of reagents and catalysts have been identified as most important [CHA95,COL92]. Therefore, by controlling these factors, it is possible to vary the structure and properties of the sol-gel derived inorganic network over wide ranges [YU03,HIR97,KAJ00a]. For example, Löbmann et al. observed that the synthesis conditions i.e. concentration of water, used for the preparation of soluble titania precursor powders determine their chemical composition and, thus, the solubility behavior in various solvents [LOE03,LOE05].

2.2 THIN FILM FORMATION

Sol-gel processing has become a versatile method for preparing thin films on an industrial level. Depending on the application, various coating techniques were in general applied: i.e. dip-coating, spin-coating, spray-coating, float-coating, doctor blade technique, printing technique and ink jet technique [MOU06, PUE04]. The most common used method besides spin coating is the dip coating technique, which can be easily applied for cost efficient production of highly uniform films for optical applications (filters, antireflective coatings) [GOM00,LOE03].

Dip coating can be used in the batch process or in the continuous process. The batch dip coating can be described as a process where the substrate is immersed in a liquid and then withdrawn with a well defined withdrawal rate [SCH97a].

During the deposition stage, the inner liquid layer moves upward with the substrate and the outer layer drains back to the bath, which causes the streamline between the mentioned layers (Figure 2). There are six competitive forces ruling the position of the streamline and, thus, the thickness of the film in the film deposition: viscosity influencing upward on the solution, gravity, surface tension in the meniscus, inertial force of the boundary layer liquid that arrives at the deposition region, surface tension and disjoining or conjoining pressure for films whose thickness is under 1 μm [BRI90].

There is a relationship between thickness of the wet film and viscosity of coating solution, as well as between thickness of film and withdrawal rate of the substrate. The more viscose the liquid and rapid the withdrawal rate, the thicker the film is. The thickness h of the wet film can be calculated from the Landau-Levich-equation (Figure 2) [BRI91].

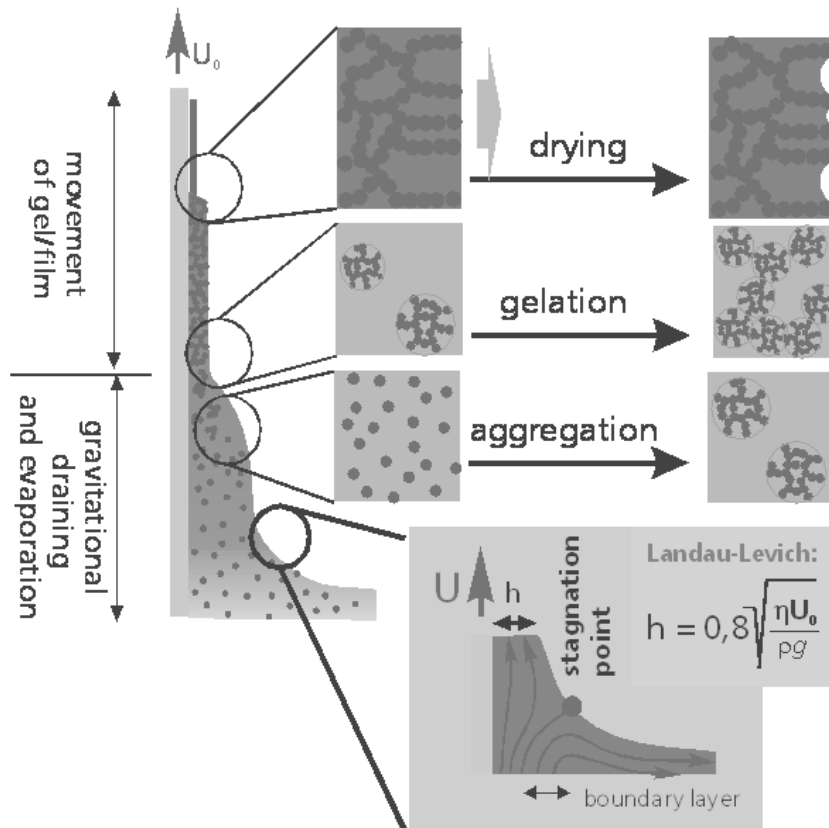


Figure 2. The schematic illustration presents the steady stage of the dip coating process (from the bottom up): formation of a wet film, aggregation of sol-particles, gelation and thin film drying. The extra display detail describes the flow patterns during dip coating. U_0 is the withdrawal rate, h is the entrained film thickness just above the stagnation point. η and ρ are the liquid viscosity and density. g is the gravitational constant. (taken from [LOE03b] and [SCH97a])

The sol-gel dip coating process includes the stages of concentrating of the polymeric species in the dilute sol on the substrate, aggregation and gelation with coincident gravitational draining and evaporation of the solvent. After the gelation, at the moment the solvent-filled and condensed network is capable to resist the gravitational flow, the xerogel might collapse or/and pore formation occurs due to solvent evaporation (Figure 2) [SCH97a].

The drying and aging of the wet film are significant stages of the film formation during and after the deposition stage. The different phenomena which occur during the film formation overlap and thus affect each other and thus the properties of the final inorganic film [KAJ98].

2.3 FILM DENSIFICATION

The formations of bulk and film material prepared by sol-gel method differ in many ways. The steps of bulk sol-gel processing may be divided in hydrolysis, condensation, gelation, aging, drying and densification stages [SCH88a]. The aggregation, gelation and drying phenomena occur mostly simultaneously and fast in film formation (Figure 3), whereas these stages are separated and may last for weeks in bulk systems [SCH97a].

Processes occurring during thin film shrinkage and densification are displayed in Figure 3. After gelation the uniaxial shrinkage causes tensile stress within the film. Further network stiffening by hydrolysis and condensation reactions occurs during drying and is promoted by air moisture.

[SCH88b] The xerogel network still contains some residual organics which are hydrolytically stable or sterically protected. Up on rising the annealing temperature the pyrolysis of organic moieties proceeds between 200 and 550 °C [KED91,KED94]. An oxidative atmosphere facilitates the decomposition reactions as opposed to pyrolysis under reductive conditions [KRU02,LOE03b].

The separation of organic residues induces further skeletal densification and promotes the intermediary formation of micro- and mesopores [ROU99]. Up on further annealing network relaxation and particle growth occurs. Crystallization in inorganic systems starts at lower temperatures as required in conventional ceramic processing [BRI90,LOE03b].

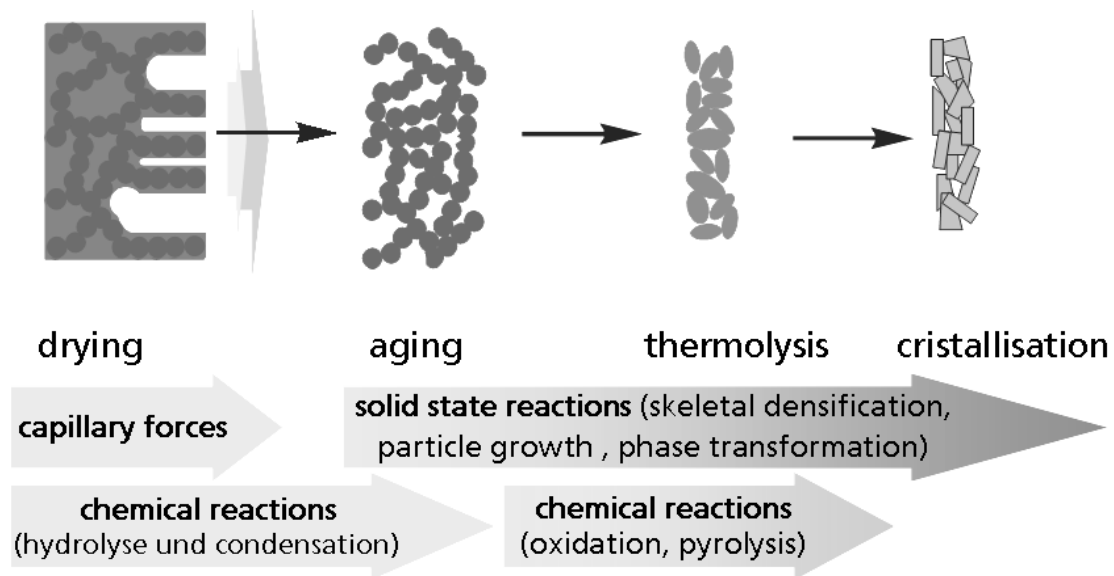


Figure 3. Schematic illustration of the chemical and structural processes occurring during thin film shrinkage and densification (taken from [LOE03b]).

2.4 STRESS FORMATION IN THIN FILMS

Virtually all thin inorganic films are in a state of stress [THO89]. Shear stresses occur near the free ends of the coated substrate, as well as in plane normal stresses in the interior region [CGI95]. The in plane stresses may be compressive or tensile [VRE92]. The total residual stress σ is composed of an intrinsic stress σ_i and a thermal stress σ_T :

$$\sigma = \sigma_i + \sigma_T$$

The thermal stress σ_T occurs during the cooling stage and is a result of thermal expansion mismatch between the coating and the substrate expansion coefficient. The thermal stress can be calculated by the following equation

$$\sigma_{th} = \frac{E_f}{1-\nu_f} (\alpha_f - \alpha_s) (T_a - T_c)$$

where E_f and ν_f are Young's modulus and Poisson's ratio, α_f and α_s the average coefficients of thermal expansion for the film and the substrate, T_a is the annealing temperature and T_c the

temperature during the measurement, respectively [THO89,BRE99]. The thermal stress σ_T is obviously a function of annealing temperature.

The intrinsic stress σ_i is a fundamental sum of many effects, i.e. the deposition method, the film shrinkage and film structure [ATA99,OTT96]. In general, thin films prepared by sol-gel processing usually exhibit tensile stress [BRE01], whereas thin films prepared by other coating techniques such as ion plating, chemical vapor deposition, or reactive evaporation, either present tensile or compressive stress [BAN97,OTT93].

During the formation of thin sol-gel films, the uniaxial shrinking mainly causes tensile stress in the coatings [BRI92]. Generally, the stress is originated by the restricting effect of the substrate on film shrinkage. For the adherent film, all of the shrinkage happens in the direction of the film thickness leading to tensile stresses parallel to the film-substrate interface (Figure 4) [SEN98].

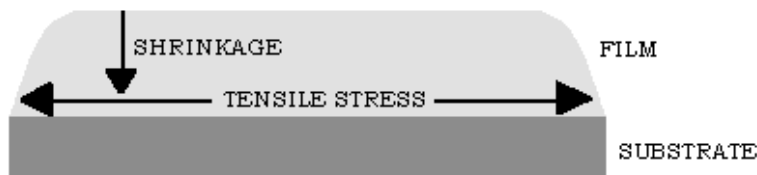


Figure 4. Shrinkage and tensile stress formation in an adherent sol-gel film.

Various techniques have been reported in literature for the determination of stresses in coatings including raman spectroscopy [EXA92], diffraction methods [MEH97,FIS96], hole drilling method [PER96], and substrate bending detection [SAN89,KOZ03,BRE01,HON02].

The commonly applied method is the mechanical deflection method. The advantage of this method is that a determination of residual stress in even amorphous coatings without knowledge of their elastic constants is possible [SKR00,MEH97,PER96]. However, one sided coatings are required [PER96].

Therefore, when the adhesion of the substrate is strong enough to suppress slippage, the residual stress σ_f can be determined as function of film curvature change occurring during the thermal treatment by the following Stoney equation:

$$\sigma_f = \frac{1}{3} \times \frac{E_s}{1-\nu_s} \times \frac{t_s^2}{t_f} \times \frac{\delta}{r^2}$$

where E_s = Young's modulus, ν_s = Poisson's ratio, t_s = thickness of the substrate, t_f = thickness of the film and δ = deflection of the substrate from the distance r of the substrate [STO09,FLI87, BRE99].

In Figure 5 the tensile stress of thin zirconia sol-gel films is displayed as function of annealing temperature and dwell time. The substrates were one side coated and afterwards first annealed at the designated temperature for 1 min. The residual stress was determined by the deflection method. Later the thermal treatment was continued and the residual stress was measured as function of dwell time. [BRE01]

At annealing temperatures of 150 and 250 °C the residual stress is approximately 20 MPa (1-10 min dwell time) and nearly doubles when the dwell time increases up to 10 hours. At this quite low annealing temperatures the content of residue organics is quite high, ensuring network plasticity and arising of tensile forces are easily reduced by structural relaxation processes. By increasing dwell time further network cross-linking by hydrolysis and condensation reactions takes place, which leads to increasing network stiffening and residual tensile stresses [SCH97b].

As the annealing temperature raise up to 350 °C the organics decompose [LOE03,BOC06]. This accompanies further film shrinkage and the residual tensile stresses increase. Nevertheless, with increasing dwell time the residual stresses decrease. In this temperature regime already viscose flow can diminish the tension created by pyrolysis and densification [SCH97b]. Of course, when the annealing temperature is further increased the film densification and tensile stress raises, but also a similar trend is observed [LOE03b].

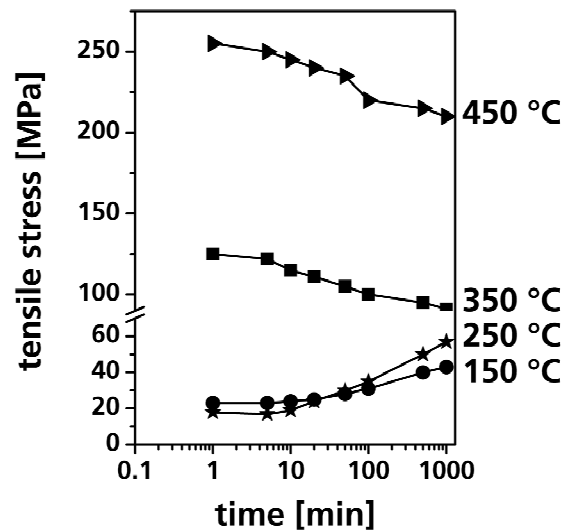


Figure 5. Tensile stress of thin zirconia sol-gel films is displayed as function of annealing temperature and dwell time. (Data taken from [BRE01])

2.5 CRACK FORMATION IN THIN FILMS

Tensile stress which exceeds the elastic limit in thin layers often causes cracking or decohesion of the layer [EVA88]. In turn some degree of compressive stress is considered to be advantageous because it closes surface cracks or can improve mechanical properties. However excessive compressive stress can lead to spallation and buckling of the film [SEN98,SKR00].

In sol-gel processing the stress and thus the cracking may be predicted by calculating the critical thickness h_c for crack propagation or the growth of pinholes by equation:

$$h_c = (K_{Ic} / \sigma W)^2$$

with K_{Ic} = critical stress intensity, σ = stress and W = function (1 for gel films). This theory describes the behavior of coatings that adhere well to the substrates. Films thinner than the critical

thickness do not crack. The critical film thickness for cracking has been observed to be typically around 1.0 μm for a variety of conditions and materials [ROE99,KOZ00b,KOZ02].

The film cracks mainly during drying or pyrolysis but not during sintering or crystallization, because of stress release through viscous flow or diffusive creep, which may occur during the last stages [BRI95,SCH97b]. In addition to the film thickness, the skeletal density of the film and the removal rate of solvents have an effect on the cracking [SEC00,CAI97]. The adhesion between film and substrate and the rate of temperature increase [KUR06] are also important on the stages of drying and sintering. The mismatch of thermal expansion coefficients of the substrates and the coating material also influences the stress development and, therefore, the crack formation. In the case of titania films on Borofloat glass with a film thickness over 750 nm the film quality is worsening, whereas higher film thicknesses of titania coatings on metal-substrate can be easily achieved [LOE03].

Several strategies to prevent film cracking or to produce thick films are mentioned and can be summarized as follows:

- 1 By using precursors containing organically-modified, non-hydrolysable groups, films with reduced network connectivity are obtained. The resulting network flexibility allows the densification without cracking, but the porosity of these films is higher than of the inorganic films [SEC00].
- 2 The condensation of the gel particles and, thus, the gelation can be prevented by the reversible complex formation of the reactive groups through drying before the gel formation. Nevertheless densification and pore formation is shifted to the pyrolysis stage [CAI97].
- 3 The condensation reactions and densification behavior of the coatings can be monitored by the environmental conditions after the deposition step [BUR99]. Nevertheless the processes are very complex and difficult to apply at an industrial scale [LOE03b].
- 4 High heating rates do prevent the cracking by promoting the densification against the crystallization. After the crystallization the sintering demands higher temperatures. [SCH97b,KED94]
- 5 To avoid the cracking polymeric additives, so called stress relaxing agents, are often used. They retard condensation reactions and film stresses can be easier released. For example, the 1.0 μm thick, single-layer and uncracked PZT ($\text{Pb}(\text{Zr}/\text{Ti})\text{O}_3$) film is achieved by adding polyvinylpyrrolidone, which hinders condensation reactions and promotes the structural relaxation in the films [KOZ00a,KOZ00b,KOZ03].

2.6 TITANIA

By the sol-gel process thin films for various applications are easily accessible [EGG04,LOE03b]. To study the interrelationship of structure and densification of thin sol-gel films in general, the system titania (TiO_2) system was chosen as a model.

The unique properties of TiO_2 , as i.e. its high refractive index and photocatalytic activity [YU02,WIN03] led to a high variety of applications in diverse areas such as electronics [ORE91], sensing [LAN06b] optics [LOE03] and catalysis [HER04].

TiO_2 naturally exists in three crystalline polymorphs: anatase, brookite and rutile. From these only rutile and anatase are used for technical applications. The third TiO_2 structure, brookite, as well as anatase, is a metastable phase and transforms into rutile at temperatures above ($>500^\circ\text{C}$). The impurities, crystal size, sample history etc. have influence on the transition temperature [LIN05,ZHU05,OKA01,TAK00,HUA06].

The bulk unit cells of both anatase and rutile (Figure 6) are tetragonal and the basic building unit is a slightly distorted octahedron. The titanium atom is surrounded by six oxygen atoms and the stacking of the octahedra results in threefold coordination of oxygen atoms.

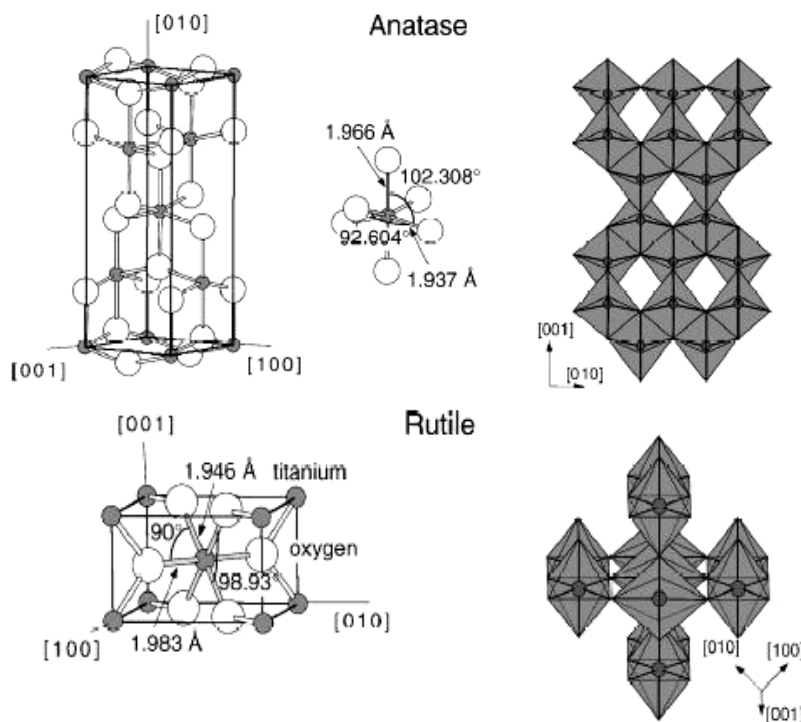


Figure 6. Bulk structures of rutile and anatase. The bond lengths and angles of the octahedral building units are presented on the left side and the stacking of the octahedra is shown on the right side. (Data taken from [DIE03])

3 OBJECTIVES OF THESIS

On the microscopic level, material deposition by sol-gel processing results from a complex interwoven sequence of interacting processes. Therefore it is crucial for all coating processes to understand the microstructural changes in the films in order to optimize the fabrication and to improve the film performance. Especially in this context macroscopic film cracking has gained high attention by industrial scientists.

The physical and chemical processes that are responsible for crack formation and prevention in thin films have already been theoretically described in literature. The experimental evidence has been poorly proved up to now, which may be partially due to a limited accessibility of sufficient amounts of material for solid state characterization. As a result of the recent invention of soluble precursor powders some new analytical perspectives are given. Therefore the aim of the thesis is to experimentally investigate the relationship between the microstructure of thin sol gel films, their densification and cracking.

Precursor powders of titania were chosen as model system, because they can be characterized as a function of annealing temperature. Furthermore, after preparation of coating solutions, the solvent can be stripped off again in order (sol powders) to separately investigate the influence of different solvents on the structure and densification of the precursors. When so-called film powders scraped off dip-coated substrates, the analysis of these film powders should take the effect of air-moisture and the unidirectional densification during drying into consideration. The microstructure of annealed film powders is probably the best match to the microstructure of sintered films, which unfortunately cannot be isolated due to their strong adhesion to the substrate. Nevertheless differences to the real coatings are anticipated and shall be pointed out.

Thereby it is interesting how the shrinkage and densification behavior of sol-gel films can be directed by the precursor chemistry and process parameters as heating rate and air moisture. Is it possible i.e. to exactly adjust the resulting film microstructure (i.e porosity, phase composition) by the respective precursor chemistry?

A new tool for the quantitative measurements of macroscopic cracks of thin films has to be created, which shall allow correlating film quality directly to the drying, shrinkage and densification behavior of the sol-gel films. The main interest is, whether it is possible to directly correlate the behavior of the thin sol-gel films to chemical properties of the used precursor types.

Further studies will be also related to the relationship of the formation of internal stresses and crack formation i.e., can the crack formation directly be correlated to the accompanied stress level.

Finally, the universal validity of the observation made shall be verified by the use of other solvents, precursor powders and coating systems i.e. zirconia.

4 EXPERIMENTAL

4.1 MATERIALS

Chemicals and solvents were used without further purification or drying procedure. Their corresponding manufacturer information and purity levels are listed in Table 1.

Table 1. Summary of used chemicals and their corresponding manufacturer information and purity levels.

manufacturer	chemical
Aldrich	acetylacetone, $\text{CH}_3\text{COCH}_2\text{COCH}_3$, $\geq 99\%$
	1,5-pentanediol, $\text{HO}(\text{CH}_2)_5\text{OH}$, 96%
	yttrium(III)-acetate hydrate, $(\text{CH}_3\text{CO}_2)_3 \cdot x \text{H}_2\text{O}$, 99.9%
ISC	deionised water, H_2O
Jäckle	ethanol, $\text{C}_2\text{H}_5\text{OH}$
	titanium(IV)-ethoxide, $\text{Ti}(\text{OC}_2\text{H}_5)_4$, 95.9%
	zirconium(IV)-propoxide, $\text{Zr}(\text{OCH}(\text{CH}_3)_2)_4$, 77.5%
Merck	hexadecyltrimethylammoniumbromide, $\text{CH}_3(\text{CH}_2)_{15}\text{N}(\text{Br})(\text{CH}_3)_3$, $\geq 98\%$
Fluka	triethanolamine, $(\text{HOCH}_2\text{CH}_2)_3\text{N}$, 98%

4.2 PREPARATION

4.2.1 PRECURSOR POWDER PREPARATION

Amorphous precursor powders were synthesized by reaction of metal alkoxides with the chelate ligand acetylacetone or triethanolamine, hydrolyzed with water and afterwards all volatile components were removed by rotational evaporation at reduced pressure. [LOE00,LOE01,LOE02,LOE03,LOE05,KRU06]

A standard TiO_2 precursor powder with a ratio Ti/ligand/ H_2O of 1/1/3 was synthesized as follows: By slow addition of 1.0 mol chelate ligand to 237.7 g (1.0 mol) titanium(IV)-ethoxide a yellow sol was obtained, which was stirred for one hour. After cooling down to room temperature 54.0 g (3.0 mol) deionised water was added. Without further delay subsequently all volatile components were removed from the reaction mixture by rotational evaporation at reduced pressure (< 40 mbar) with a maximum bath temperature of 80°C .

In contrast to the TiO_2 precursor powder synthesis the 8YSZ precursor powder was modified, because of the dopant addition. Therefore a standard 8YSZ precursor powder with a ratio Zr/ligand/ H_2O of 1/1/3 was prepared as follows: By slow addition of 1.0 mol chelate ligand to 237.7 g (1.0 mol) zirconium(IV)-propoxide a yellow sol was obtained, which was stirred for one hour. After cooling down to room temperature 54.0 g (3.0 mol) deionised water and 58.8 g

(173 mmol) yttrium-acetate hydrate were added. The sol was stirred for 30 minutes at room temperature followed by 30 minutes at 80 °C. Without further delay subsequently all volatile components were removed from the reaction mixture by rotational evaporation at reduced pressure (< 40 mbar) with a maximum bath temperature of 90 °C.

4.2.2 SOL PREPARATION

Coating solutions were prepared by dissolution of the amorphous precursor powder in different solvents and solvent mixtures with an oxide yield respective to crystalline TiO₂ or 8YSZ of 6 mass %. After stirring over night, they were filtered through a 0.45 µm membrane. [LOE03, KRJ06]

As typical basis solvents ethanol and water were used. When water based sols were prepared the cationic surfactant hexadecyltrimethylammoniumbromide was added below the critical micelle concentration (0.1 mass % respectively to water content) in order to improve the substrate wetting abilities. Solvent mixtures in principle were consisting of the basis solvent and an additive component like 1,5-pentanediol. The notation "90:10" indicates that a solvent mixture consisted of 90 mass % basis solvent and 10 mass % additive component.

4.2.3 PREPARATION OF SOL POWDER AND FILM POWDER

Sol powders were obtained after rotational evaporation of all volatile components from the sols at reduced pressure (< 20 mbar) with a maximum bath temperature of 80 °C.

Film powders were prepared by multiple dip-coating (~30 times, withdrawal rate: 50 cm/min) of 30 cm * 30 cm glass plates with a drying time of each single thin sol-gel film of 10 min. Then the multi-layer gel film was dried at 60 °C for 15 min and scraped off with a razor blade. The obtained sol powders and film powders were placed in a furnace (Model M110, Heraeus Instruments, Hanau, Germany) preheated to the designated temperature and held for 60 min. [BOC06]

4.2.3 THIN FILM PREPARATION

Thin films were prepared by dip coating either of borosilicate glass (Schott, Borofloat® 3.3, 3 mm × 100 mm × 100 mm, 2.2 g/cm³) that was pre-cleaned in a laboratory dishwasher at 93 °C with alkaline detergent (Neodisher A8, Dr. Weigert GMBH & CO.) or Si-wafer (150 mm, Si-Mat Silicon Materials, Germany).

The glass plates were treated with compressed air to remove dust from the surface before the coating. Thin film preparation was carried out in clean room atmosphere under constant humidity conditions using a climate control unit. The substrate was dipped in the dip-coating container and the solution was let to settle down for 15 seconds. The coating was made with a withdrawal rate depending on the desired end film thickness, varying in the range of 5 – 80 cm/min. [LOE03, BOC07]

If not otherwise mentioned constant humidity conditions of 20 % relative humidity (RH) at 24 °C (4.4 g H₂O/m³) were used. The freshly coated plates were dried in a fume hood for two minutes. After the pre-drying, calcinations of the sol-gel films were achieved by rapid thermal annealing

(RTA) for 10 min using a vented oven (Model Thermicon P, Heraeus Instruments, Hanau, Germany), pre-heated to the designated temperature (100 °C – 700 °C).

Coated samples for stress measurements were prepared on borosilicate glass (Schott, Borofloat® 3.3, ~0.14 mm × 50 mm × 50 mm, 2.2 g/cm³) by dip-coating. To ensure one-sided coatings, one surface side was protected by an adhesive foil, which was carefully removed before the final calcinations step.

4.3 CHARACTERIZATION

4.3.1 ANALYTICAL ULTRACENTRIFUGATION

Measurements of particle size distribution were carried out by Analytical Ultracentrifugation (AUC) at the Max Planck Institute of Colloids and Interfaces, Department of Colloid Chemistry, MPI Research Campus Golm, Potsdam, Germany (H. Cölfen) [COE04].

4.3.2 CHEMICAL ANALYSIS

Chemical analysis of the carbon content by pyrolysis method was performed by the micro analytic laboratory "Beller" in Göttingen, Germany. Investigations regarding to residue silicon (Si) or iron (Fe) content in scraped off film powders were performed by inductively coupled plasma-atomic emission atom spectroscopy (ICP-AES) analysis (ISC-FHG, analytical group).

4.3.3 DEFECT ANALYSIS

Depending on the current type of defect pattern light microscope images or SEM images were used for defect analysis. The evaluation procedure was performed with the picture evaluation program IMAGE C™ (Imtronic GmbH, Germany, Berlin).

Before starting the actual evaluation process, it was standard procedure to handle the images with an especially programmed IMAGE C™ "makro", which includes the following steps: (1) image scaling, (2) operation "color contrast", (3) filter "mean", (4) filter "convolve". For the defect quantification by counting, the EPQ analysis mode was used [IMA97,JUV04].

Thereby an array of a minimum of 10 virtual horizontal lines was laid over the image and the software counted every interception of the virtual lines with the cracks, detected by the strong contrast variation. The quantity of defects was obtained as "defects per millimeter [mm⁻¹"]

The second type of method for defect quantification was also performed by using IMAGE C™. After scaling of the image and adjusting of the grayscale threshold setting, the area of exposed glass surface, due to film cracking, was automatically detected [%] [IMA97,JUV04].

From each sample a minimum of 5 images from different areas of the glass plates were analyzed, wherefrom the standard deviation was calculated.

4.3.4 ELLIPSOMETRIC POROSIMETRY

Ellipsometric porosimetry (EP) measurements were performed at IMEC (Leuven, Belgium) using an EP tool equipped with an in situ spectro-ellipsometer from Sopra [MAE03,BAK00,BAK02]. EP measures the change of ellipsometric values $\cos\Delta$ and $\tan\Psi$ of thin films during the vapor

adsorption and desorption. All measurements were carried out at RT using toluene as sorptive. Further analysis included the calculation of the refractive index (n) of the film during adsorption using the fundamental equation of ellipsometry.

The isotherm of adsorption is calculated from the change of refractive index occurring during the adsorption using the Lorentz-Lorenz equation [BOI05]. The pore size distribution is calculated from desorption isotherms using the Kelvin model [ROU99].

4.3.5 FILM THICKNESS AND REFRACTIVE INDEX

Film thickness and refractive index of the thin films was calculated from UV-Vis reflection spectra with a wavelength area of 300 – 1800 cm^{-1} (UV-Vis spectrometer, Shimadzu UV-3100, Kyoto, Japan) using the Swanepoel method [DIA04,SWA84]. Barium sulfate was used as reference material. For the evaluation of the film thickness and refractive index an in-house developed computer-program Panker 43 was used (Panker 43, © Rainer Jahn, ISC-FHG, Würzburg, Germany).

For the determination of refractive index and film thickness only maxima and minima between 400 – 800 cm^{-1} were evaluated. The calculation of overall porosity from refractive index was performed using the Lorentz-Lorenz equation [CHR98,LAU96].

4.3.6 INFRARED SPECTROMETRY

FT-IR measurements were carried out using a Magna-IR 760 Spectrometer (FT-IR; Nicolet Instrument Corporation, Waltham, USA).

Powder samples were prepared as KBr pellets, whereas thin films are deposited on polished alumina or Si-wafer as substrate and measured in reflection geometry.

4.3.7 MICROSCOPY

Images of macroscopic cracks in thin films on glass were made with a Leica DC 300 (Wetzlar, Germany) or a Leica ARISTOMET (Wetzlar, Germany) using the Leica Image Manager.

Scanning electron microscopy (SEM; Model S-800, Hitachi Ltd., Japan; or LEO 1530 Gemini) was made on thin films coated either with a thin film of gold or platinum.

For transmission electron microscopy (TEM; Model JEM-2010, Jeol Ltd., Tokyo, Japan; Model CM 200 FEG/ST, Phillips, Nederland) samples were embedded in epoxy resin, ground with SiC abrasive paper and finally thinned with Ar-ions (Model RES 101, Bal-TEC, Balzer, Liechtenstein).

4.3.8 NITROGEN SORPTION

Nitrogen sorption was measured with an automated volumetric analyzer (Model Autosorb 3B, Quantachrome Instruments, Boynton Beach, USA). Prior to nitrogen adsorption analysis, samples were dried at 110 °C for 16 h at reduced pressure. The multipoint-method was used to determine the specific surface area according to Brunauer, Emmet and Teller (BET).

4.3.9 PENCIL HARDNESS TEST

Film hardness was tested by pencil test similar to ISO 15184. Though pencil-to-surface-angle was defined as 90 ° and surface was cleaned prior to testing with compressed air. As pencils Faber Castell 9000 pencils from 9B to 7H and pencils Derwent Cumberland pencils (Keswick, England) from 8H – 9H with a down-force of 1.25 N were used. The test was classified as ‘not passed’ when the coating was destroyed up to the substrate surface.

4.3.10 PHOTOCATALYTIC ACTIVITY

The photocatalytic activity of TiO₂ thin films on Borofloatglas™ was determined by using an in-house build-up testing method. Thereby coated glass plates of 5 * 5 cm² in size were irradiated with UV_A light while immersed in an aqueous/methanol solution. Methanol is easily degraded to formaldehyde by photocatalytic reactions. Formaldehyde in aqueous solutions can be detected in very small concentrations by a color reaction with special reagents by using a photometer. Color intensity depends on the formaldehyde concentration and thus for the photocatalytic activity of the coating. [HER06]

4.3.11 3-POINT BENDING TEST

The 3-point bending tests were performed in the middle of the 50 mm long, unbent fiber bundles on a test machine (Model Zwicki 1120, Zwick GmbH and Co., Ulm, Germany) with a crosshead speed of 1.5 mm/min. Span of the lower bearings was 3.2 mm, bearing diameters were 1.0 mm. Further details are given by Krüger and coworkers [KRU06].

4.3.12 REFRACTIVE INDEX OF POWDERS

Refractive index of powders was measured by the immersion method using refractive index liquids (Cargille Labs, Cedar Grove, USA). [KLE90]

4.3.13 SKELETAL DENSITY

Helium pycnometry (Model Accupyc 1330, Micromeritics Instrument Corp., Norcross, USA) was applied to determine the skeletal densities. Prior to analysis, samples that were prepared at calcinations temperatures > 150 °C were dried in a vented oven at 150 °C for 24 h and afterwards cooled down in an exicator filled with silica gel. Samples prepared using lower calcinations temperatures were stored in an exicator filled with silica gel for at least 48 h prior to analysis.

4.3.14 STRESS MEASUREMENTS

The curvatures of the substrates were measured by a MicroProf® laser profilometer (Fries Research & Technology GmbH, Germany). The residual stress σ_f in the thin film was calculated by the Stoney's equation [STO09,FLI87,KOZ03,BRE01]:

$$\sigma = \frac{1}{3} \frac{E_s}{1-\nu_s} \frac{t_s^2}{t_f} \frac{\delta}{r^2}$$

where E_s , ν_s , and t_s are Young's modulus (64 kN/mm²), Poisson's ratio (0.2) and thickness of the substrate (~0.14 mm), respectively, t_f is the thickness of the thin film, and δ the deflection of the substrate at a distance r from the center of the substrate.

4.3.15 THERMO ANALYSIS

Differential thermal analysis (DTA) and thermogravimetric analysis (TGA; Setaram TAG24, Caluire, France) of the sol powder and film powder were performed with a heating rate of 10 K/min in dry air atmosphere.

4.3.16 VISCOSITY

The kinetic viscosity [mm²/s] of the sols was measured with a capillary viscometer (Schott AVS 400) at 20 °C temperature. The capillary constant was 0.1029 and the measurements were made four times with 15 repetitions. The density ρ [kg/m³] of the sols was calculated from the mass of 50 ml solution. Using the value of the sol density and the kinetic viscosity $\eta_{kinematic}$ [m²/s], the dynamic viscosity $\eta_{dynamic}$ [mPas] was calculated as follows:

$$\eta_{dynamic} = \eta_{kinematic} \times \rho$$

4.3.17 X-RAY – DIFFRACTOMETRY

Powder X-ray diffractometry (XRD; Siemens D-5005, Bruker AXS GmbH, Karlsruhe, Germany) in Bragg- Brentano geometry with CuK α radiation was used to verify phase development.

Lattice parameter and microstrain analysis of the powders were performed by the evaluation program "Topas" (Bruker AXS GmbH, Karlsruhe, Germany). The program is based on the rietveld method [YOU95, CHE92] and is generally able to calculate the instrumental peak broadening of the diffractometer from the used instrumental parameters.

The Siemens D-5005 is equipped with a göbel mirror, which influence on the instrumental profile is not clear until now. For that reason the instrumental peak broadening was defined by measuring a standard. For powder X-ray diffractometry a certified LaB₆-standard (NIST, USA) was used.

Thin film grazing incidence X-ray diffractometry (GIXRD; Siemens D-5005, Bruker AXS GmbH, Karlsruhe, Germany) was performed at angle of incidence γ of 0.5°.

The average grain size was determined from the Integral breath by using Fourier analysis of the XRD peaks, refined by a split Pearson 7 function (Software EVA 6.0, Siemens, München, Germany) of the (101) reflection using the Debye-Scherer equation. The instrumental peak broadening of the diffractometer in grazing incidence geometry was determined by measuring certified Corundum (Al₂O₃) – standard (NIST, USA). The instrumental broadening (IB_i) was eliminated from Integral breath by the Warren Biscoe equation [RUP06].

4.3.18 X-RAY – REFLEKTOMETRY

Macroscopic film density was measured by X-ray reflectometry (XRR) using a Siemens D-5005 diffractometer (Bruker AXS GmbH, Karlsruhe, Germany) equipped with a reflectometry sample

stage [AND04]. The sample height was adjusted by the edge slit. The used measurement parameters are presented in Table 2. Thin film density was evaluated by fitting the measured X-ray reflectometry (XRR) data with DIFFRACplus REFSIM 2.0 (Bruker AXS GmbH, Karlsruhe, Germany) [BRU00]. Pure titania was assumed as uniform layer and borosilicate glass with a density of 2.2 g/cm³ was defined as substrate.

Table 2. X-ray reflectometry (XRR) measurement parameters.

2 θ angle [°] scan range	0.2 – 2.0
Generator voltage [kV]	40
Generator current [mA]	40
Time/Step [s]	2 - 50
Step size [°]	0.002
Scan mode	Step scan
Scan type	Locked coupled
Divergence slit	1.0
Anti-scattering slit	0.1
Detector slit	Out
Divergence blend [cm]	0.2
Detector blend [cm]	0.1
Edge – sample distance [μ m]	15

5 RESULTS AND DISCUSSION

5.1 SOLUBLE PRECURSOR POWDERS

The chemical modification of titanium precursors has been proved to be highly versatile for the preparation of sol-gel coating solutions [BRI90,LIV89,DOE87,KEM00,LOE00,LIV05,KAJ98,PEL98,TAK00,KOZ00]. Recently the synthesis of novel soluble precursor powders was reported, which can be dissolved in various solvents, resulting in ready to use long-term stable coating solutions [LOE00]. The use of these precursor powders has been demonstrated to be beneficial for the production of TiO₂ thin sol-gel films on an industrial level [LOE03].

A general preparation scheme of the TiO₂ precursor powders is shown in Figure 7. When titanium alkoxides are chelated with acetylacetonate (AcAcH), hydrolyzed and afterwards all volatile components are distilled off, an amorphous precursor powder is obtained. This powder is indefinitely stable under ambient conditions. This preparation route ensures the synthesis of highly reproducible soluble precursor powders on an industrial level and can be scaled up to batches of 50 kg. [LOE03]

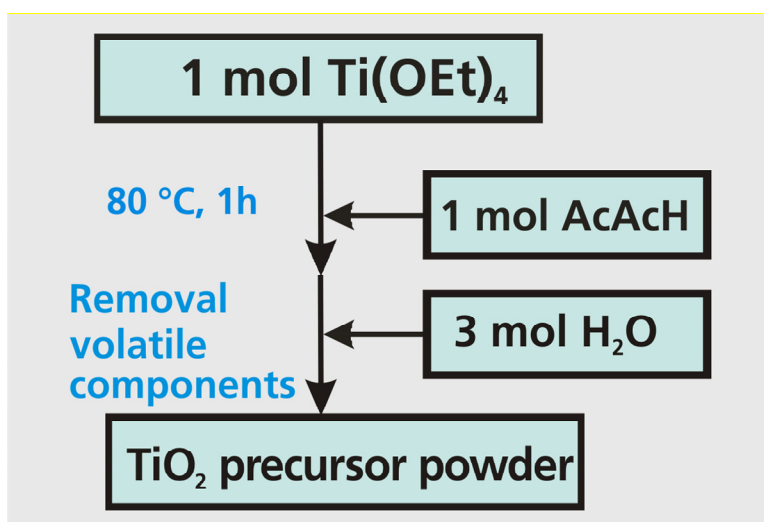


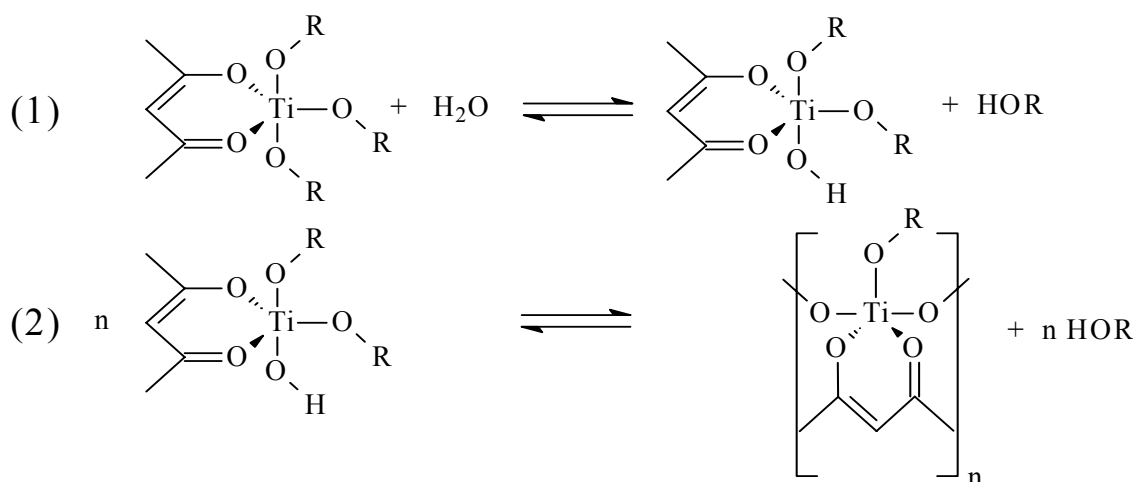
Figure 7. Scheme of soluble TiO₂ precursor powder synthesis using Ti(OEt)₄, acetylacetonate and water in the molar ratio of 1/1/3. (Data taken from [LOE03])

The molar ratio of Ti/AcAcH/water can be varied over a wide range of compositions. An overview is presented in Table 3. As it can be seen, most experiments yield fine grained amorphous powders, but with a low water content ($Y = 1$) for hydrolysis a liquid was obtained if the molar ratio of Ti/AcAcH is 1 ($X = 1$).

Table 3. TiO₂ precursors prepared with different molar ratios of Ti/AcAc/water. (Data taken from [LOE05])

	water Y					
	1 mol	3 mol	5 mol	7 mol	10 mol	20 mol
AcAcH X						
0.5 mol		Powder	Powder			
1.0 mol	Liquid	Powder	Powder	Powder	Powder	Powder
1.5 mol		Powder	Powder	Powder	Powder	Powder

One equivalent of water can only hydrolyze one alkoxide functionality per monomer (Figure 8, (1)). Therefore the possibilities for condensation reactions of these monomers are restricted. In ideal case only linear polymer chains or at least rings are formed (Figure 8, (2)). For that reason a low water content (Y=1) prevents the formation of sol-gel particles, which can be isolated as a powder.

**Figure 8.** Reaction scheme of hydrolysis reaction (1), condensation reaction (2) using Ti(OR)₄, acetylacetonate and water in the molar ratio of 1/1/1.

For further investigations on the influence of the preparation conditions on the chemical environment of the powders, thermogravimetric analysis and differential thermal analysis experiments were carried out by Löbmann [LOE05]. Since these investigations are essential for the understanding of the following investigations, these results are considered and discussed again.

The results for two powders prepared with different amounts of acetylacetonate for the complexation reaction of Ti (X = 1.0 and 1.5) are presented in Figure 9. Generally the thermal decomposition of the two powders can be divided up in two major temperature regimes, RT - 400 °C and 400 - 800 °C. Though the total mass loss (~54 %) of both powders is nearly equal, the powders present significant different decomposition behavior depending on the preparation conditions.

The powder synthesized with a higher amount of AcAcH presents higher mass loss up to 400 °C and a lower mass loss above 400 °C (Figure 9 (left)). This correlates with the corresponding

exothermal signal intensities in the differential thermal analysis, which are higher for an increasing ratio of AcACh/Ti in the first temperature regime (< 400 °C) and are lower in the second regime (> 400 °C) (Figure 9 (right)). [LOE05]

A higher ratio of AcACh/Ti leads to an increasing coordination of AcACh to the metal atoms in the powder. This complexation reaction also results in an increasing hydrolysis reaction of alkoxide moieties leading to a lower content of alkoxide groups. In summary it can be suggested that the thermal decomposition reaction of AcACh takes place between 200 and 400 °C, whereas the alkoxides are removed in a separate reaction up to 600 °C. Apparently the thermal stability of the organic groups behaves opposite their hydrolytic stability. [LOE05]

These results are also confirmed by investigations in the literature on molecular precursors chelated with acetylaceton. Poncelet [PON90] and Brenier [BRE01] observed a thermal induced chemical transformation of acetylaceton via a retro-Claisen type reaction to acetone and acetate at around 200 °C. Acetone immediately decomposes, whereas the oxidative elimination of the acetate ligands is proposed to be finished at 350 °C.

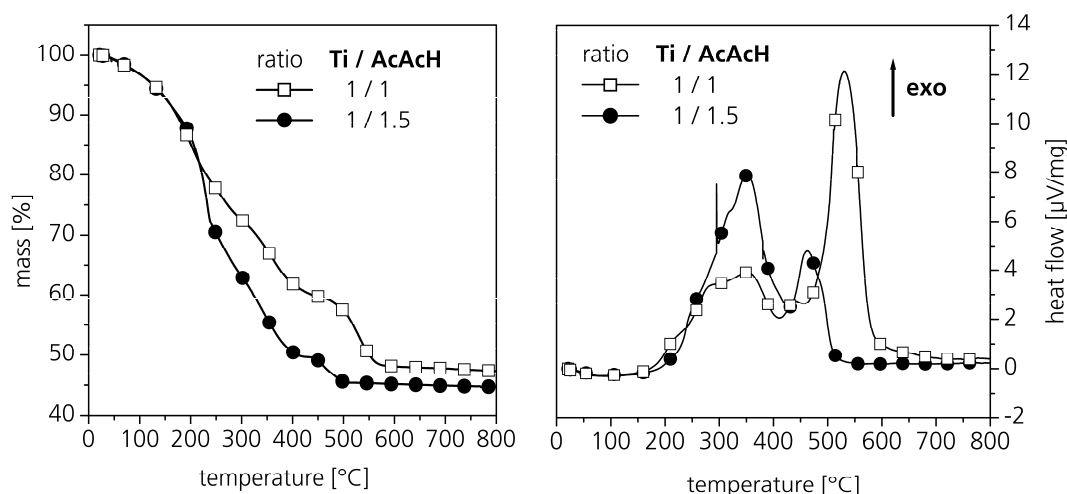


Figure 9. Thermogravimetric analysis (left) and differential thermal analysis (right) of soluble TiO_2 precursor powder synthesized using $\text{Ti}(\text{OEt})_4$, acetylaceton and water in the molar ratio of 1/1/3 and 1/1.5/3. (Data taken from [LOE05])

Furthermore this assumption is confirmed by DTA/TG investigations on a series of TiO_2 precursor powders prepared with different ratios water/Ti ($Y = 3 - 20$) and with a fixed ratio of AcACh/Ti (1/1). From the thermogravimetric analysis in Figure 10 (left) it can be seen that with increasing water content the total mass loss decreases from ~53 mass % up to ~35 mass %. Higher water content during the distillation at 80 °C results in a higher rate of hydrolysis reactions and so one in a lower content of alkoxide groups. [LOE05]

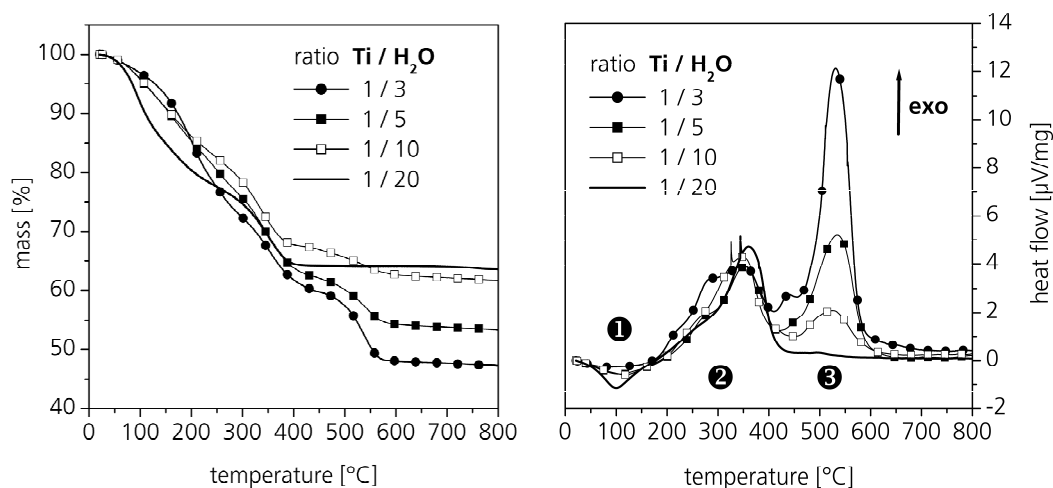


Figure 10. Thermogravimetric analysis (left) and differential thermal analysis (right) of soluble TiO₂ precursor powder synthesized using Ti(OEt)₄, acetylacetonate and water. The molar ratio of Ti/AcAc was fixed (1/1). (Data taken from [LOE05])

In the DTA (Figure 10 (right)) the signal between 200 – 400 °C (②), attributed to AcAcH, remains nearly unchanged, whereas the signals for the alkoxide groups (③) are decreasing with increasing water/Ti ratio. So the low hydrolytic stability of the alkoxide groups leads to a higher oxide yield of the resulting powders with increasing water content.

When a high water content ($Y = 20$) in the hydrolysis step of the precursor powder preparation is used, an additional endothermic signal around 100 °C appears (①) in the DTA, which can be explained with the evaporation of residual incorporated water.

SUMMARY OF 5.1 "SOLUBLE PRECURSOR POWDERS"

A synthesis route for the preparation of long term stable amorphous TiO₂ precursor powders can be utilized. Depending on the synthesis conditions and the initial chemical compositions the chemical structure of the resulting powders can be adjusted.

5.2 ETHANOL BASED COATING SYSTEMS

5.2.1 SOLUBILITY AND STABILITY

The preparation of ready-to-use coating solutions by simple dissolution of precursor powders in polar solvents was recently reported by Löbmann [LOE03]. As shown by Löbmann the solubility of the precursor powders in various polar solvents critically depend on the processing parameters. [LOE05]

The results of the solubility experiments in ethanol as solvent are presented in Table 4. Powders synthesized with a ratio of AcAcH/Ti smaller than 1 ($X = 0.5$) were insoluble in ethanol, whereas with an equimolar ratio of AcAcH and Ti the powders dissolve easily (Table 4). Obviously, when a ratio of AcAc/Ti of 0.5 is used half of the $Ti(OEt)_4$ is not coordinated by acetylacetonate. The unstabilized metal-alkoxide are unprotected against hydrolytic attack and condensation reaction. Therefore during the hydrolysis step of the precursor powder synthesis, partly amorphous titanylhydroxide species are formed, which are obviously not dissolvable in ethanol anymore [JOL00].

When the concentration of water is further increased ($Y > 7$) the powders are insoluble again. But when a ratio AcAc/Ti of 1.5 is used the concentration of water can be extended to $Y = 10$. With increasing water content, the hydrolysis rate increases and the amount of residual -OEt groups in the powders decreases. Based on the explanation of the thermoanalysis data it was concluded, that the solubility and stability of TiO_2 precursor powders is a function of the balance of acetylacetonate and alkoxide groups within the precursor-clusters. When the content of polar -OEt groups is decreasing in the amorphous particles the solubility in polar solvent like ethanol is also decreasing. For instance commercial pure $Ti(AcAc)_4$ is insoluble in ethanol, too [GOE07].

Table 4. Solubility of TiO_2 precursors prepared with different molar ratios of AcAc/water in ethanol. The Ti content is fixed to 1 mol. (Data taken from [LOE05])

	water Y					
	1 mol	3 mol	5 mol	7 mol	10 mol	20 mol
AcAcH X						
0.5 mol		Insoluble	Insoluble			
1.0 mol	(Liquid)	Good	Good	Soluble	Insoluble	Insoluble
1.5 mol		Soluble	Soluble	Soluble	Soluble	Insoluble

For standard dip-coating experiments a precursor powder, prepared with a ratio $Ti/AcAc/H_2O$ of 1/1/3, dissolved in solvent mixtures of ethanol and 1,5-pentanediol was favored [LOE03]. Therefore an investigation on the long-term stability of a sol prepared with this precursor powder ($Ti/AcAc/H_2O$ ratio of 1/1/3) dissolved in a solvent mixtures of 90 % ethanol and 10 % 1,5-pentanediol was carried out by measurements of the particle size distribution using Analytical Ultracentrifugation (AUC) [COE04]. A representative selection of those measurements over a period of half a year is presented in Figure 11. Even if the sol is aged up to half a year no obvious

change in the particle size distribution is noticeable. So the dissolution of amorphous precursor powders in alcohol-based solvent mixture yields in long-term stable coating solutions. However it seems that the amount of smaller particle (< 1 nm) is decreasing with increasing aging time and therefore a narrower particle distribution is achieved. Since particles of the same size have the same surface energy this is energetically favored.

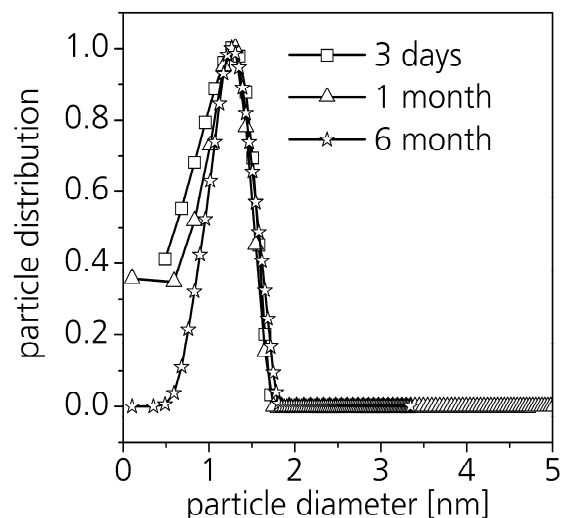


Figure 11. Measurements of particle size distribution by Analytical Ultracentrifugation (AUC) of a sol prepared with a precursor powder (ratio Ti/AcAc/H₂O of 1/1/3) dissolved in a solvent mixtures of 90 % ethanol and 10 % 1,5-pentanediol.

SUMMARY OF 5.2.1 "SOLUBILITY AND STABILITY"

The solubility of the precursor powders in ethanol based solvents critically depends on the balance of acetylacetonate and alkoxide groups within the precursor-clusters. For the preparation of long term stable coating solutions a solvent mixture of ethanol and pentanediol was favored. The long term stability was proved by particle size measurement over half a year.

5.2.2 CHANGES INDUCED BY THE SOLVENT COMPOSITION

In addition to the practical advantages shown by Löbmann et al. [LOE00,LOE03] there are some new analytical perspectives: The precursor powders can be characterized as a function of annealing temperature. Additionally coating solutions may be stripped off again in order to investigate the role of different solvents during a drying process (Figure 12), which are called "sol powders". When as-dried films are scratched off a substrate, the solid state analysis of these "film powders" (Figure 12) provides valuable information on the effect of air moisture and the unidirectional densification during drying. The microstructure of annealed film powders is probable the best match to the actual film material, which unfortunately cannot be isolated in bulk quantities because of their strong adhesion to the substrate. However to exclusively study the changes induced by the solvent, first a systematical comparison between the precursor and different sol powders is made. [BOC06]

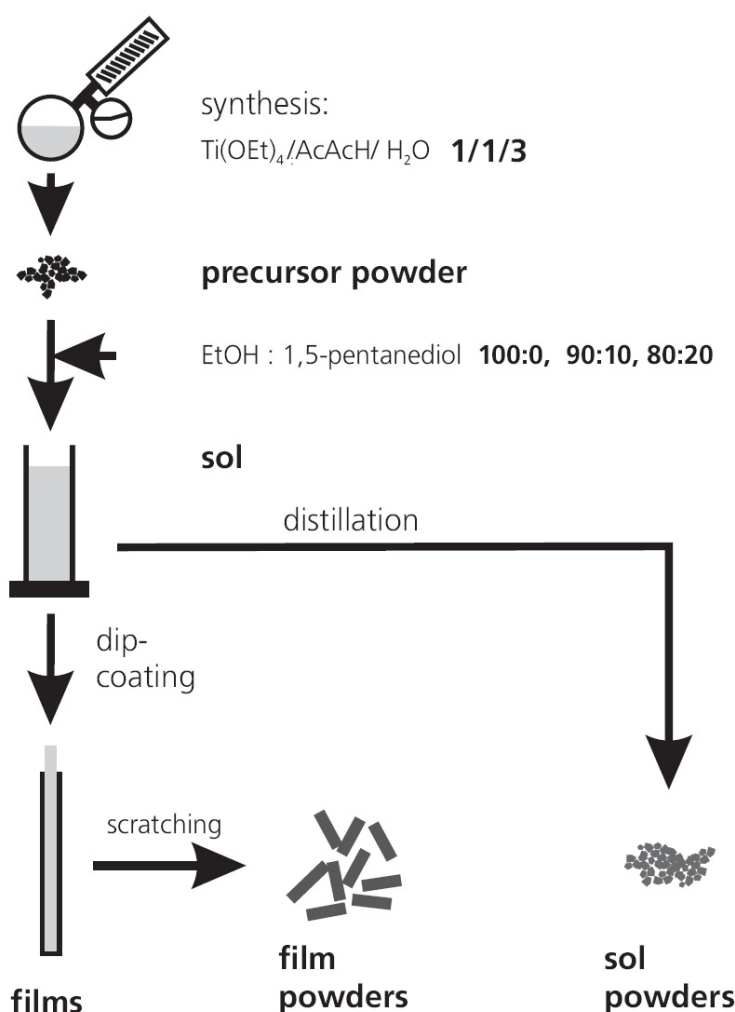


Figure 12. Illustration of different amorphous TiO₂ materials used for the characterization of the thin film formation and densification. (Illustration taken from [BOC06])

The thermoanalysis is an often applied powerful method for the study of thermal degradation behavior of isolated materials. This method is restricted by its relative slow heating rate (< 20 K/min). Nevertheless in laboratory praxis often isothermal annealing is used. Therefore the results of representative TGA experiments of a typical used soluble TiO_2 precursor powder with a molar ratio of $\text{AcAcH/Ti/H}_2\text{O}$ (1/1/3) are given in Figure 13. Samples that were isothermally annealed at temperatures below 600 °C for one hour in a preheated furnace (Figure 13) generally achieve the same mass loss at lower temperatures than those in the experiments with constant heating rates. Even though this observation is predictable, this systematic offset must be considered when results from different experimental setups are compared. [BOC06]

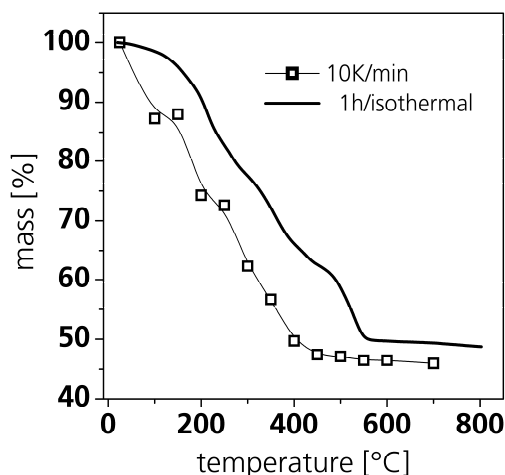


Figure 13. Thermogravimetric analysis of soluble TiO_2 precursor powder synthesized using $\text{Ti}(\text{OEt})_4$, acetylacetone and water in the molar ratio of 1/1/3. The experiment was performed simultaneously under dry air atmosphere with a heating rate of 10 K/min. In mass losses are given (open symbols) for samples isothermally annealed for one hour at the respective temperature. The line is drawn as guide for the eyes. (Data taken from [BOC06])

When pure ethanol is used as solvent and all volatile components are again removed by rotational evaporation, the resulting sol powder exhibits the identical thermal decomposition pattern as the soluble precursor powder employed. Obviously the initial synthesis conditions have established a stable configuration of the precursor that remains unaffected in the presence of ethanol as solvent.

This situation changes when the solvent mixture contains 1,5-pentanediol (Figure 14). In this case the material isolated after rotational evaporation is a highly viscous liquid rather than a powder. Apparently the vacuum conditions employed are not sufficient to completely remove the diol (b.p. 242 °C) as additionally indicated by higher total mass losses during thermogravimetric analysis (Figure 14 (left)). This assumption is corroborated by the DTA measurements performed on the different residues (Figure 14 (right)). As already mentioned the DTA pattern of powders from purely ethanol-based sols does not differ from those of the respective precursor powder (Figure 14 (right)). When 10 % 1,5-pentanediol were present in the sol, the signals assigned to the decomposition of AcAc and -OEt groups are broadened indicating partial replacement by the diol. When its content is increased to 20 %, the first exothermic signal is superimposed by the endothermic evaporation of the diol (~ 242 °C). [BOC06]

Based on these observations one could expect that during drying of films 1,5-pentanediol should become enriched and thus may maintain some plasticity of the deposited material [KOZ03].

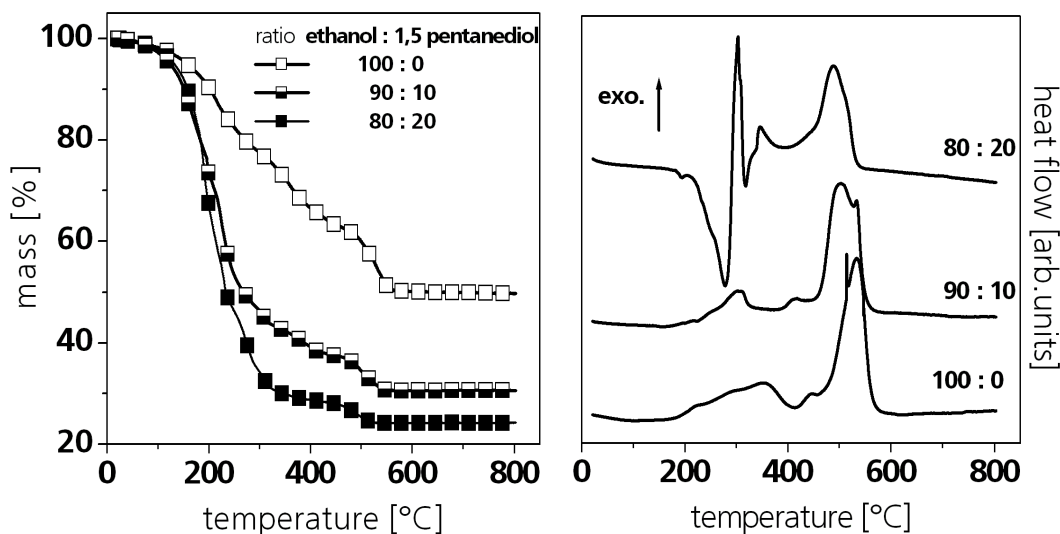


Figure 14. Thermogravimetric analysis (left) and differential thermal analysis (right) of sol powders obtained from ethanol based coating solutions containing 0 % (□), 10 % (◻) and 20 % (■) 1,5-pentanediol (compositions 100:0, 90:10 and 80:20 respectively). The experiments were performed under dry air atmosphere with a heating rate of 10 K/min. (Data taken from [BOC06])

Measurements of the skeletal “backbone” densities of the powders as a function of isothermal annealing temperatures (Figure 15) provide additional insight into the influence of the solvent mixture. Sol powders prepared from purely ethanol based solutions exhibit the highest initial skeletal density, increasing amounts of 1,5-pentanediol in the sol decrease the density of the respective material. As it could be seen in the DTA/TG analysis, the vacuum conditions are not sufficient enough to remove the 1,5-pentanediol from the sol powders and so the 1,5-pentanediol is still present and reduces because of its low density (1.0 g/cm^3) the overall density of the 1,5-pentanediol containing sol-powders. [BOC06]

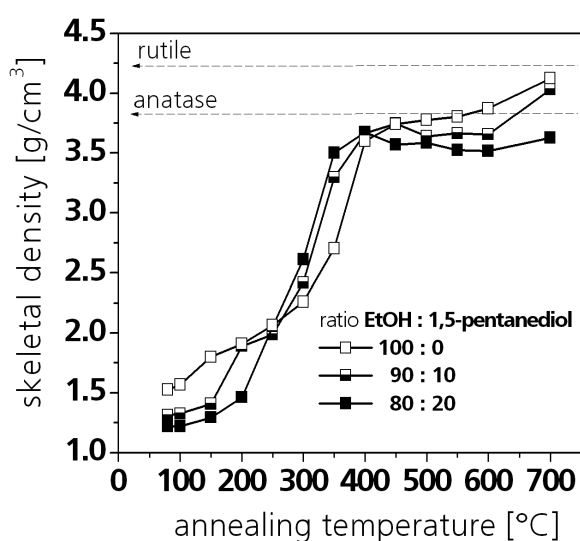


Figure 15. Skeletal densities of sol powders prepared from different sols as a function of annealing temperature. The theoretical densities of rutile (4.24 g/cm^3) and anatase (3.84 g/cm^3) are given as references [CRC94]. (Data taken from [BOC06])

Upon annealing the powders prepared from sols containing 1,5-pentanediol undergo a steeper skeletal densification than the samples from purely ethanol based sols. This densification behavior is associated with the higher mass loss up to 350 °C in the thermogravimetric analysis (Figure 14 (left)) and can be related to the thermal degradation and evaporation of 1,5-pentanediol. However for all materials a value of approximately 3.6 g/cm³ is measured after treatment at 400 °C. [BOC06]

Above this temperature, the presence of organic residues cannot account for any differences in the backbone densities, because no significant mass loss takes place during isothermal sintering above 400 °C (Figure 13). Nevertheless, powders which are treated up to 400 °C are nearly colorless, but show a grayish to black appearance in an intermediate temperature range and become quite colorless at 700 °C again. This visual observation indicates the transitional presence of at least small volume fractions of carbon due to an incomplete oxidative decomposition of organic moieties.

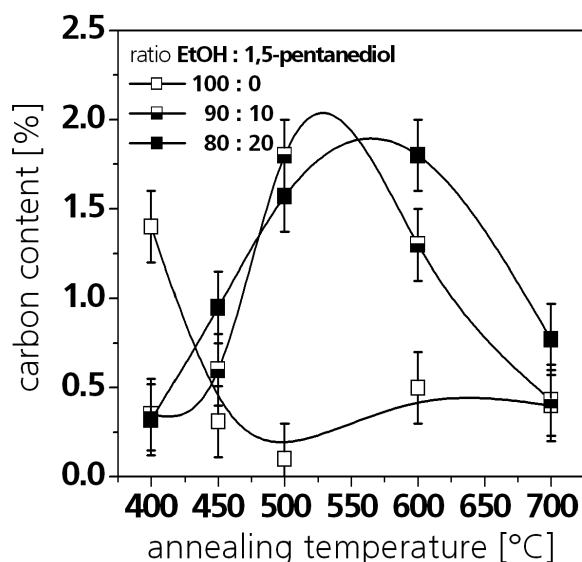


Figure 16. Carbon content of sol powders prepared from different sols as a function of RTA annealing temperature.

Measurements of the carbon content in the sol powders (Figure 16) confirm this assumption. At temperatures > 400 °C powders from pure ethanol based sols contain only minor residues of carbon, whereas a higher content of 1,5-pentanediol in the sol mostly results in an increasing carbon content at intermediate temperatures. Though, it has to be noted that this phenomena of increasing carbon content is due to the sample preparation by isothermal annealing at the designated. When a constant heating rate is used such a behavior is not expected. Nevertheless in this case it can not be totally clarified whether all carbon is incorporated as elementary carbon, or also partly substituted some lattice oxygen atoms or formed a carbonate species [LI05].

These small amounts obviously do not significantly contribute to the TGA-results above 400 °C (Figure 13 (left), open symbols). Nevertheless, the increase of skeletal density correlates with the initial solvent composition: the lower the content of 1,5-pentanediol, the better the densification with increasing temperature. In turn powders from sols with 20 % diol do not reach the skeletal density expected for crystalline anatase (3.84 g/cm³) even after sintering at 700 °C. [BOC06]

Further investigations by X-ray diffraction experiments were carried out which reveal different contents of crystalline phases (Figure 17) above 500 °C: Even though only anatase is found as product of the initial phase of crystallization for all samples, rutile starts to crystallize at 600 °C and becomes the dominating phase at 700 °C for samples that contained no or only 10 % pentanediol. In contrast to this, if the initial sol comprised 20 % diol, no rutile can be detected at 600 °C and at 700 °C still only minor amounts of this phase are found. The fact, that the skeletal density of this sample is still below the theoretical density of anatase (Figure 15), can be partly explained by the existence of carbon, but also suggests the existence of significant volume fractions of amorphous or at least strongly disordered TiO₂. The existence of closed pores, which also could reduce the skeletal density, was not favored as discussed in the following Paragraph. In contrast to this, only rutile is found in powders from purely ethanol based solutions, even though these samples do not reach the theoretical skeletal density of rutile. [BOC06]

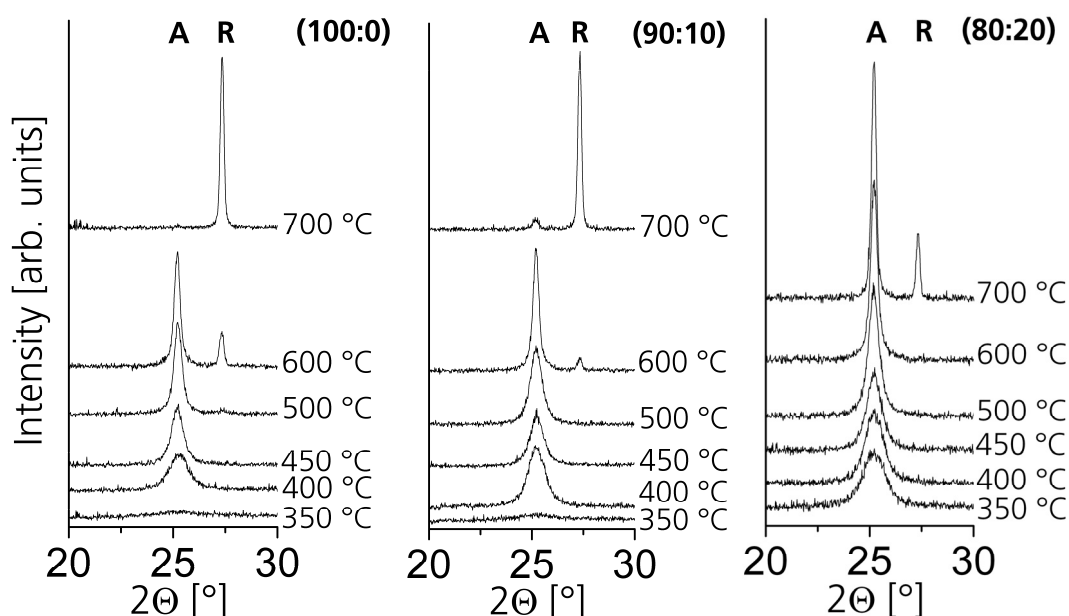


Figure 17. X-ray diffraction pattern of sol powders prepared from sols containing 0 % (left), 10 % (middle) and 20 % (right) 1,5-pentanediol respectively. The samples were annealed at temperatures between 350 °C and 700 °C as indicated at the right side of the Figure. Peaks assigned to anatase (A) and rutile (R) are marked individually.

To explain this observation, investigations by N₂-sorption experiments were done. Since the existence of macropores can be ruled out by SEM, open mesoporosity can be estimated by combining the skeletal densities and the cumulative pore volumes. Generally all systems are showing an evolution of surface area (Figure 18 (left)) and open mesoporosity (Figure 18 (right)) that has already been observed for other sol-gel material [LOE96, KRU02].

The arising of microporosity and surface area at a calcination temperature of 350 °C is directly linked to the degradation of organics also leading to the skeletal densification (Figure 15). A further increase in the calcination temperature up to 400 °C leads to a formation of a mesoporous network that is densified at higher temperatures. However, with increasing 1,5-pentanediol content, especially with the addition of 20 % 1,5-pentanediol, the surface area and porosity is significantly reduced after annealing temperatures between 400 °C and 500 °C. This

faster densification process then leads to an incomplete thermal oxidative decomposition of organic residues resulting in trapped carbon. [BOC06]

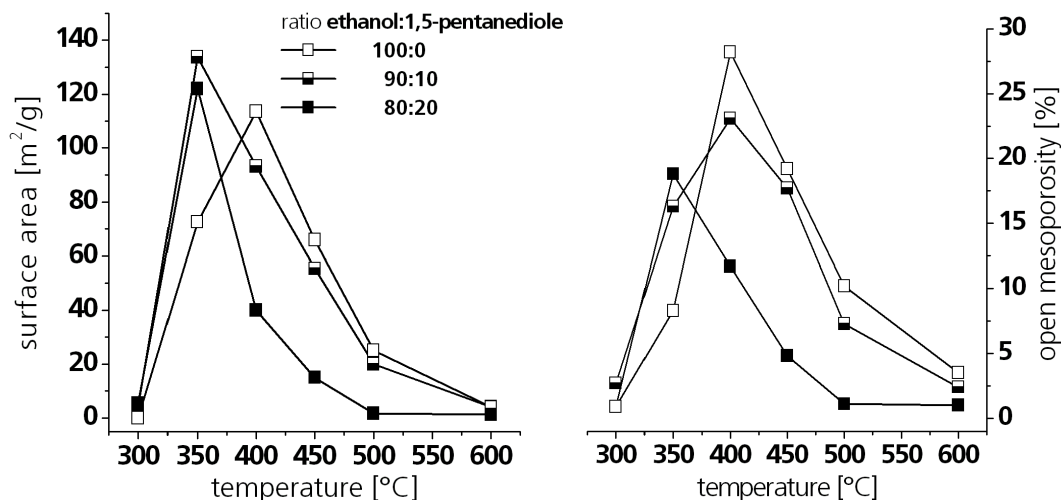


Figure 18. Surface area (left) and open mesoporosity (right) as a function of annealing temperature from sol-powder prepared from sols containing 0 %, 10 %, 20 % 1,5-pentanediol respectively. (Data taken from [BOC06])

SUMMARY OF 5.2.2 "CHANGES INDUCED BY THE SOLVENT COMPOSITION"

In summary, a high densification rate caused by the addition of 1,5-pentanediol, results in a dense microstructure with trapped carbon. The inclusion of carbon impurities after the calcinations step of titania sol-gel precursors has been already reported [SAK03,KRU05]. These impurities can retard the phase transformation of anatase to rutile [LIN05] as already been shown for increasing concentration of other organic additives like Pluronic™ [CHO04]. This effect may be utilized for the preparation of photocatalytic films, because only the anatase phase of TiO₂ is sufficiently active for such applications [FUJ99]. Furthermore the usage of carbon-doped titania has been reported as promising option to increase the visible light photocatalytic activity of titania [LI05,KHA02].

5.2.3 DENSIFICATION OF ETHANOL BASED FILM POWDES

5.2.3.1 GENERAL CONSEQUENCE OF LARGE SURFACE-TO-VOLUME RATIO AND AIR MOISTURE DURING FILM FORMATION

According to the experimental approach outlined in Figure 12, the results obtained for sol powders have to be compared with experiments using material scraped off from substrates after coating experiments (film powders) in order to elucidate the changes induced by the large surface-to-volume ratio and the presence of air moisture during the dip coating procedure. In a first step film powder from a purely ethanol based solution will be investigated.

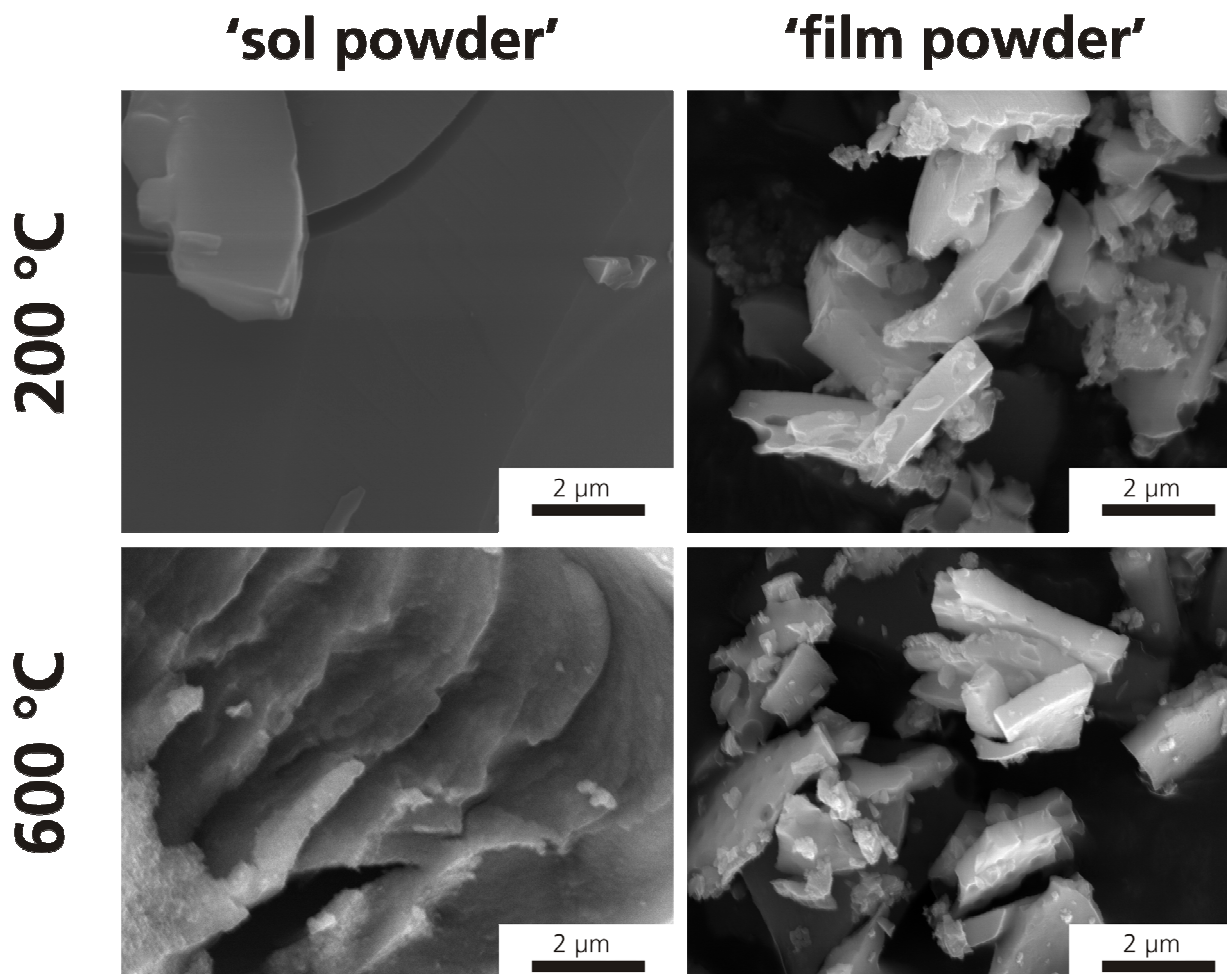


Figure 19. SEM images of sol powder (left) and corresponding film powder (right) at calcinations temperatures of 200 °C (top) and 600 °C (bottom). Pure ethanol was used as solvent. (Data taken from [BOC06])

At first sight the two types of “powders” differ significantly concerning their microscopic shape. As it can be seen in Figure 19 the SEM images of the sol powder present a coarser structure, with a high content of particles larger than several μm. Film powder on the other hand exhibit a high amount of fine film fragments, which have the typical proportions of thin films with a medium film thickness lower than 1 μm. However these SEM images present no clear differences between samples whether annealed at 200 °C or 600 °C. Therefore further insights into the changes induced by thermal treatment on those materials are given by the thermogravimetric analysis and the differential thermal analysis in Figure 20. [BOC06]

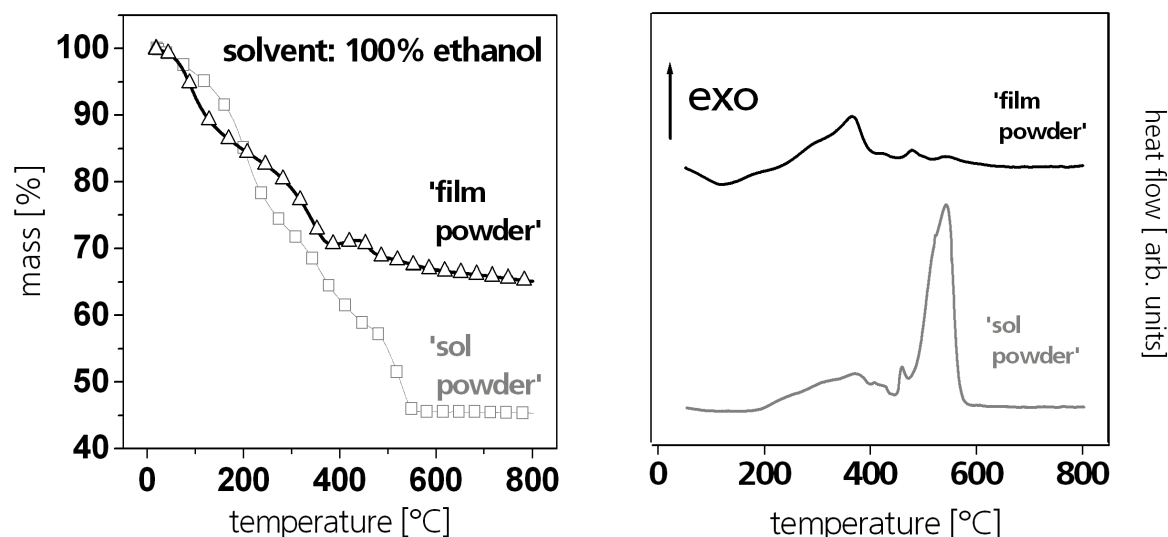


Figure 20. Thermogravimetric analysis (left) and differential thermal analysis (right) of film powder obtained from a purely ethanol based coating solution (black lines). Additionally the data of the respective sol powder is given (grey lines). All experiments were performed under dry air atmosphere with a heating rate of 10 K/min. (Data taken from [BOC06])

Up to temperatures between 350 °C and 400 °C film powders and sol powders show similar mass losses under a constant heating rate of 10 K/min, also the associated broad DTA-signals both indicate exothermal decomposition reactions. Since these reactions are attributed to the oxidative decomposition of acetylacetonate groups, these organic residues were obviously stable against hydrolysis during film deposition under ambient conditions. Above 400 °C the mass of film powders is only diminished by a few percent and just a small exothermal peak is found in the DTA analysis. The -OEt groups, that are known to decompose in this temperature region, had apparently undergone a hydrolytic cleavage during the coating procedure. This observation can be directly attributed to the influence of the large surface-to-volume ratio and air moisture during thin film formation. [BOC06]

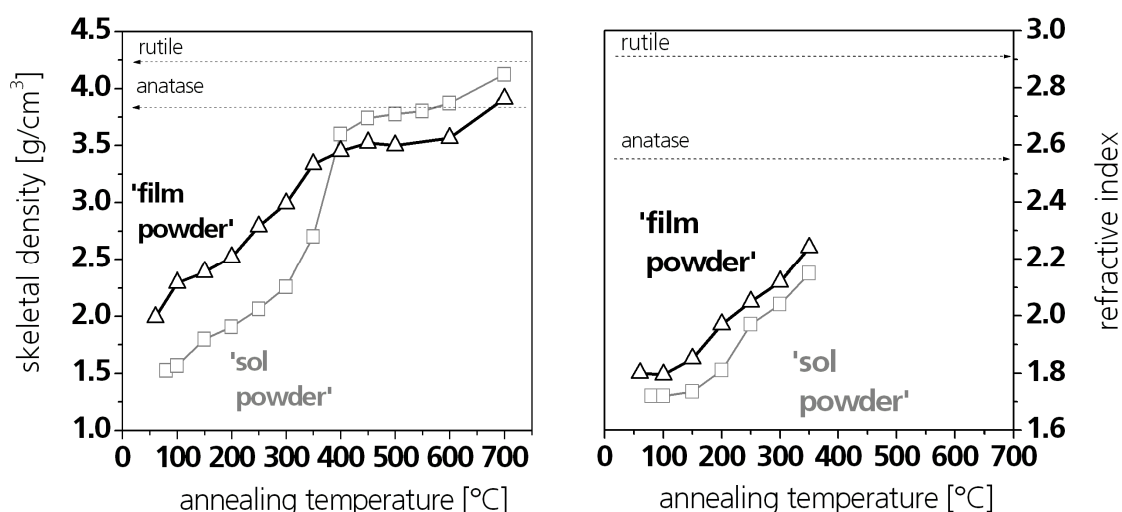


Figure 21. Skeletal density (Data taken from [BOC06]) and refractive index (left) of film powder prepared from a purely ethanol based sol as a function of annealing temperature (Δ). For comparison the data of the respective sol powder from Figure 15 are shown (\square). The refractive index and the theoretical densities of rutile and anatase are given as references [CRC94].

As a consequence of the lower content of residual -OEt groups, the film powder exhibits a higher skeletal density than the sol powder at low isothermal treatment temperatures (Figure 21 (left)). This difference is observed up an annealing temperature of 350 °C.

Measurements of the refractive index of these powders seem to confirm that results. The refractive index in solids is determined by the polarizability of elementary bondings [BOG75,MA02] and meso/microporosity in the network. Since it was proved by N₂-sorption measurements, that below 300 °C no porosity exists (Figure 18) this factor can be ruled out. It is known that mostly covalent bondings as found in the -OEt groups are less polarizable than the more ionic metaloxide bondings [HOI95], which might be formed after hydrolysis of the -OEt groups by condensation reactions. Therefore it is reasonable why the film powder shows a higher refractive index than the respective sol powder.

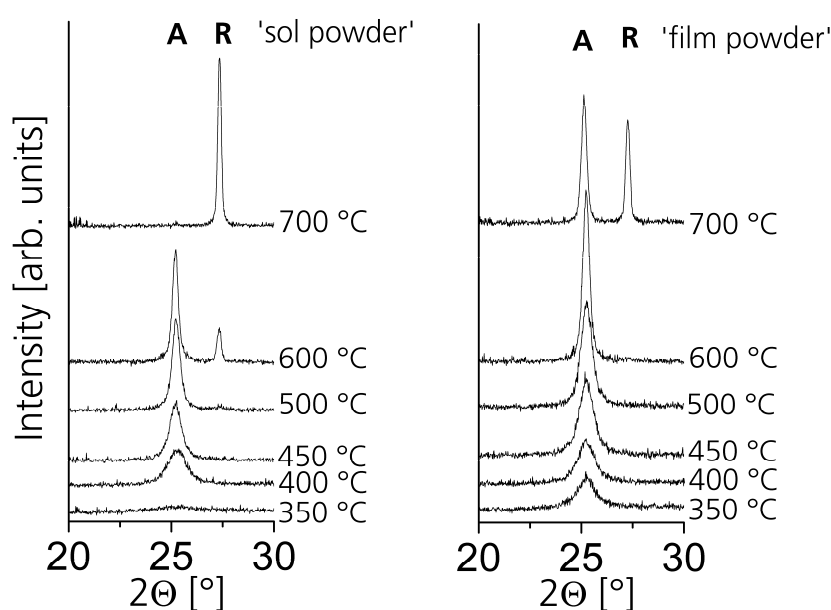


Figure 22. X-ray diffraction pattern of sol powders and film powders prepared from purely ethanol based sols. The samples were annealed at temperatures between 350 °C and 700 °C as indicated. Peaks assigned to anatase (A) and rutile (R) are marked individually.

After annealing at 400 °C, skeletal densities around 3.5 g/cm³ are measured for the inorganic backbone of both samples regardless of their initial properties. Nevertheless the sol powder goes through a better skeletal densification at higher temperatures. This hindered skeletal densification of the film powders is accompanied by the phase evolution of the respective powders: When compared to the sol powders (Figure 22), a delayed formation of rutile is observed.

Now the question comes up if this residue carbon is also responsible for the observed differences concerning the skeletal densification above 300 °C and phase evolution as it was seen in the case of the sol powder in Paragraph 5.2.2. The visually appearance of the film powders compared to the sol-powder is indicating a similar behavior: film powders present at all temperatures more or less a grayish color, whereas the sol powders were nearly colorless at temperatures ≥ 450 °C. Comparing the carbon content of sol powder and the respective film powder a corresponding development is observed (Figure 23). The carbon content in film powder is significantly higher than in the complementary sol powder even at 700 °C.

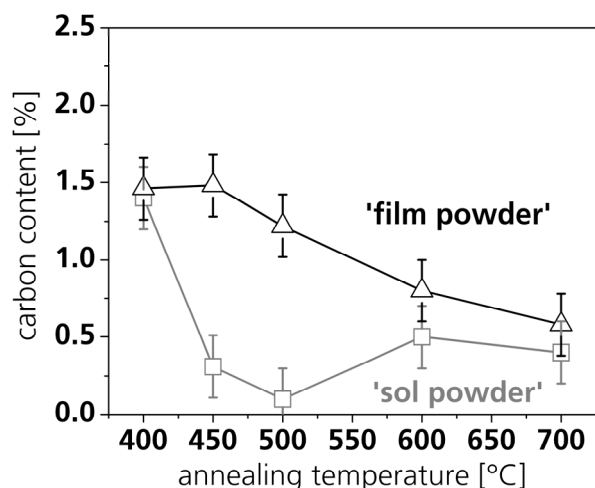


Figure 23. Carbon content of sol powders (\square) and film powders (\triangle) prepared from pure ethanol based sols as a function of annealing temperature.

When the phase transformation is affected by an additional phase, often the crystallite growth is also influenced [OKA01,TAK00,LIU05,ZHU05]. For that reason in Figure 24 the crystallite size and microstrains as a function of annealing temperature are displayed. For the film powders the anatase crystallite size increase continuously from 4 nm (350 °C) up to 85 nm (700 °C), whereas the sol powder presents at intermediate temperatures (450 – 500 °C) a high increase in crystallite size compared to the corresponding film powder. Even the crystallite size of rutile reached at 700 °C is significantly lower for the film powder (202 nm) compared to the sol powder (350 nm). The impurities of carbon in the film powders seem to slow down the crystallite growth of the film powders.

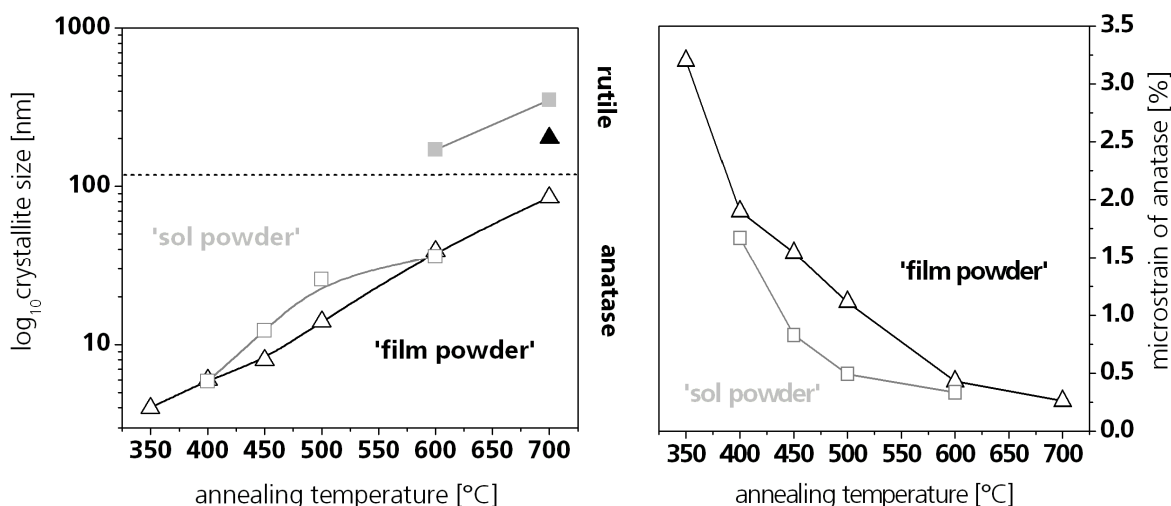


Figure 24. Crystallite size (left) and microstrain of sol powders (\square) and film powders (\triangle) prepared from pure ethanol based sols as a function of annealing temperature.

The microstrain of the anatase crystallites is displayed in Figure 24 (right). Generally, microstrain arises from imperfections (i.e. dislocations, vacancies, interstitials, substitutionals) in the crystal lattice and results in variation of the lattice spacing leading to increased line broadening. With the crystallization onset of anatase, both samples exhibit a high degree of microstrain. For film

powders, the microstrain decreases continuously upon annealing to 700 °C. However, the microstrain of the sol powders diminishes more rapidly from 400 to 500 °C.

The degree of microstrain in the anatase crystallites seems to depend on the carbon content in the powders. When assumed that the incorporated carbon substitutes some of the lattice oxygen atoms, the formed Ti-C bond [LI05] is shorter than a Ti-O bond. This should lead then to a distortion of lattice spacings around the substitutionals. Although, it can not be clarified whether the microstrain arises from inclusion of elementary carbon or other carbonate species. Nevertheless always when the crystal lattice of anatase is disturbed this results in a high degree of microstrain and this deformation energy must be released for crystallite growth and phase transformation to occur [HUN04,ROD97].

To explain the reduced skeletal density additional factors must be considered, because at a calcinations temperature of 600 °C, the carbon content decreases, but the skeletal density remains nearly constant. IR spectra measured from the film powders (Figure 25) surprisingly indicate the presence of gaseous CO₂ in samples sintered between 350 °C and 600 °C. Such results were never obtained for any precursor or sol powders, artifacts from faulty baseline corrections (atmospheric CO₂ in beamline of spectrometer) were ruled out. [BOC06]

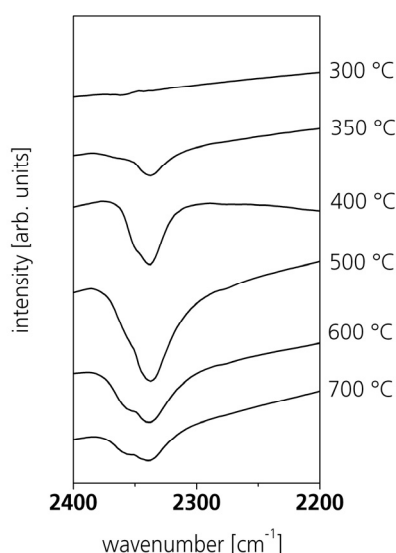


Figure 25. IR spectra of film powders that had been isothermally annealed for 1 hour at the temperatures indicated. (Data taken from [BOC06])

In order to explain the appearance of closed pores, one has to consider that due to the high surface-to-volume ratio of the drying films the densification of the material is much faster than the densification of sol powders prepared by rotational evaporation. Therefore, it is much more likely that some organics are trapped in the rapidly shrinking film. Upon annealing some CO₂ as product of the thermal decomposition above 300 °C [KRU05] may be trapped (in closed porosity) [COL92] within the film and is gradually removed during sintering above 500 °C. To support this assumption some more microstructural information of the different materials are required. [BOC06]

N_2 -sorption experiments on isothermally annealed film powders were performed and compared with the corresponding sol powders. Regardless of the annealing temperature, the scraped off and sintered films have a much denser microstructure than the comparable sol powder. Only the sample annealed at 300 °C exhibits a Type-I isotherm (Figure 26 (right)) that results from micropores with a pore diameter below 2 nm (Figure 27 (right)). At higher calcination temperatures the N_2 -sorption experiments do not indicate open porosity. Because closed pores, which contain gaseous CO_2 cannot be accessed by N_2 molecules, they will not be detected.

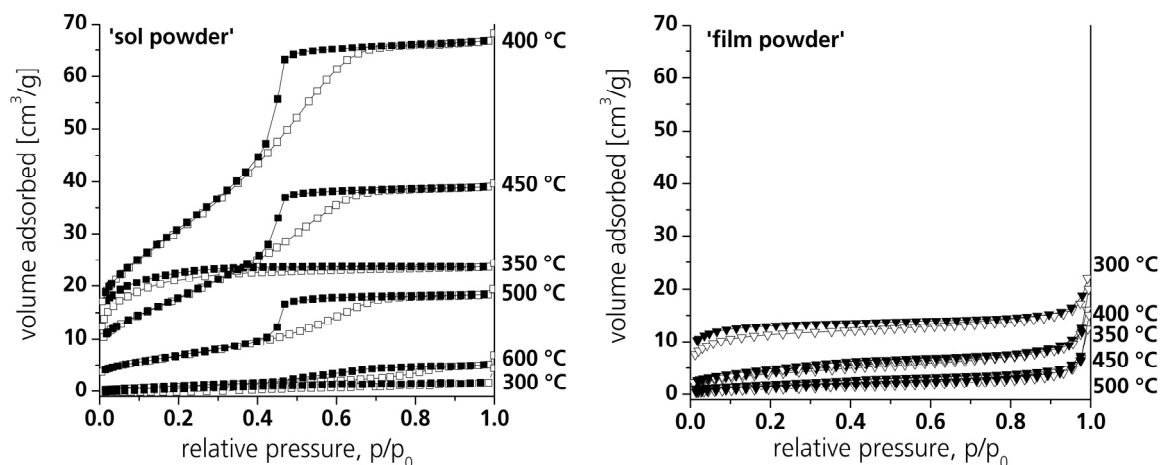


Figure 26. N_2 -adsorption isotherms for sol powders (left) and film powders (right) obtained from purely ethanol based solutions that had been isothermally annealed for 1 hour at the temperatures indicated. (Data taken from [BOC06])

Sol powders annealed at 350 °C also result in Type-I isotherm (Figure 26 (left)) with an average pore diameter below 1 nm (Figure 27 (left)). Upon annealing at 400 °C the pores transform to larger mesopores with a medium pore diameter of 4 nm and a typical Type-IV isotherm. Similar formations of pore systems due to the removal of organic residues have been reported for xerogels [LOE96] and sol-gel derived fibers [KRU02]. Upon further annealing, the volume of these pores is significantly reduced and the sol powders have lost their porosity accessible to N_2 -sorption experiments above 500 °C.

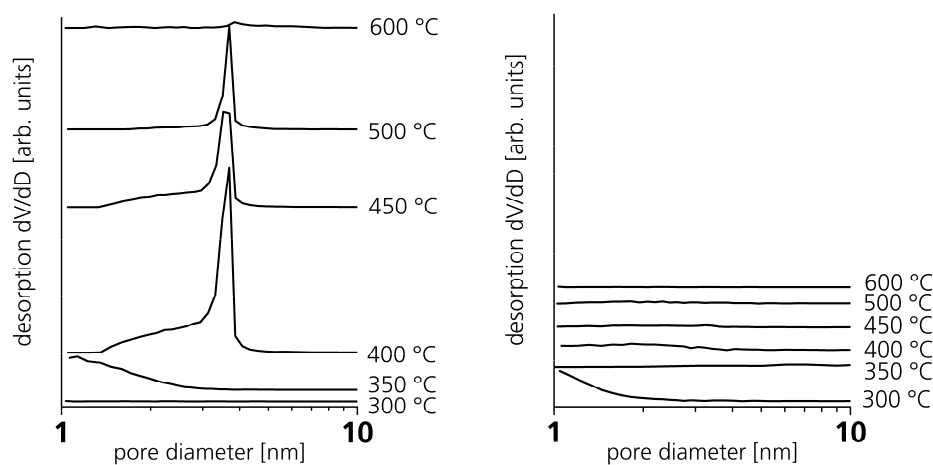


Figure 27. Pore diameter as function of dV/dD [$cm^3g^{-1}nm^{-1}$] for sol powders (left) and film powders (right) obtained from purely ethanol based solutions that had been isothermally annealed for 1 hour at the temperatures indicated.

5.2.3.2 CHANGES INDUCED BY 1,5-PENTANEDIOL

In the following chapter is reported, how these features of the film powders and thus the dip-coated films on glass are changed by the presence of 1,5-pentanediol. In Figure 28 thermogravimetric analysis and differential thermal analysis of different film powders are summarized. Samples prepared from coating solutions that contained 1,5-pentanediol undergo a stronger mass loss than the film powder isolated from the purely ethanol based system, but the overall oxide yield is about 50 % for both samples regardless of the diol concentration in the initial sol.

As already shown in Figure 20, the differential thermal analysis of film powders obtained from the coating solution based on pure ethanol presents the exothermal decomposition pattern typical for acetylacetonate groups between 200 °C and 400 °C followed by a very weak signal which was assigned to residual -OEt moieties (Figure 28 (right)). When the sols contain 1,5-pentanediol, this component is expected to be enriched during solvent evaporation and film drying due to its lower volatility. The first DTA decomposition peak (Figure 28 (right)) between 200 °C and 400 °C is significantly altered when the sols contained 10 % 1,5-pentanediol and consists of one sharp exothermal signal at 290 °C for higher contents of the diol (80:20). When the respective sol powder was measured (Figure 28 (right)), this peak was partially superimposed by the endothermic evaporation of the diol. From the absence of this evaporation process during the DTA analysis of film powders (Figure 28 (right)) can be concluded that 1,5-pentanediol is covalently linked to the film material. If the diol (b.p. 1,5-pentanediol = 242 °C) is in equilibrium with acetylacetonate groups (b.p. AcAcH = 139 °C) during film drying, it is reasonable to assume that preferably the more volatile component will evaporate.

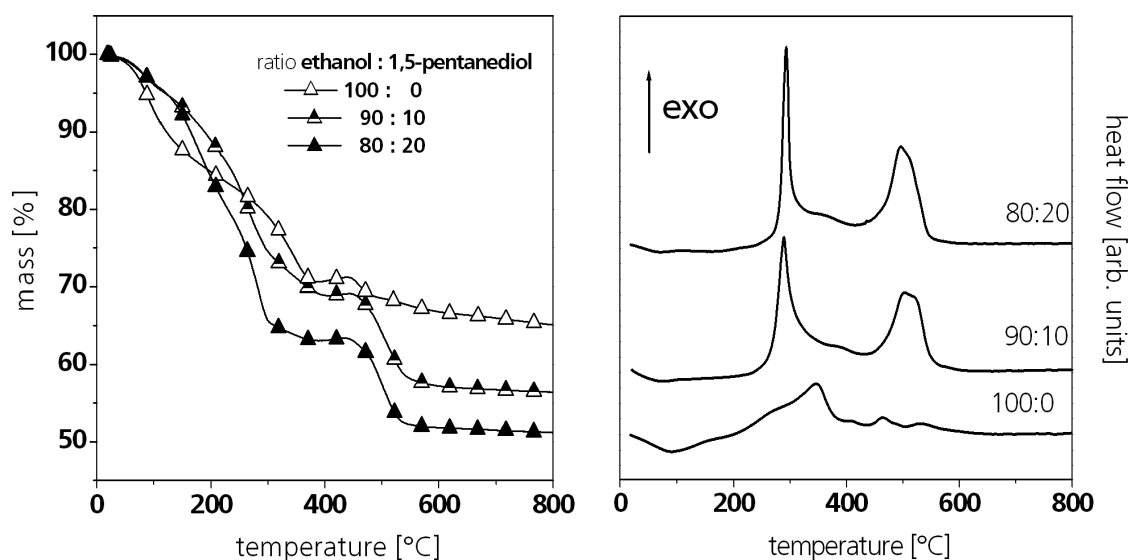


Figure 28. Thermogravimetric analysis (left) and differential thermal analysis (right) of film powder prepared from coating solutions that contained 0 %, 10 % and 20 % 1,5-pentanediol. All experiments were performed under dry air atmosphere with a heating rate of 10K/min. (Data taken from [BOC06])

These chemical modifications also have an influence on the decomposition pattern at higher temperatures (Figure 28): In contrast to material from purely ethanol based sols the film powders prepared in the presence of the diol exhibit distinct exothermal signals above 500 °C,

which were assigned to alkoxy groups for sol powders (Paragraph 5.2.2, Figure 14). Only based on Figure 28 it cannot be decided, though, whether these peaks originate from 1-5 pentanediolate groups in a different chemical environment as those decomposed around 300 °C or if the diol has a protective function for -OEt moieties during drying of the film. [BOC06]

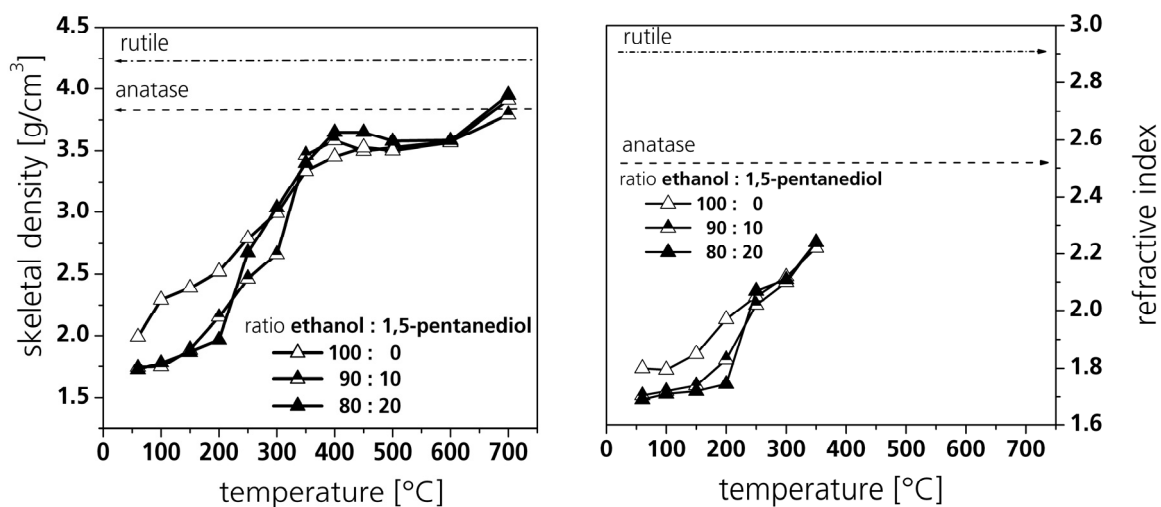


Figure 29. Skeletal densities (left) (Data taken from [BOC06]) and refractive index (right) of film powder prepared from sols containing 0 % (Δ), 10 % (\blacktriangle) and 20 % (\blacktriangle) 1,5-pentanediol as a function of annealing temperature. The theoretical densities and refractive index of anatase and rutile are given as references.

As already shown in Figure 21, film powders generally exhibit higher initial skeletal densities (Figure 29 (left)) after drying than the respective sol-powders (Paragraph 3.2.2, Figure 15). Nevertheless up to 250 °C film powders prepared from sols containing 1,5-pentanediol show significantly lower skeletal densities than the respective material from purely ethanol-based sols (Figure 29 (left)). This can be directly attributed to the higher content of organics due to presence of the diol. [BOC06]

The refractive index up to 350 °C (Figure 29 (right)) behaves analogous. According to the explanation given in Paragraph 5.2.3.1, the refractive index of film powders is also linked to the content of organics. The incorporation of 1,5-pentanediol by itself reduces the overall refractive index because of its low refractive index (1.45). Additionally without the addition of 1,5-pentanediol, the xerogel can undergo more hydrolysis and condensation reactions. This leads to a higher content of Ti-O-Ti metal-oxide bondings, that results in a higher refractive index and preserves some network plasticity.

At annealing temperatures above 350 °C no significant differences between the skeletal densities of the film powder were measured. However the theoretical density of anatase is never reached below 700 °C. As already mentioned in section 5.2.3.1, closed pores that contain gaseous CO₂ from the decomposition of organic residues are partly responsible for the low backbone density of the film powders.

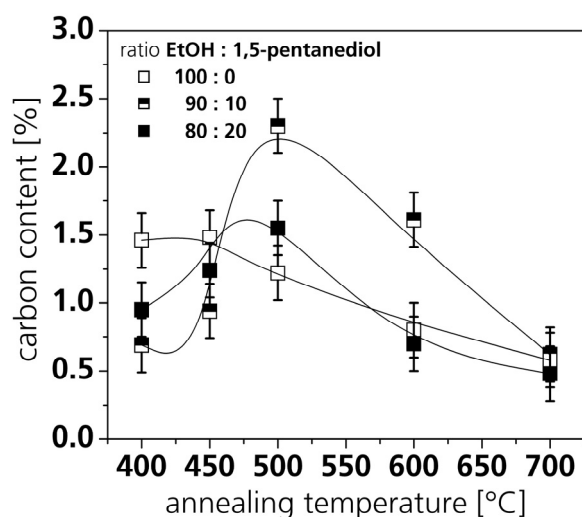


Figure 30. Carbon content of film powders, prepared from sols containing 0 % (□), 10 % (◐) and 20 % (■) 1,5-pentanediol as a function of annealing temperature.

Furthermore the inclusion of carbon due to an incomplete thermal decomposition of organic moieties can reduce the skeletal densities of the powders as seen in Paragraph 5.2.2. Below 700 °C all film powders show a grayish color, indicating an incorporation of carbon due to an incomplete decomposition of organic moieties. Therefore, the carbon content in the samples was determined as function of the annealing temperature (Figure 30).

The carbon content for all film powders decreases up to ~ 0.5 % at 700 °C. Samples prepared from the pure ethanol based coating solution exhibit a continuous decrease in their carbon content. As it has been already noticed for the sol powders (Paragraph 5.2.2, Figure 16), a maximum in the carbon content appears at an annealing temperature of 500 °C when 1,5-pentanediol containing sols were used. Thereby comparing the film powders, the addition of 10 % 1,5-pentanediol induces a slightly increased content of carbon at 500 – 600 °C.

All film-powders show a microstructure not accessible to N₂-sorption experiments (data not shown). This has been already exemplary shown for the film powder (100:0) prepared from a pure ethanol based sol (Figure 26 and 27).

Apparently, as been seen for the sol powders the high densification rate leads to a densification of the material before the oxidative decomposition of residue organics is finished. This results in partly reductive conditions and the formation of elementary carbon. At higher temperatures than 500 °C this still leads to inclusion of residue carbon. However the oxidation reactions of carbon residues and sintering processes are also increasing with annealing temperature. Therefore carbon impurities can be degraded by relieve of gaseous CO and CO₂. However, as it has been noted before (Paragraph 5.2.2), based on this data it can not be clearly distinguished, which sort of carbon (i.e. elementary carbon, organic carbon, gaseous carbonoxides, etc.) is responsible for this intermediate increase.

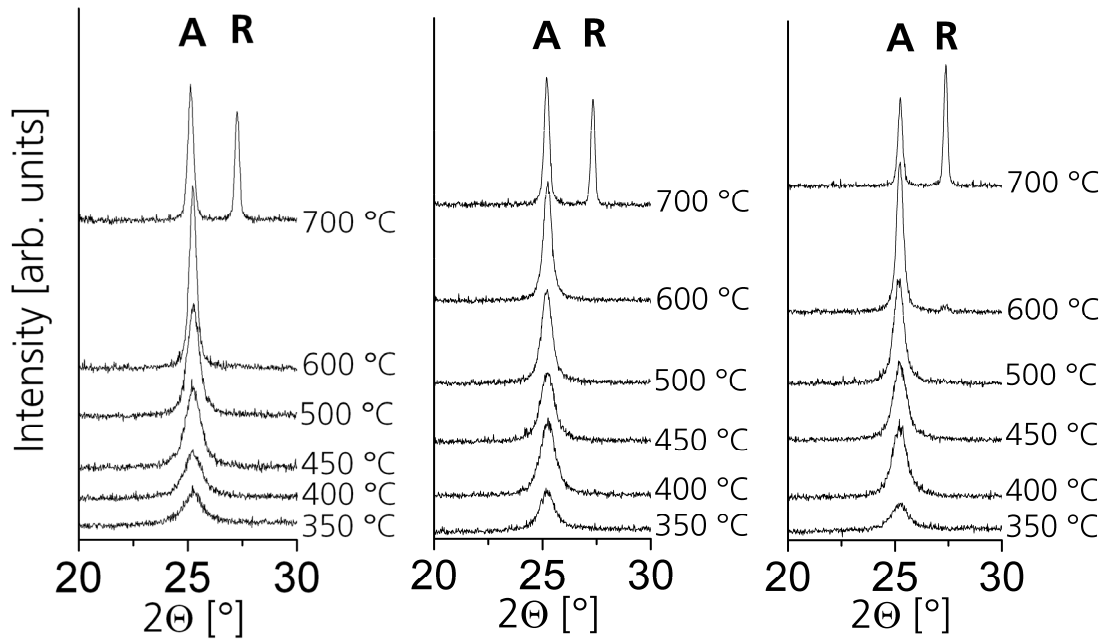


Figure 31. X-ray diffraction pattern of film powders prepared from sols containing 0 % (left), 10 % (middle) and 20 % 1,5-pentenediol respectively. The samples were annealed at temperatures between 350 °C and 700 °C as indicated at the right side of the Figure. Peaks assigned to anatase (A) and rutile (R) are marked individually.

Regarding the evolution and transformation of the anatase phase all film powders exhibit nearly a similar behavior. At 350 °C all film powders started the formation of anatase (Figure 31), but their further phase transformation of anatase to rutile is significantly retarded compared to sol powders (Figure 17). The presence of carbon impurities delay the formation of rutile as already demonstrated for the sol powders and the film powder (100:0) as well.

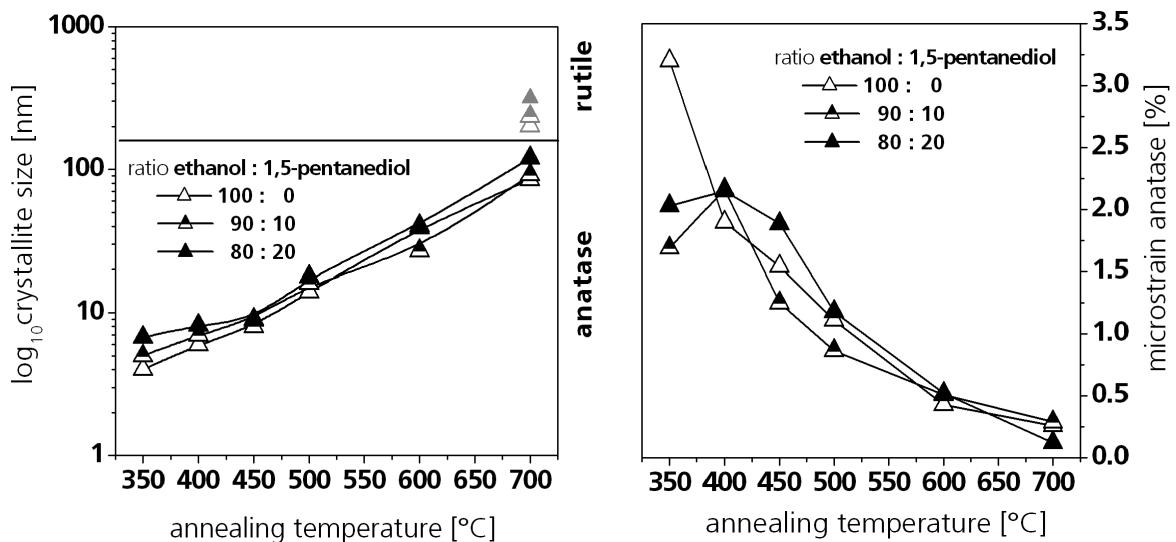


Figure 32. Crystallite size (left) and microstrain (right) of film powders as a function of annealing temperature prepared from sols containing 0 % (Δ), 10 % (\blacktriangle) and 20 % (\blacktriangle) 1,5-pentenediol.

Furthermore, these impurities are also known to influence the whole process of crystallite growth (Paragraph 5.2.3.1). The anatase crystallite size (Figure 32 (left)) of the film powder increases continuously from 4-7 nm up to 80-120 nm by raising the calcinations temperature from 350 °C

to 700 °C. The decrease in microstrain (Figure 32, (right)) is also accompanied with increasing of crystallite size. Additionally, the lattice parameters of the anatase crystallites are displayed in Figure 33. Whereas the lattice parameter *a* exhibits no change over the whole temperature regime, the lattice parameter *c* nearly continuously converge to the theoretical value by raising the annealing temperature. Similar behavior has been reported for dopants like Si⁴⁺, Al³⁺ and Nd³⁺, too [OKA01,YAN97,BUR04,HUA06].

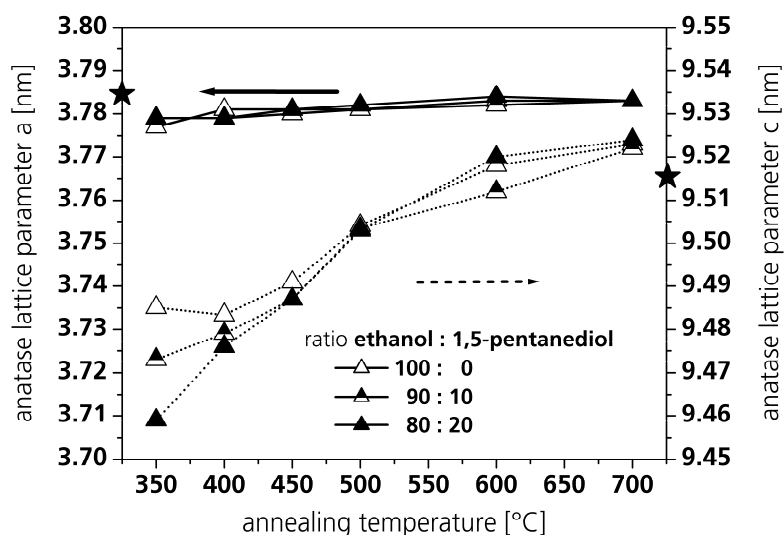


Figure 33. Anatase lattice parameters *a* and *c* of “film powders” as a function of annealing temperature prepared from sols containing 0 % (△), 10 % (▲) and 20 % (▲) 1,5-pentanediol. The literature lattice parameters are individually marked (★) on the axes [HOR72].

In general, no significant differences regarding phase transformation, crystallite size, microstrain and lattice parameters were noticeable between the different sorts of film powders. As mentioned before, the inclusion of carbon seems to be responsible for the retarded phase transformation from anatase to rutile and the observed microstrain. Since the lattice parameter *c* is also significantly reduced at temperatures below 600 °C and the Ti-C bond length is smaller than the Ti-O bond length it is presumed that part of the carbon substitutes some of the lattice oxygen atoms. Furthermore it has to be noticed, that the carbon impurities affect only the length of the lattice parameter *c*. This suggests that substitution of O by C reduces the distortion of the octahedral angle, which preferentially should decrease the lattice parameter *c* of the anatase structure [LAN06].

SUMMARY OF 5.2.3 “DENSIFICATION OF THIN SCRAPED OFF FILMS”

In conclusion, drying as a thin film results in the formation of closed pores and a much denser microstructure than the respective sol powder.

Without the addition of 1,5-pentanediol, the high surface-to-volume ratio and air moisture during the thin film formation leads to an separation of -OEt moieties by hydrolysis. The following condensation reactions cause the formation of a rigid network. The presence of 1,5-pentanediol during thin film drying and aging retards this hydrolysis and condensation reactions preserving some network plasticity.

Above an annealing temperature of 300 °C no significant differences in the microstructure of the different film powders were recognized. Depending on the annealing temperature, film powders contain residues of carbon due to their dense microstructure. These inclusions of carbon suppress the crystallite growth and therefore enhance the phase transition temperature of anatase to rutile.

5.2.4 MICROSTRUCTURE OF THIN FILMS

5.2.4.1 CONSTRAINT OF SHRINKAGE BY THE SUBSTRATE: GENERAL CONSEQUENCE

Thin films prepared with amorphous sol-gel precursors, mostly possess a high scratch resistance, i.e. their pencil hardness is ~5H at annealing temperatures above 250 °C [MAL07]. Since this high scratch resistance, most of the analyzed thin films could not be scraped off the glass substrate at all. Therefore to obtain sufficient material for microstructural investigations, so called film powders were introduced (Paragraph 5.2.3).

However, the question remains to what extent the microstructure of film powders is related to real thin films. In detail, what is the difference between a thin sol-gel film that is once annealed as scraped off film powder and once annealed in direct contact to the glass substrate. Generally during annealing, the film powder can undergo shrinkage in all three dimensions whereas the film itself mainly can only shrink unilaterally. This matter will be discussed by the comparison of thin film and film powder using the 100:0 system.

A method, which can be easily applied to both, film powders and films, is the IR spectroscopy. Using the IR spectroscopy the thermal degradation behavior of both materials can be monitored. Therefore film powders are prepared as KBr pellets whereas thin films are deposited on polished alumina or Si-wafer as substrate and measured in reflection geometry. The IR-spectra of the film powders and the corresponding thin films as a function of annealing temperature are displayed in Figure 34.

At an annealing temperature of 100 °C between both sorts of xerogels no significant differences in the spectra are noticeable. A broad IR band at 3600 – 3000 cm^{-1} belongs to the hydroxyl groups confirming the hydrolysis of the alkoxide groups. The peaks at 2923 cm^{-1} , 2860 cm^{-1} and 794 cm^{-1} are attributed to the C-H vibrations. In the spectra at ~1640 cm^{-1} a shoulder is visible which is characteristic for the bending vibration of H_2O . The vibrations at 1578, 1534, 1430 and 1029 cm^{-1} correspond to the conjugated C-O vibrations [C=C-(C=O) and C=C-(C-O)-] of the acetylacetonate ligand. Regarding the peak at 1358 cm^{-1} , which belongs to the CH_3 umbrella, it can not be determined whether it is originated from the acetylacetonate or the -OEt group. However the vibrations at 1288 and 1123 cm^{-1} clearly correspond to the -OEt group. Finally the absorption band at 661 cm^{-1} represents the Ti-O vibration. [JUN99, KRU05, RYU99, DJA02b]

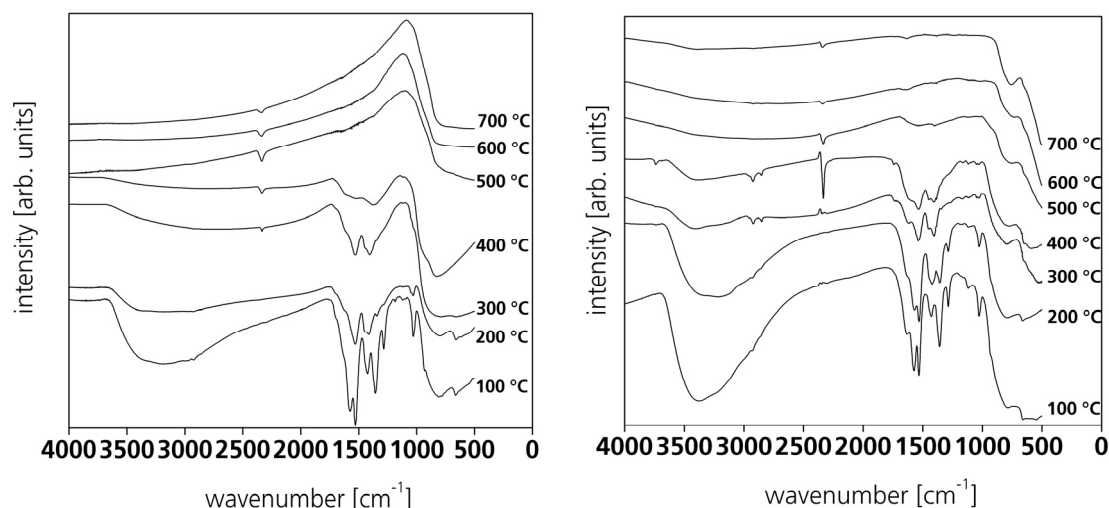


Figure 34. IR spectra of film powders (left) and films (right) prepared from 100:0 ethanol based sols as a function of annealing temperature. The film powder samples were isothermally annealed for 1 h, whereas films samples were isothermally annealed for 10 min at the respective temperatures.

In general with increasing annealing temperature a decrease in peak intensity and a broadening of the bands is presented, which can be attributed to decomposition reactions of organic moieties [KED94]. Film powders and films present at annealing temperatures ≥ 300 °C the arising of an additional peak at 2334 cm^{-1} . As already mentioned before (Paragraph 5.2.3.1) this can be explained by the incorporation of gaseous decomposition products as CO_2 in closed pores. However the film at 400 °C presents a significant stronger CO_2 peak.

Furthermore it seems that with increasing temperature the peaks of the film powders disappear at lower annealing temperatures than the corresponding peaks from the films. This indicates that at an equal annealing temperature, the decomposition reactions of the organic moieties of the film powders are in further advance compared to the respective films. This can be explained with the differently used dwell times: thin films were annealed for 10 min and film powders for 60 min. But beside this observed thermal offset, the degradation behavior of the film powders seems quite similar to the respective films.

A further method, which enables to directly investigate the microstructure of thin films, is the ellipsometric porosimetry (EP) [GRO06]. The EP is a sort of adsorption porosimetry comparable to N_2 sorption on powders. Thereby the change of the refractive index by simultaneous sorption of a measurement gas in the pores is detected. More detailed information about EP is given by Mogilnikov et. al. and Grill et al. [MOG02,GRI03]. To achieve measurements in a sufficient high resolution, thin films were prepared on Si-wafers.

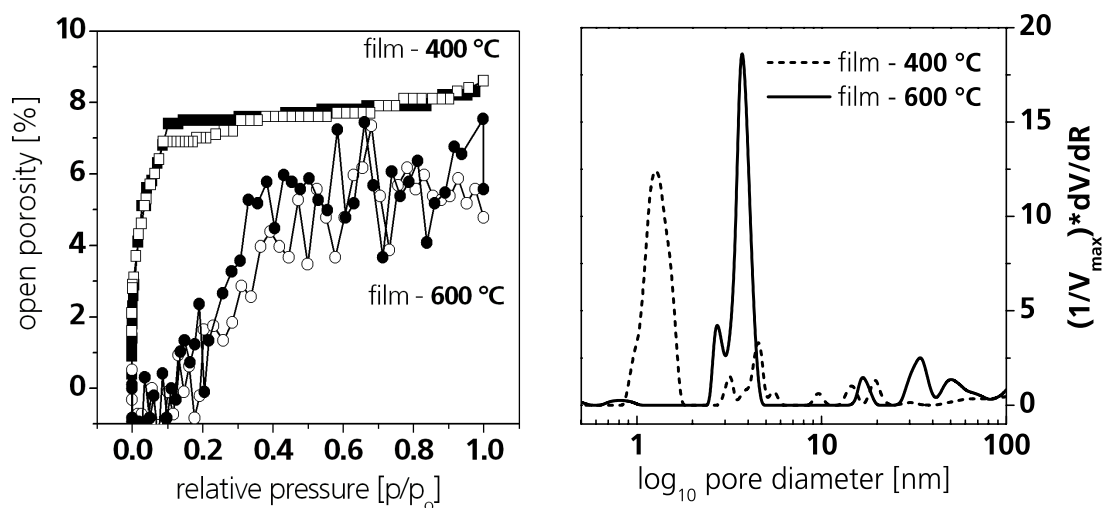


Figure 35. Ellipsometric porosimetry isotherms (left) and desorptive pore diameter (right) of thin films that had been prepared from purely ethanol based coating solutions and afterwards isothermally annealed for 10 min at the temperatures indicated.

Figure 35 shows adsorption/desorption isotherms (left) and pore size distribution (right) during the toluene adsorption and desorption. A film annealed at 400 °C results in a Type I isotherm generated by micropores with a medium pore diameter of ~1.3 nm. Upon annealing to 600 °C these pores have been transformed to larger mesopores (Type IV isotherm) with a medium pore diameter ~3.7 nm. The amount of measured open porosity is in principle very low and slightly decreases during annealing from ~8 % (400 °C) to ~6 % (600 °C) (Figure 35 (left) and Table 5). Generally this behavior is typical for sol-gel materials and has been seen before (i.e. Paragraph 5.2.3.1).

When it is supposed that the thin films consist of pure anatase the overall porosity can be calculated by the Lorenz-Lorentz equation [CHR98, LAU96]. The relative volume of closed pores is calculated by comparing the EP results obtained with empty and filled pores (Table 5). The overall porosity for both temperatures is nearly equal (15-16 %) and is significantly higher than the open porosity. So additionally in all films a significant number of closed pores (7-10 %) exist, that slightly increase up to 600 °C. These results confirm the former IR investigations on thin films (Figure 34 (right)), which pointed out the presence of closed pores as well.

Table 5. Porosities of films that had been prepared on Si-wafer from purely ethanol based coating solutions and afterwards isothermally annealed for 10 min at 400 °C and 600 °C. The refractive index and open porosity were measured by ellipsometric porosimetry. The overall porosities were calculated by using the theoretical refractive index of anatase [CHR98].

	refractive index (empty pores)	overall porosity [%]	open porosity [%]	closed porosity [%]
400 °C	2.134 ± 0.005	15.6 ± 0.3	8.0 ± 0.5	7.6 ± 0.8
600 °C	2.129 ± 0.005	15.7 ± 0.3	6.0 ± 1.0	9.7 ± 1.3

In the case of the film powders the existence of closed pores was supposed, too (Paragraph 5.2.3). There the closed pores turned out to be mostly responsible for their reduced skeletal density. With the assumption that the skeleton consists of pure anatase and the reduction of the

skeletal density is only attributed to the closed pores, an overall porosity for the film powders can be calculated. In combination with the pore volume obtained from the N₂-sorption experiments the amount of open and closed porosity is given (Table 6). However, a quantitative comparison is quite arbitrary, because of the unconsidered influence of the incorporated carbon and the different used dwell times for films and film powders. Nevertheless, beside the lower overall and open porosity of the film powders compared to the films, the quantity of closed pores is in the same order of magnitude.

Table 6. Comparison of porosities for film powder that had been prepared from purely ethanol based coating solutions and afterwards isothermally annealed for 60 min at 400 and 600 °C.

	skeletal density [g/cm ³]	overall porosity [%]	open porosity [%]	closed porosity [%]
400 °C	3.46 ± 0.02	14.4 ± 1.5	4.5 ± 1.0	9.9 ± 0.5
600 °C	3.56 ± 0.02	9.9 ± 1.5	2.6 ± 1.0	7.3 ± 0.5

Finally the phase evolution and crystallization behavior of film powders and films were investigated. Since the distinctive influence of the dwell time on the crystallization behavior is known [MEH97], the investigations of film powders and films were performed on samples which were prepared by using an equal dwell time (60 min). At a temperature of 350 °C the corresponding X-ray diffraction patterns are displayed in Figure 36. The film powders already present reflections for anatase, whereas the films start the building of anatase just at 400 °C. Furthermore, at an annealing temperature of 700 °C the film powders partly transform to rutile, whereas thin films never exhibit any reflections of rutile.

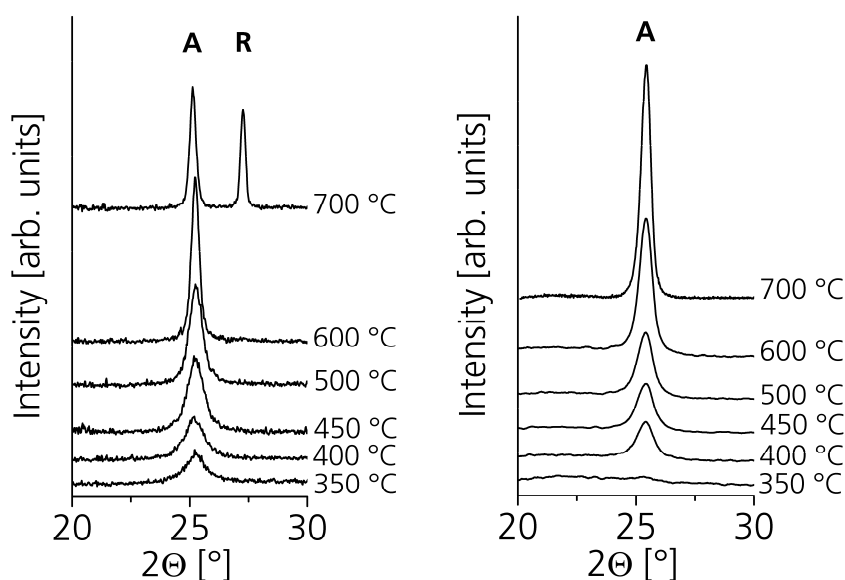


Figure 36. X-ray diffraction pattern of film powder (left) and film (right) prepared from 100:0 ethanol based sols. The samples were isothermally annealed for 1 h at temperatures between 350 °C and 700 °C as indicated at the right side of the Figure. Peaks assigned to anatase (A) and rutile (R) are marked individually.

The crystallite size of the film-powders and films as function of the annealing temperature is displayed in Figure 37. The anatase crystallites of the film powders increase in size from 4 nm (350 °C) up to 85 nm (600 °C) and finally partly transform to rutile crystallites with a size of

~200 nm. The films present a smoother increase in the anatase crystallite size from 10 nm up to 67 nm. This implies that below 500 °C the crystallites of the films are larger than the film powder and in reverse order above 500 °C. A similar behavior has also been reported in a comparable case in the literature [FAN02]. As already seen in Paragraph 5.2.3.1, a hindered phase transformation is often associated with a smaller anatase crystallite size [HIR05].

In the case of the sol and film powders the hindered phase transformation was linked to a clear degree of microstrain in the crystallites caused by carbon impurities. Unfortunately the GIXRD – patterns of thin films were recorded in glancing incidence geometry, which affects the deflection conditions. This lead to different peak intensities and a shift of peak positions compared to normal XRD – pattern recorded in $\Theta/2\Theta$ geometry [PIT96]. A measurement of thin films in $\Theta/2\Theta$ geometry is not possible in a sufficient resolution. Therefore an evaluation of microstrain from GIXRD – patterns by Rietveld analysis is barely possible.

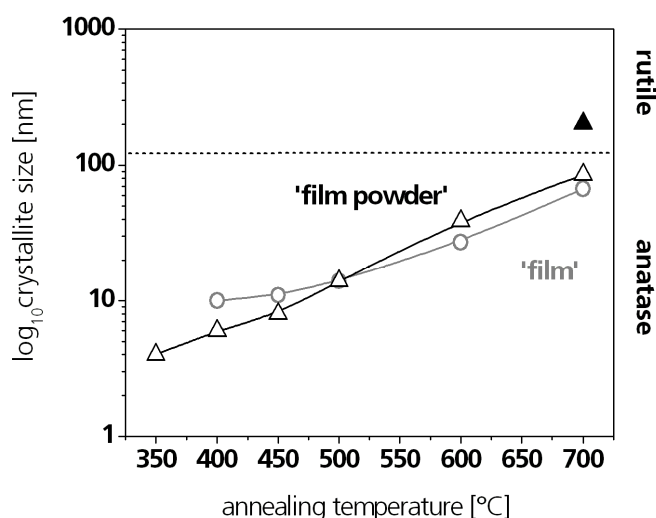


Figure 37. Crystallite size of film powders (Δ) and films (\circ), as a function of annealing temperature, prepared from purely ethanol based sols.

Furthermore microstrain can be obtained from XRD patterns by a numerical evaluation of the integral breath, i. e. by the Halder Wagner plot [MEH97,RUP06,XU04,AQU66]. However in this case the glancing incidence geometry, the overlapping of reflections, the hexagonal anatase geometry and the available reflection of anatase make a usable numerical evaluation of microstrain in thin anatase films almost impossible.

Nevertheless the results concerning the phase evolution can be interpreted as follows. When the phase formation of the sol powder and film powder (Paragraph 5.2.3.1) was inspected, the observed differences were mainly explained by carbon impurities causing microstrain. Carbon impurities can hinder the phase transformation of anatase to rutile (Paragraph 5.2.2). Even when a microstrain measurement on thin films is not possible, for the here observed differences concerning the phase formation of films and film powders (Figure 36 and 37) this explanation is not favored, because: (1) the equal chemical composition should ensure a similar decomposition behavior, leading to a similar content of residual carbon, (2) usually for films treated at 600 °C and 700 °C no elementary carbon is observed (3) their porosity is comparable.

Beside the influence of impurities on the phase transformation also tensile stress, that is effective in the case of thin films under constraint by the substrate can influence phase transformation. The phase transformation of anatase to rutile is accompanied with a decrease of specific volume (~9 %) and therefore additional shrinkage, which is hindered by tensile forces [POP05, LIU05].

5.2.4.2 CHANGES INDUCED BY THE SOLVENT COMPOSITION

Different solvents and solvent mixtures can be used to prepare coating solutions from the amorphous TiO_2 powder. The dynamic viscosity of TiO_2 sols with identical oxide yield (6 %) increases as the amount of 1,5-pentanediol in the solvent rises (Table 7). The film thickness can significantly influence the microstructure of thin films [SCH06b]. For that reason conditions have to be chosen that result in films with identical final thickness. The final film thickness after treatment at 600 °C for different sols is given in Figure 38 as a function of withdrawal rate. Unless otherwise noted the subsequent experiments were performed at a relative humidity of 20 % (24 °C).

Table 7. Dynamic viscosity [mPas] of sols prepared from soluble TiO_2 precursor powder containing 0 %, 10 %, 20 % 1,5-pentanediol respectively.

	ratio ethanol :1,5-pentanediol		
	100:0	90:10	80:20
dynamic viscosity [mPas]	1.6 ± 0.1	2.3 ± 0.1	3.1 ± 0.1

The data basically follow hyperbolic contours consistent with the Landau-Levich theory for the formation of films by dip-coating [BRI90]. Using Figure 38 it is possible to adjust withdrawal rates to prepare single coatings with comparable thickness from different solutions. The effect of withdrawal rate and 1,5-pentanediol content on the film thickness after calcination at 600 °C (10 min) was investigated. The increasing withdrawal rate results in increasing film thickness, the trend is in conclusion with the Landau-Levich equation (Figure 38) [BRI90].

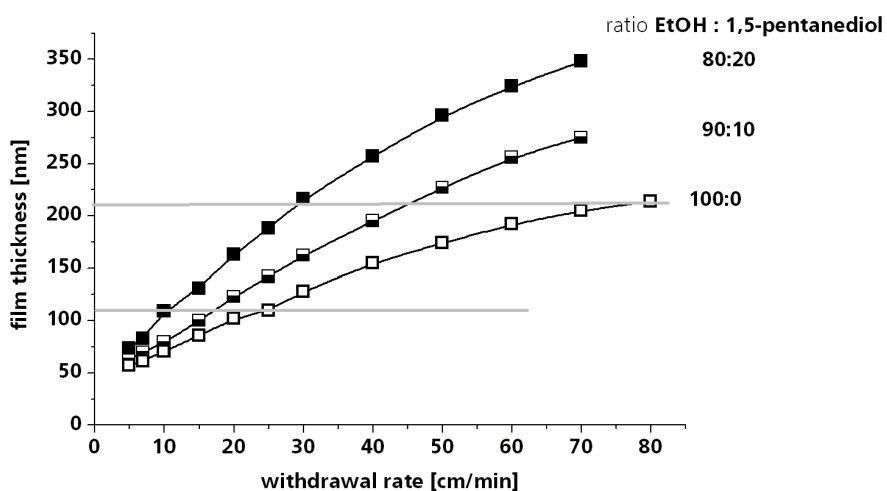


Figure 38. Thickness of TiO_2 films as a function of withdrawal rate. The samples were obtained from ethanol based coating solutions containing 0 % (\square), 10 % (\square) and 20 % (\blacksquare) 1,5-pentanediol. The withdrawal rates at the intersection of the grey lines with the experimental data were used to prepare films of 110 nm and 220 nm thickness from the different solutions respectively. (data taken from [BOC07a])

The addition of 1,5-pentanediol also of course influences the chemical composition of the sol-gel films. In the IR-spectra of thin films prepared with different content of 1,5-pentanediol and annealed at 100 °C for 10 min are presented in Figure 39. The bands of the O-H vibrations (3300 cm^{-1} , 1130 cm^{-1}), the C-H vibrations (2930 cm^{-1} , 2860 cm^{-1}) and C-O vibrations (1081 cm^{-1} , 1057 cm^{-1} , 1033 cm^{-1}) significantly increasing with increasing content of 1,5-pentanediol. They can be directly referred to the addition 1,5-pentanediol. Simultaneously the intensities of the bands corresponding to the acetylacetonate ligand (i.e. the conjugated C-O vibrations) are decreasing. This can be explained, because the ratio of AcAc/1,5-pentanediol is decreasing with increasing content of 1,5-pentanediol.

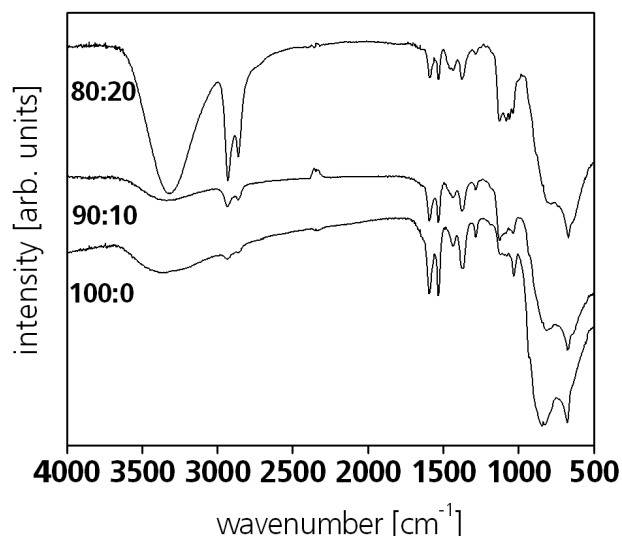


Figure 39. IR spectra of sol-gel films prepared from ethanol based coating solutions containing 0 %, 10 % and 20 % 1,5-pentanediol. The film samples were isothermally annealed for 10 min at 100 °C.

Of course the different content of 1,5-pentanediol influences the degradation behavior, as it has been already pointed out in Paragraph 5.2.3.2 by DTA/TG analysis of film powders (Figure 28). 1,5-pentanediol can partly coordinate to the titania atom and prevents hydrolysis and condensation reactions of the sol-gel material. This affects the content of organics and the skeletal densification of the sol-gel material.

The shrinkage (Figure 40) of the corresponding films behaves in agreement with these investigations. In order to compare samples that had undergone a comparable total densification, in initial experiments coating conditions (withdrawal rates) were determined that lead to films with similar film thickness after annealing at 600 °C. As one would expect the as-dried films from sols that contained only ethanol as solvent show the lowest thickness corresponding to the highest skeletal density of the respective film powder (Figure 29). Both coatings comprising 1,5-pentanediol show nearly similar densification as the data in Figure 40 would suggest.

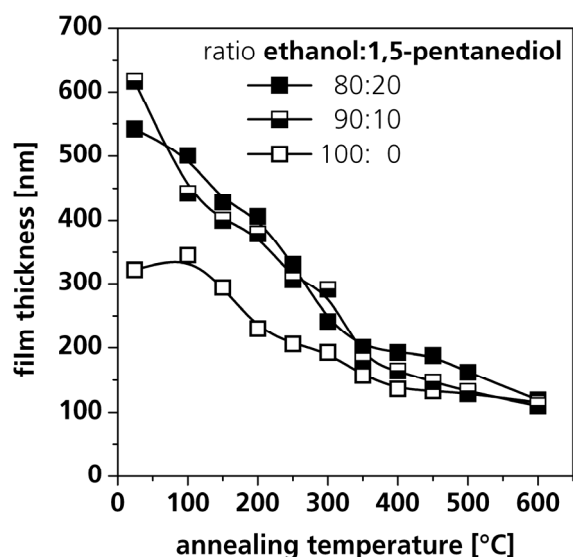


Figure 40. Film thickness of TiO_2 films as a function of annealing temperature. The films were obtained from ethanol based coating solutions containing 0 % (\square), 10 % (\square) and 20 % (\blacksquare) 1,5-pentanediol. The lines are drawn as guide to the eyes. (Data taken from [BOC07a])

The phase evolutions of the films differ not significantly (data not shown). However, except when a dwell of 10 min is used, the films prepared without the addition of 1,5-pentanediol start the formation of anatase already at an annealing temperature of 400 °C. Whereas films prepared with the addition of 1,5-pentanediol exhibit reflections for anatase first at 450 °C. When a dwell time of 60 min is used, no differences regarding the onset temperature are noticeable.

As seen before films prepared with the addition of 1,5-pentanediol have a higher content of organics. So it turns out that a dwell time of 10 min is apparently at 400 °C too short for the uptake of enough thermal energy to complete the decomposition reactions and form anatase crystallites.

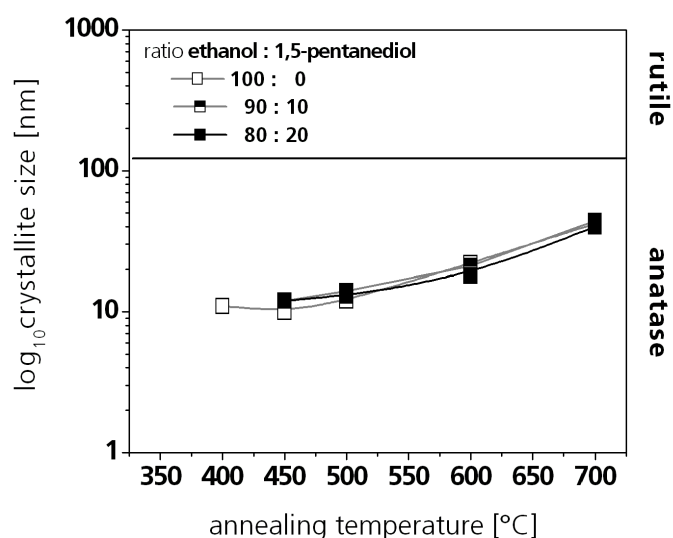


Figure 41. Crystallite size of TiO_2 films as a function of annealing temperature (annealing time 10 min). The films were obtained from ethanol based coating solutions containing 0 % (\square), 10 % (\square) and 20 % (\blacksquare) 1,5-pentanediol.

The evaluation of crystallite size of the films do not differ (Figure 41) despite different contents of 1,5-pentanediol in the starting xerogel films. When a dwell time of 10 min is used a growth in

crystallite size generally is noticeable from ~10 nm (400-450 °C) up to ~45 nm (700 °C). A similar behavior has already been noticed for the film powders. There the crystal growth also was unaffected by the precursor chemistry, too (see Paragraph 5.2.3.2).

In Figure 42 TEM images of films from sols based on pure ethanol as solvent and a mixture of 80 % ethanol and 20 % 1,5-pentanediol are shown, that were prepared with withdrawal rates of 40 cm/min and 10 cm/min, respectively. The two film thicknesses of 150 nm and 110 nm are in good agreement with the value anticipated and with independent measurements by UV-Vis spectrometry using the Swanepoel method [DIA04]. Generally both films exhibit a similar microstructure with a granular coating structure and no visible pores. The average crystallite sizes of 30 nm and 25 nm correspond with the analysis of X-ray diffraction experiments (Scherrer formula, data not shown). Neither bright- nor dark-field images show any microstructural differences between the films after annealing at 600 °C. Nevertheless in each film itself variations of the crystallite size occur.

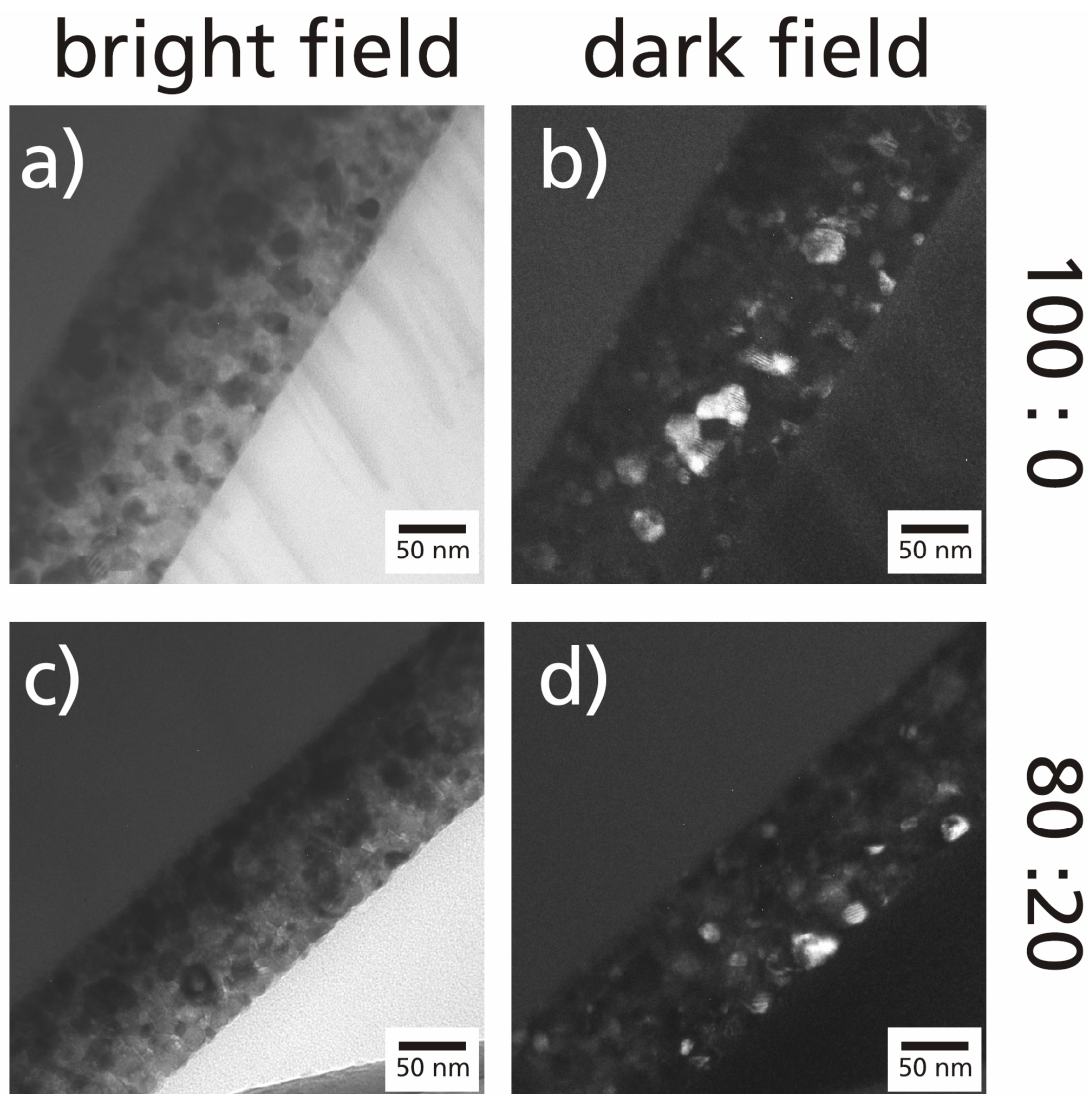


Figure 42. TEM bright field images (left column, a & c) and corresponding dark field images (right column, b & d) of TiO_2 films annealed at 600 °C. Images a & b were prepared from a coating solution based on pure ethanol (100:0), the solvent mixture for the images c & d contained 20 % 1,5-pentanediol (80:20). (Data taken from [BOC07a])

Additionally crystalline films were characterized by X-ray reflectometry (XRR) [AND04]. The measurement data and the fitted values are presented in Figure 43. Evaluation of the slope and frequency of the interference rings revealed a surface roughness of ~ 1.6 nm and a film thickness of ~ 110 nm for all three films. Additionally, film densities were obtained from the critical angle, the angle where the total reflection decreases.

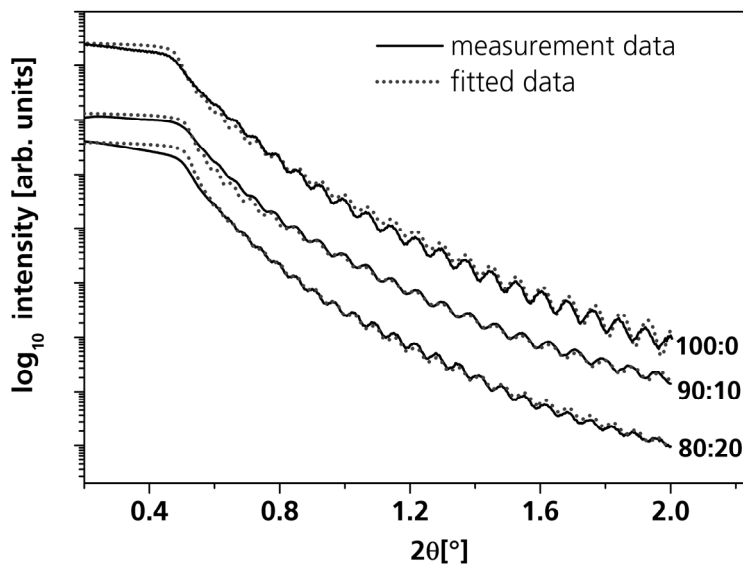


Figure 43. X-ray reflectometry data (black lines) and corresponding fitted value (grey dots) of TiO_2 films prepared from ethanol based coating solutions containing 0 %, 10 % and 20 % 1,5-pentanediol and annealed at 600 °C for 10 min.

With these “apparent” film densities, it is possible to estimate the total porosities (open + closed porosity) of the films, considering that our ceramic films consist of pure anatase with a density of 3.84 g/cm^3 [CRC93]. Total porosity can also be calculated from the refractive index obtained from UV-Vis measurements using the Lorentz-Lorenz equation [CHR98, LAU96]. Both results are summarized in Table 8. Both methods are in good agreement considering the margin of error. However it must be noted, that as explained in Paragraph 5.2.3.2 the skeletal densities of the corresponding film powders are significantly lower than the theoretical density of anatase, which is mainly explained with the existence of closed pores [BOC06].

Table 8. Estimation of the porosity of TiO_2 films annealed at 600 °C from macroscopic density (XRR) and refractive index (UV-Vis) using the density of anatase (3.84 g/cm^3) [CRC93] and the refractive index of anatase (2.5235) [CHR98]. (Data taken from [BOC07a])

solvent composition EtOH:1,5-pentanediol	macroscopic density [g/cm^3]	porosity [%]	refractive index	porosity [%]
100 : 0	3.25 ± 0.05	15.4 ± 1.3	2.11 ± 0.02	16.6 ± 1.0
90 : 10	3.50 ± 0.05	8.9 ± 1.3	2.24 ± 0.02	10.8 ± 1.0
80 : 20	3.45 ± 0.05	10.2 ± 1.3	2.21 ± 0.02	12.1 ± 1.0

Films from sols containing 1,5-pentanediol seem to have small residual total porosities that do not exceed 10.2 % (XRR), whereas with 15.4 % (XRR) the value for the sample from purely ethanol based solution is significantly higher.

Nevertheless the films show a quite different defect pattern, even though their thickness is basically identical (Figure 44): Film surfaces prepared from a purely ethanol based sols show a coarse crack pattern that separates undamaged film regions with diameters often exceeding 500 μm (Figure 44 (a)). The addition of 10 % or 20 % 1,5-pentanediol strongly improves the film quality since only few short cracks and star-like defects can be found. It has to be mentioned, that Figure 34 (b) was even taken from a relatively poor region near the edge of a 10*10 cm^2 substrate in order to facilitate focusing of the image at the single defects, most parts of the coated glass are virtually faultless. [BOC06]

The reasons concerning the prevention of crack formation by the addition of 1,5-pentanediol are going to be discussed in detail in the following Paragraph 5.2.5. Though regarding the different porosities (Table. 8) it has to be mentioned that cracks in the films can influence the calculated porosity values obtained both by XRR or UV-Vis measurements. These cracks result in uncovered glass surface and therefore do not contribute neither to the macroscopic density nor to the refractive index [MAL07]. In other words, the highly cracked film pattern might be the only reason for the higher observed porosity of the coating prepared from pure ethanol based sol.

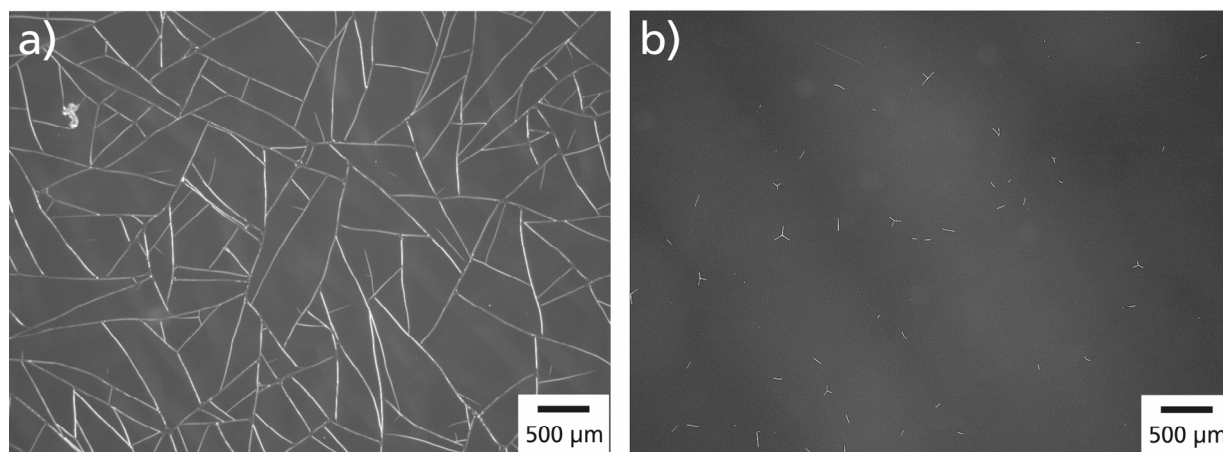


Figure 44. Light microscope surface images of TiO_2 films on glass prepared from coating solutions containing 0 % (a), 10 % (b) 1,5-pentanediol. Both samples were annealed at 600 $^{\circ}\text{C}$ for 10 minutes and have a final film thickness of ~ 110 nm. (Data taken from [BOC06])

Additionally EP measurements were performed of thin films that had been prepared on Si-wafer from ethanol based sols containing 0 %, 10 % and 20 % 1,5-pentanediol. For this comparative study thin films were chosen, which were annealed at 400 $^{\circ}\text{C}$. The corresponding isotherms are shown in Figure 45. Open porosity increases from sample 90:10 (0 %) to 80:20 (1-1.5 %) to 100:0 (8 %).

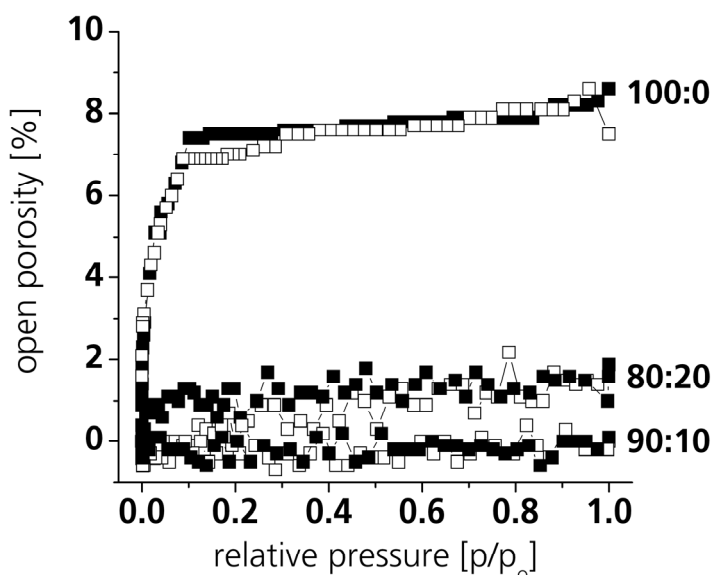


Figure 45. Ellipsometric porosimetry isotherms of thin films that had been prepared from ethanol based coating solutions containing 0 %, 10 % and 20 % 1,5-pentanediol and annealed at 400 °C for 10 min.

Although this tendency qualitatively correlates with difference in initial refractive indices, the difference in initial n -values can not explain such significant difference in the measured porosity. Further analysis of the EP data (Table 9) rather reveals that all coatings have a certain overall porosity of > 13 %. Though the films prepared with the addition of 1,5-pentanediol have mostly only closed pores. Regarding the overall porosity of the 100:0 sample, the influence of cracks on the refractive index measurement has to be kept in mind.

Table 9. Porosities of films that had been prepared on Si-wafer from ethanol based coating solutions containing 0 %, 10 % and 20 % 1,5-pentanediol and annealed at 400 °C for 10 min. The refractive index and open porosity were measured by ellipsometric porosimetry. The overall porosities were calculated by using the theoretical refractive index of anatase [CHR98].

solvent composition EtOH:1,5-pentanediol	refractive index (empty pores)	overall porosity [%]	open porosity [%]	closed porosity [%]
100 : 0	2.134 ± 0.005	15.6 ± 0.3	8.0 ± 0.5	7.5 ± 0.8
90 : 10	2.189 ± 0.005	13.0 ± 0.3	0 ± 0.5	13.0 ± 0.8
80 : 20	2.165 ± 0.005	14.2 ± 0.3	1.0 ± 0.5	13.2 ± 0.8

The main difference between the samples is, that films prepared with a pure ethanol based sol (100:0) present a completely cracked film, whereas the samples prepared with sols containing 1,5-pentanediol were not cracked at all (90:10) or show only small, star like cracks (80:20) (pictures not shown).

The EP-results can be explained as follows. All these films form during thermolysis a dense crust on their interface coating/air (Figure 46, indicated by fat black line). Coatings without any defects have only closed pores, which are not accessible to the measurement gas (Figure 46 (a)). Cracks in the films, arising after formation of this crust, can burst this crust so that pores can be detected

(Figure 46 (C)). Whereas cracks that occur just before the thermal densification, during film drying and aging, not burst this crust (Figure 46 (B)).

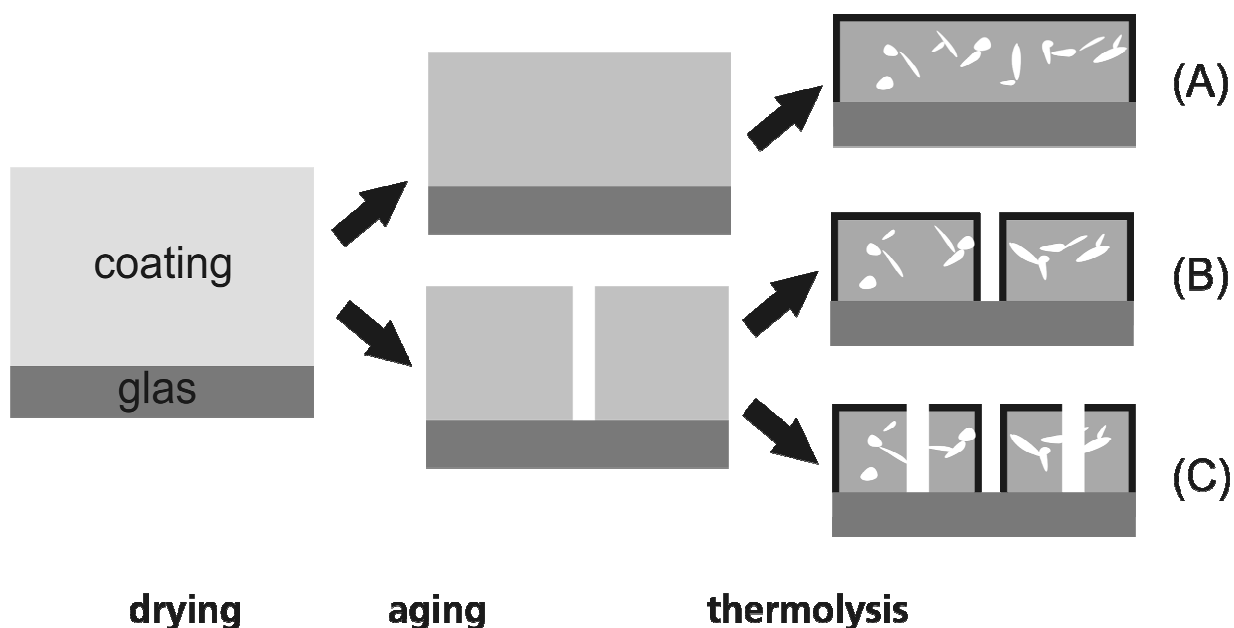


Figure 46. Schematic model of the generation of open and closed porosity during thin film shrinkage. After thermolysis a dense crust is formed on the top of all coatings. (A) Thin film without cracks, without open porosity. (B) Thin film with cracks formed only during drying. The crust is not burst by the cracks and only closed pores exist. (C) Thin film with cracks that burst the crust during thermolysis leading to open porosity.

The differences concerning the open porosities should also affect the accessible surface area of the samples. First at all the accessible surface area of films with cracks ("100:0"; open pores) should be higher than films without cracks ("90:10"; only closed pores). Furthermore the absolute accessible surface area of films with cracks should rise with increasing film thickness. This affect should not occur in the case of films without cracks.

This argumentation was proved by investigations on the photocatalytic activity of thin TiO_2 films. Generally it is a common observation in literature that the photocatalytic activity of TiO_2 increases with increasing accessible surface area [HEI00,XAG99]. Hence the photocatalytic activity of cracked (100:0) and not cracked (90:10) thin films as function of film thickness was determined (Figure 47). When films were cracked (100:0) an increase of activity can be noticed with increasing film thickness. By doubling of film thickness from ~ 120 nm up to ~ 250 nm the activity is also nearly doubled. According to the former argumentation, the photocatalytic activity of films, which exhibit no cracks and no open porosity, remain nearly constant.

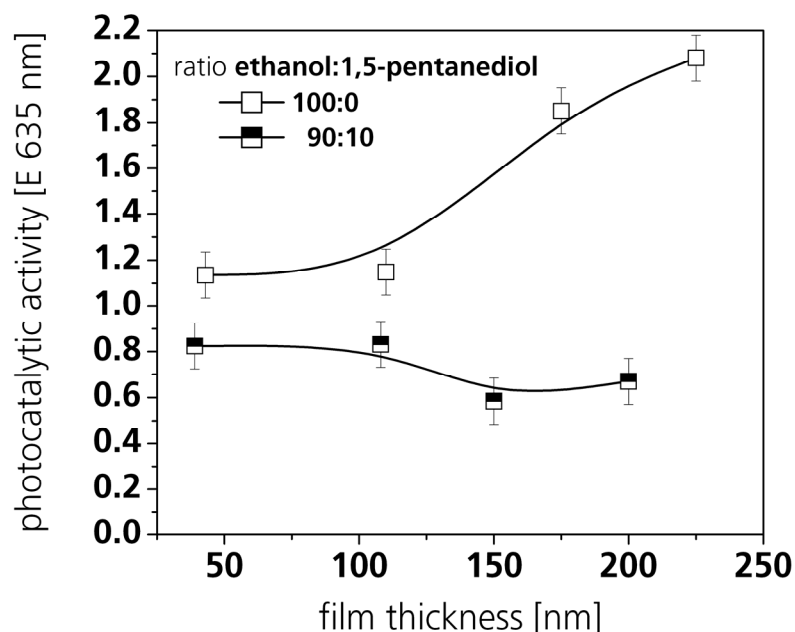


Figure 47. Photocatalytic activity of thin films that had been prepared on glass (borofloat™) from ethanol based coating solutions containing 0 % and 10 % 1,5-pentanediol as function of film thickness. Samples were annealed for 10 min at 500 °C.

Though, it has to be noted that even cracked films present at relatively low film thicknesses no increase in photocatalytic activity. Nevertheless, the overall porosity of all investigated films is comparable (data not shown). This might indicate that in these films with thicknesses below 110 nm mostly cracks exist, which do not generate open porosity (Figure 46 (B)). When the film thickness increases also cracks appear, which break through the crust (Figure 46 (C)). Thereby open porosity is generated and the photocatalytic activity increases with increasing film thickness.

SUMMARY OF 5.2.4 "MICROSTRUCTURE OF THIN FILMS"

Generally the microstructure of thin films is comparatively close to the microstructure of the film powders, whether the thermal offset due to differently long used dwell times has to be considered. In thin films and in film powders as well a comparable amount of closed pores are formed during annealing. However, thin films never transform to rutile, even at 700 °C. This behavior can be attributed the additional tensile stress, which is only active in the case of the films.

Basically the densification and shrinkage of thin films corresponds to the investigations made on the film powders. The observed results confirm the property of 1,5-pentanediol to prevent hydrolysis and condensations reactions. Thus films prepared from sols with and without the addition of 1,5-pentanediol present a different shrinkage and densification behavior during film drying and aging (< 250 °C). Nevertheless, the further densification at higher annealing temperatures of all films results in a quite similar microstructure, except crack formation.

Ellipsometric porosimetry measurements revealed that films with cracks partly present a certain amount of open pores, whereas coatings without cracks have only closed pores. In conclusion with these results the photocatalytic activity of cracked films increases with raising film thickness,

because of the simultaneously increasing surface area. In contrast to that the photocatalytic activity of crack free films shows no dependence on film thickness.

From this was predicted that generally thin TiO_2 sol-gel films, during annealing form a crust on top. Therefore crack free films have only closed pores. When this crust is burst by cracks, which are originated from the densification stress, a certain amount of open porosity is generated.

5.2.5 RESIDUAL STRESS AND CRACKING OF THIN FILMS

5.2.5.1 INFLUENCE OF SOLVENT COMPOSITION ON RESIDUAL STRESS OF THIN FILMS

In the initial state of wet-film formation the coating solution is still a viscous liquid and thus is able to undergo isotropic shrinkage [BRI92]. Up on drying of the thin film the solvent evaporates and the viscosity of the colloidal sol increases. The more volatile components of the sol will evaporate first increasing the concentration of water and catalyst which in turn will promote further hydrolysis- and condensation reactions of precursor particles [SCH92,SCH97]. As most coating procedures are performed under ambient conditions, air moisture significantly contributes to this process [BUR99,BRE01]. This sol-gel transformation leads to a stiffening of the network [CAI97]. Further thermal processing steps result in decomposition reactions of organic moieties. By simultaneous densification the xerogel is converted film to a ceramic thin film.

All these drying and pyrolysis steps associated with a volume changes constrained in the plane of the substrate induce tensile stresses [ROE99]. As a visualization the height profile of a $50 \times 50 \text{ mm}^2$ glass slide that carries a single sided TiO_2 -coating, is given in Figure 48. The microscope glass slide is bent in a cylindrical shape by the tensile forces originated from the coating [HYE81].

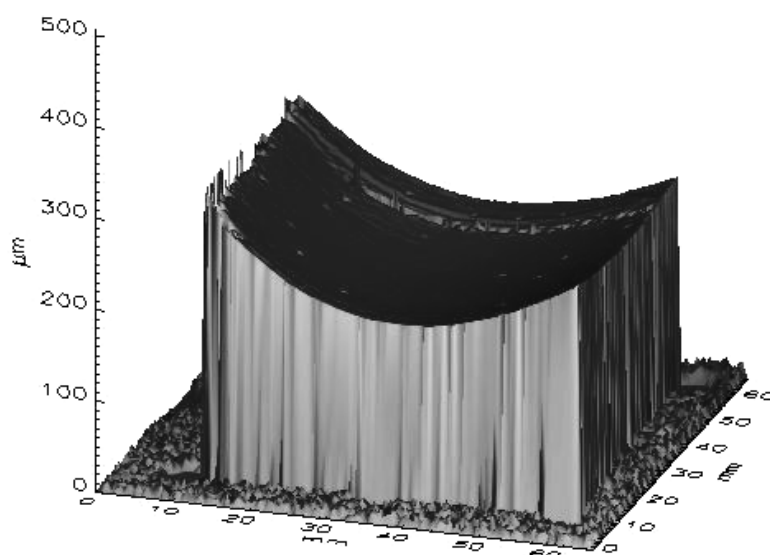


Figure 48. Typical image of a one side TiO_2 coated thin microscope glass slide that is bent by the tensile forces originated from the coating.

Tensile stress which exceeds the elastic limit causes cracking in surface coatings, perpendicular to the direction of the tensile stress [PER96,BRI95,MEH05]. Generally, cracking occurs when the internal stresses exceed the cohesive strength of the film [ROE99]. Thus the magnitude of stress

places a limit on the film thickness [ZHO05,EVA88] and therefore numerous strategies to avoid stress-related damage have been developed [KOZ00b,VRE90,KOZ03].

Several methods are commonly employed for residual stress measurements [PER96,SKR00]. Beside the X-ray diffraction methods which require crystalline films the mechanical deflection method is frequently applied. Therefore the average stress in a coating can be determined from the deflection δ of the glass substrate, as caused by a stressed coating deposited on one side of it [STO09,FLI87,KOZ03,BRE01,BRE99,SEN98].

Though, it has to be noted, that the residual stress is the sum of intrinsic and thermal stress [BRE01]. Since the thermal expansion coefficients and Young's modulus of the thin films are not known at any temperature the thermal stresses can not be calculated accurately. In the case of titania a large portion is from thermal mismatch [KOZ03,VRE90]. If assumed that at 500 °C the coating consists of pure dense anatase, the thermal stress contributing to the overall stress is around 0.6 GPa. Certainly when lower annealing temperatures are used the thermal stresses decrease.

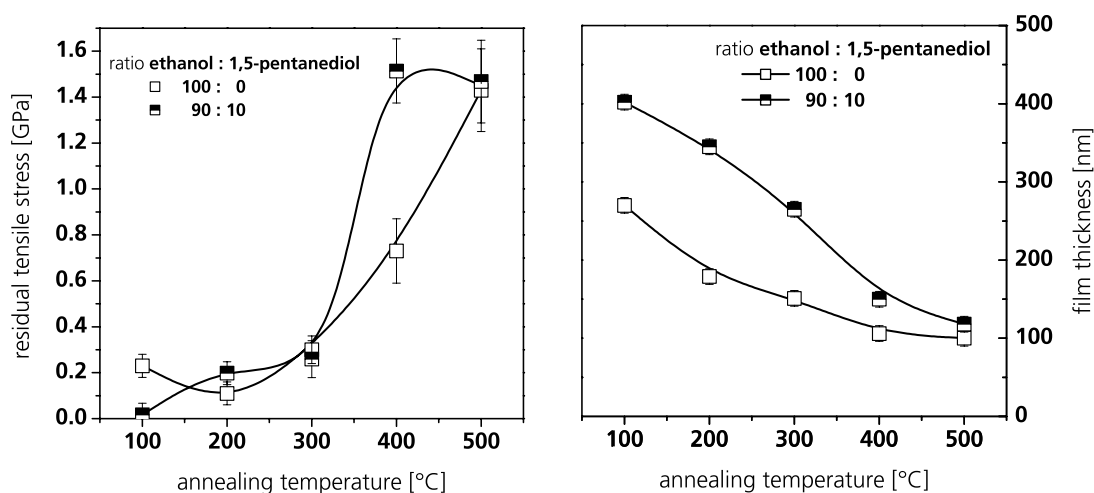


Figure 49. Residual tensile stress (left) and film thickness (right) of TiO₂ coatings prepared from sols with (■) and without (□) the addition of 1,5-pentanediol as a function of annealing temperature.

The residual stress of TiO₂ coatings prepared from sols with and without the addition of 1,5-pentanediol as function of annealing temperature is presented in Figure 49 (left). The stress of both sorts of TiO₂ coatings is tensile and basically increases with increasing annealing temperature up to around 1.4 GPa. At an annealing temperature of 100 °C in a coating prepared from pure ethanol based coating solution a significant amount of residual stress (~0.2 GPa) is determined, whereas in a coating prepared from a coating solution containing 1,5-pentanediol nearly no stress (~0.02 GPa) is present. Nevertheless even at 400 °C this coating already reaches the maximum level of residual stress, whereas the coating prepared without the use of 1,5-pentanediol just at 500 °C.

Constraint shrinkage of a thin film often results in tensile stress [ROE99]. Therefore the respective film thickness as function of the annealing temperature is displayed in Figure 49 (right). Both coatings present continuous shrinkage up to around 110 nm at 500 °C. Coatings prepared from

pure ethanol based coating solution have in the investigated temperature range a lower overall shrinkage than coatings prepared from a solution containing 1,5-pentanediol.

At the initial state of wet-film formation both coatings should have a comparable film thickness of several micrometers, because of the identical oxide yield (6 mass %) in the sols. However at 100 °C the coating prepared from a purely ethanol based solution presents a significantly lower film thickness than the coating prepared with a solution containing 1,5-pentanediol. This indicates that films prepared from pure ethanol based coating solutions undergo a larger shrinkage during drying and aging, which induces a higher degree of tensile stress at 100 °C (Figure 49 (left)). As already seen in Paragraph 5.2.3, the addition of 1,5-pentanediol prevents the gel-network from hydrolysis and drying reactions, whereas without 1,5-pentanediol a more rigid network is formed. Though, the addition of 1,5-pentanediol brings more plasticity in the network and can therefore better release/reduce stress. [BOC07a]

Generally the large increase of residual stress at higher temperatures is linked to further thin film densification because of decomposition reactions and the crystallization of anatase [MEH97,BRE99,SEN98]. Though the steep increase of the residual stress in coatings prepared from coating solutions containing 1,5-pentanediol at 400 °C might be explained with the high shrinkage from 300 °C to 400 °C. However in the case of the coating prepared without the addition of 1,5-pentanediol this explanation is not valid.

Certainly differences in the thermal stress could be responsible for the different observed residual stresses. But variations in the elastic constants of the two coating systems can not be as high to exclusively take account for the differences in the residual stresses. In fact structural changes, e.g. viscous flow or crack formation during the densification can also reduce residual stress. From earlier paragraphs it is known that the considered coatings differ significantly regarding their cracking tendency. Therefore to explain this behavior in detail crack formation of these coatings will be more thoroughly investigated in the following paragraphs.

5.2.5.2 CHARACTERIZATION AND ANALYSIS OF CRACKING IN THIN FILMS

It turned out that when as-dried films are annealed at intermediate temperatures, defects may be observed that are not present for samples immediately treated at higher temperatures. In order to optimize sol-gel processing of thin films it is important to understand the origin of defects, which are related to both the chemical precursors and the experimental parameters such as heating rates and humidity. Unfortunately the evaluation of defects is often rather arbitrary and depends on subjective ratings which make the comparison between different experimental series rather difficult. Therefore a method for the evaluation of defect densities based on the automated analysis of surface images was established. In the following paragraphs the results on TiO₂ films will be correlated to the film densification and the microstructural changes associated with the processing parameters.

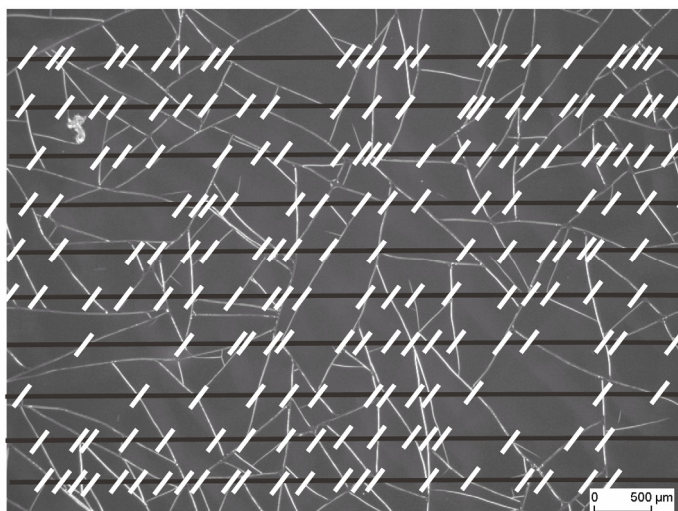


Figure 50. Surface image (light microscopy, 20-fold magnification) of a typical crack pattern observed on a sol-gel derived TiO_2 thin film. Points on the vertical lines detected as defects by the data analysis software IMAGE C™ are marked with white bars. (Data taken from [BOC07a])

In Figure 50 typical image of a cracked sol-gel film is given. Polygons of undamaged film are separated by straight cracks. At higher magnifications (data not shown) it is obvious that the cracks originate from the retraction of film material from the surface under tensile stress. Using IMAGE C™ an array of virtual lines with equal spacing can be laid over the image and the software is able to detect strong contrast variations along the lines. Since these incidents are obviously associated with cracks one can define the quantity “defects per millimeter [mm^{-1}]”. [BOC07a]

In order to check the validity of this approach, the image of a cracked surface was investigated at different magnifications by varying the length of the virtual lines but using always the same number of test lines (Figure 51 (right)). For a line length of $800\ \mu\text{m}$ a sampling area of $800\ \mu\text{m}$ by $800\ \mu\text{m}$ was chosen, which then was divided by 10 evenly spaced parallel lines, the defect density was averaged and the respective standard deviation was calculated. Figure 51 (left) shows the defect density as a function of length of virtual lines for the sample. When the area analyzed is too small (small line length, ❶ in Figure 51), no defects are detected at all – an undamaged surface is investigated. At a larger line length (❷), a single defect lies within the area of analysis crossing some of the grid lines resulting in some finite defect density associated with a large error. When the square area is further enlarged, all virtual grids cross the defect (❸) and the standard deviation becomes zero. For all larger sampling areas the data evaluation becomes more and more reliable as long as the defect size is still resolved at the respective magnification. This is achieved if every virtual line is crossed by at least more than 5 cracks, as indicated by the gray line in Figure 51 (left). In all cases investigated the orientation of the virtual lines had no significant influence on the defect density, i.e. the crack pattern is isotropic. [BOC07a]

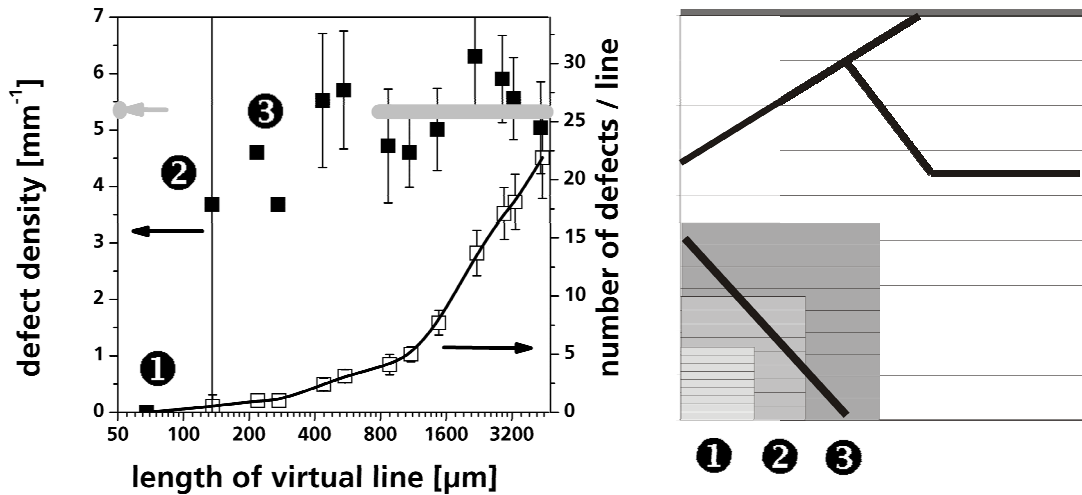


Figure 51. Left: Defect density defined as contrast variation along a virtual grid line (see Figure 50) as a function of the distance between grid lines (left axis). The values were determined for 10 parallel grids located in a square with a side length equal to the respective grid length. On the right axis the average number of defects found on the lines is given. The gray line denotes the range for which a reliable analysis is assumed. Right: Scheme of the data analysis procedure. The numbers correlate to the respective data points on the left. (Data taken from [BOC07a])

An alternative paradigm for defect quantification would be to relate the exposed glass surface area (area of cracks) due to cracking to the total area analyzed. This type of analysis was performed on films that showed different crack densities as a function of annealing temperature. In Figure 52 these results are compared with the respective values obtained from counting the intersection of a virtual grid with defects. For the damaged sol-gel surfaces investigated in this study no differences between the two methods can be found. This simply reflects the fact that the crack width, in the present case, is very small as compared to the distance between the cracks. Since the determination of the area of defects seems to be more dependent on the operator's grayscale threshold setting, for the further investigations the counting of defect densities was chosen. [BOC07a]

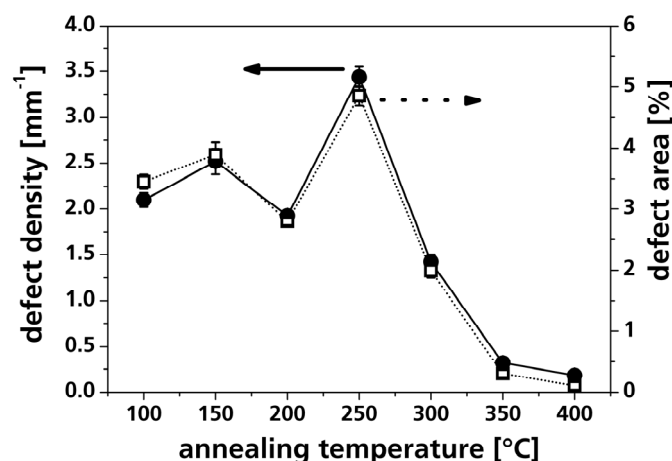


Figure 52. Defect density [mm^{-1}] as counted along virtual grids and the defect area measured by the area evaluation of cracks for TiO_2 thin films as a function of annealing temperature. (Data taken from [BOC07a])

Only if the conditions of data analysis are carefully chosen as described, reliable data can be obtained using image processing software [EXN94]. As will be considered in a following Paragraph (5.2.5.4) it is important to make sure that qualitative changes of the defects do not

invalidate the comparability of different samples. In the next Paragraph the crack formation of TiO_2 films induced by different solvent compositions is discussed.

5.2.5.3 INFLUENCE OF SOLVENT COMPOSITION ON CRACKING OF THIN FILMS

In order to investigate the formation of defects due to the densification process, conditions have to be chosen that result in films with identical final thickness, i.e. the systems must have undergone a comparable shrinkage during their preparation.

Coatings with a single layer thickness of up to 110 nm do not show significant defect levels irrespective of the solvent composition and pyrolysis temperatures employed. However, these coatings are used for UV-Vis measurements because of the fact that with increasing film thickness the portion of absorption in the films due to incorporated carbon is increasing which results in an increasing measurement error. To systematically investigate the formation of defects on a sufficiently high defect density level the withdrawal rates were increased according to Figure 38 in order to achieve a single layer thickness of 220 nm after sintering at 600 °C. [BOC07a]

Based on surface images of these samples their defect densities were determined as a function of annealing temperature (Figure 53). Purely ethanol-based coatings exhibit a small but significant amount of cracks already after drying under ambient conditions. Upon annealing at 150 °C the density of defects is increased by an order of magnitude. If as-dried samples are RTA annealed up to 450 °C, the rate of defects decreases to a low level, but at a higher annealing temperature crack free films were never obtained. [BOC07a]

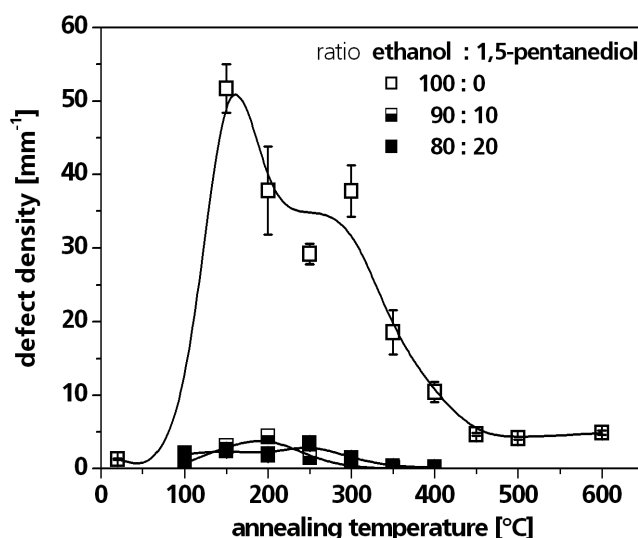


Figure 53. Defect densities for TiO_2 coatings based on different solvent compositions as a function of annealing temperature. The lines are drawn as guide to the eyes. (Data taken from [BOC07a])

Films dip-coated from solutions that contained 1,5-pentanediol can be dried at room temperature without cracking. A few cracks occur if these samples are treated at intermediate temperatures between 100 °C and 400 °C. The as-dried films do not show any cracking if directly treated at 450 °C or above. [BOC07a]

Previous results on the properties of “film powders” scraped off substrates (Paragraph 5.2.3) offer an explanation for the different behavior of the systems: If no 1,5-pentanediol is present

("100:0") drying in the presence of air moisture leads to the hydrolytic cleavage of most Ti-OEt groups in the film, a rigid xerogel network is formed due to condensation reactions. These condensation reactions are retarded in the presence of 1,5-pentanediol, that partially stabilizes the reactive alkoxide moieties. This had been demonstrated by thermogravimetric analysis and measurements of the backbone density by He-pykometry. [BOC07a]

This interpretation is further supported by the analysis of film thickness and refractive index summarized in Figure 54. These measurements have been performed on samples with final film thicknesses of 110 nm in order to get reliable UV-Vis measurements. The general trend is assumed to be the same as for the thicker samples prepared for defect analysis.

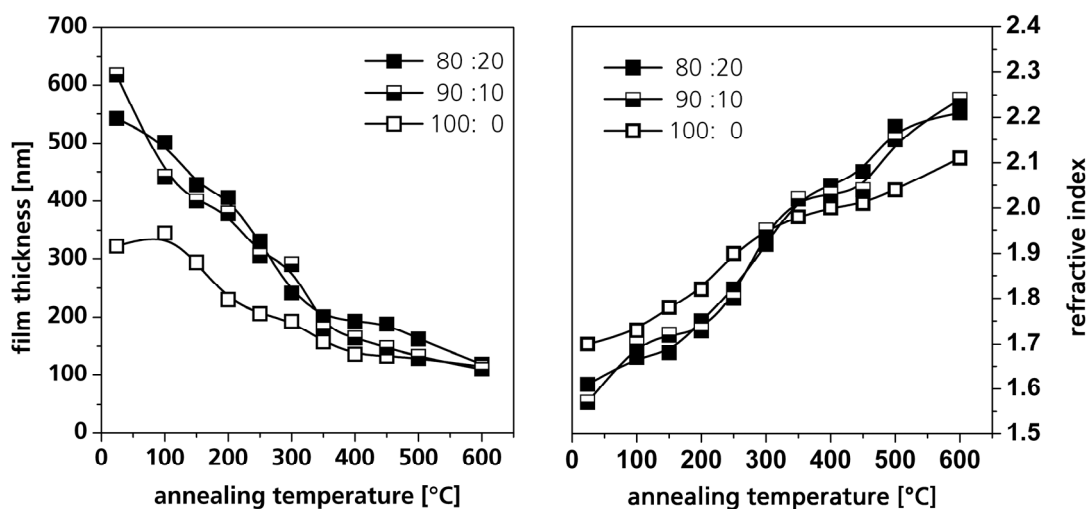


Figure 54. Film thickness (left) and refractive index (right) of TiO₂ films as a function of annealing temperature. The films were obtained from ethanol based coating solutions containing 0 % (□), 10 % (◻) and 20 % (■) 1,5-pentanediol. (Data taken from [BOC07a])

Indeed as already seen before (Figure 40 and Figure 49 (right)) the purely ethanol-based films initially show lower film thickness and higher refractive index indicating a higher degree of densification. Whereas the film thickness converges at higher annealing temperatures, the refractive index of films prepared with pure ethanol as solvent falls behind the samples from sols containing 1,5-pentanediol. This is in good agreement with the comparably high porosity calculated from XRR (Table 8) and can be explained by the different defect densities, which affect both the measurement of macroscopic density and refractive (Paragraph 5.2.4.2).

In conclusion films from sols that only contain ethanol as solvent already undergo strong shrinkage and form a rigid xerogel network during drying. This rigid xerogel induces at an annealing temperature 100 °C a relatively high tensile stress in the film compared to films, which contain 1,5-pentanediol (Figure 49 (left)). At an annealing temperature of 200 °C, when the crack density is significantly increasing, the tensile stress is lowered, because the stress is released by the formation of cracks. In contrast to this the presence of 1,5-pentanediol obviously facilitates even higher shrinkage by preserving a required degree of network relaxation. [BOC07a]

Thus, the question remains why the density of defects decreases at higher isothermal annealing temperatures as shown in Figure 53. In general there is no direct correlation between the degree of tensile stress (Figure 49) and the quantity of cracks noticeable. As already has been discussed

cracks generally appear when the tensile stress exceeds the inner coherence of the film. Unfortunately, the inner coherence of thin films is only barely accessible. Of course it can be assumed that the inner coherence of the films here investigated significantly depends on the used annealing temperature. For example a dense ceramic thin film usually has a higher inner coherence than a rigid xerogel. Hence it can be concluded that the inner coherence of a thin film annealed at high temperature is even high enough to tolerate high tensile forces. At lower temperatures however, even relatively low tensile forces, originating from drying and aging processes, can exceed the inner coherence of the thin films.

In summary the reduction of defects with increasing annealing temperature can be explained as follows: The short drying time (2 min) of the sol-gel film prevents the formation of a rigid network. When the temperature is rapidly raised the solidification leads to an increase of the inner coherence by strengthening of the interparticular connections. Therefore these thin films can easier withstand the high tensile forces without cracking.

5.2.5.4 INFLUENCE OF AIR MOISTURE DURING COATING PROCEDURE

It is a common but poorly quantitatively documented observation [BUR99,KAJ00a,KAJ00b,SUR04,CRE02,CHO04b] that the quality of sol-gel films critically depends on the atmospheric humidity during coating experiments. Thus this topic was systematically investigated by preparing TiO_2 coatings under climate controlled conditions. The RH was varied between 20 and 80 % at 24 °C using a constant RTA annealing temperature of 600 °C and constant withdrawal rate for a final film thickness of 220 nm. [BOC07a]

Major differences can be observed for films prepared from ethanol based coating solutions dried at different RH. The film dip-coated and dried at 20 % RH was transparent whereas films dried at higher RH were highly opaque. SEM images of these films calcinated at 600 °C are presented in Figure 55 and Figure 57. On the microscopic level significantly different cracking patterns are induced by variation of the RH. At RH of 20, 40 and 80 % generally closed cracking patterns consisting of cracks down to the glass surface are observed. However, at a RH of 60 % additionally a large amount of round cracks shaped like "holes" appear, which generally not expose the bare glass surface. [BOC07a]

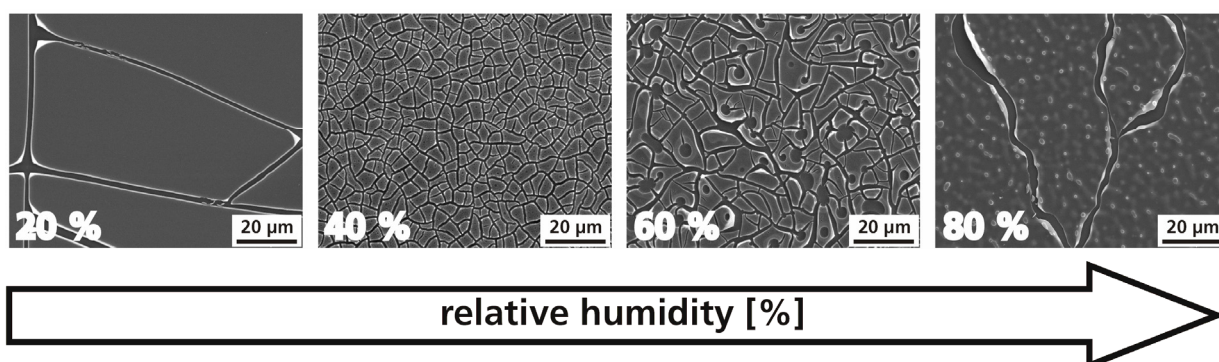


Figure 55. SEM images of TiO_2 coatings prepared at 600 °C from pure ethanol based coating solution under different RH at 24 °C. (Data taken from [BOC07a])

Based on surface images of these samples, their defect densities were determined (Figure 56). The defect density of purely ethanol-based coatings seems to be highly sensitive to increasing RH. Upon raising the RH from 20 to 40 % the defect density is increased by a factor of 70. At higher RH the defect density slightly decreases.

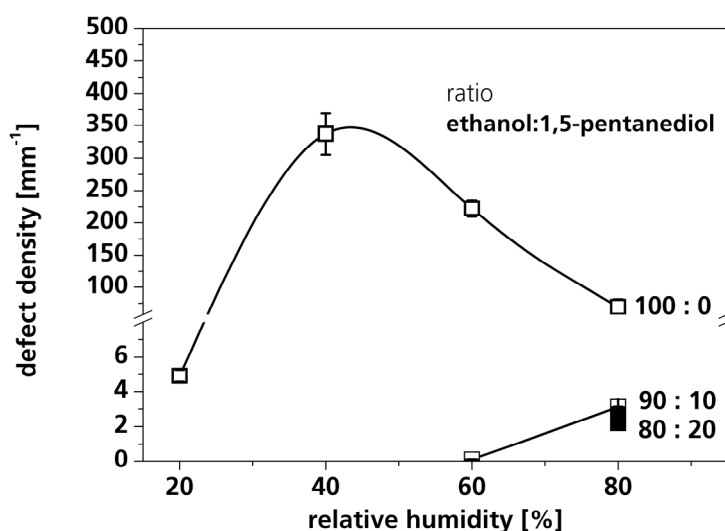


Figure 56. Defect densities for TiO₂ coatings calcinated at 600 °C from different solvent compositions as a function of RH. The lines are drawn as guide to the eyes. (Data taken from [BOC07a])

Raising the RH from 40 % up to 60 % leads to a slight reduction of the counted defects. This is associated with an increase of width and shape of the cracks. The changed crack type leads to a lower defect density, but the defect area is nearly the same (40 % RH = 20.2 % ± 0.2, 60 % RH = 21.6 % ± 0.9). If the air moisture is further increased up to 80 % RH crack density is significantly reduced. However, simultaneously nearly all straight lined cracks disappeared. [BOC07a]

SEM-images (Figure 57) of the cross section of the coatings show an increase of the film thickness from 20 % RH up to 40/60 % RH. Higher film inhomogeneity was only observed at damaged film parts (holes, cracks). Whereas at 80 % RH major variation in film thickness from 100 nm up to 600 nm was observed. In conclusion films dried at 20-60 % RH should not significantly differ in their microstructure except for defect density. However, if the coating was dried at 80 % RH, the properties of the coatings (i.e. surface roughness) have changed. [BOC07a]

It is proposed, that when the RH is raised from 20 % up to 40/60 % the hydrolysis and condensation reactions during thin film drying and aging also increase. This leads to a higher linked network and a more rigid xerogel with a higher brittleness and thus increasing defect density. Further increase of humidity up to 80 % RH still promotes hydrolysis and condensation reactions leading to a favored gelation before drying of the thin films, especially at the interface of the wet film to the atmosphere. This might lead to the formation of a gelly skin on top of the wet film, which could be the reason for this substructure formation and accompanied high surface roughness. Furthermore this change of the drying/gelation behavior [CAI97] of course influences the film densification, which could be the explanation for the reduction of crack density.

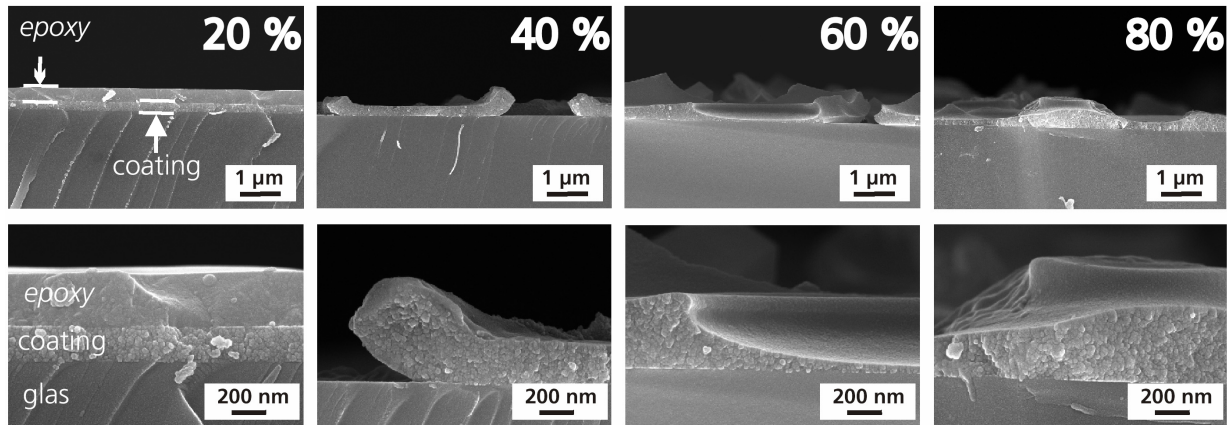


Figure 57. SEM images of cross section of TiO_2 coatings prepared at 600 °C from pure ethanol based coating solution under different RH at 24 °C. (Data taken from [BOC07a])

Coatings prepared from sols containing 1,5-pentanediol, however, are completely transparent after drying. There are no cracks at RH of 20-40 % and even at higher RH only a very low defect density is found. According to Paragraph 5.2.3 and the results on the properties of film powders scraped off substrates, we can conclude, that in the presence of 1,5-pentanediol the reactive alkoxide moieties are partially stabilized. This results in a more flexible xerogel network with lower tensile stress. Further on, compared to films prepared with pure ethanol based sols, defect free coatings or at least only slightly damaged films at high RH were obtained. [BOC07a]

Nevertheless, even with addition of 1,5-pentanediol cracks appear at higher RH. An explanation for this behavior is given by the evolution of film thickness and refractive index from coatings prepared at 20 % RH and at 80 % RH in Figure 58. Coatings prepared under higher RH have a lower film thickness and a higher refractive index directly after drying. This indicates a more densified xerogel because of increasing hydrolysis and condensation reactions resulting in a more rigid network.

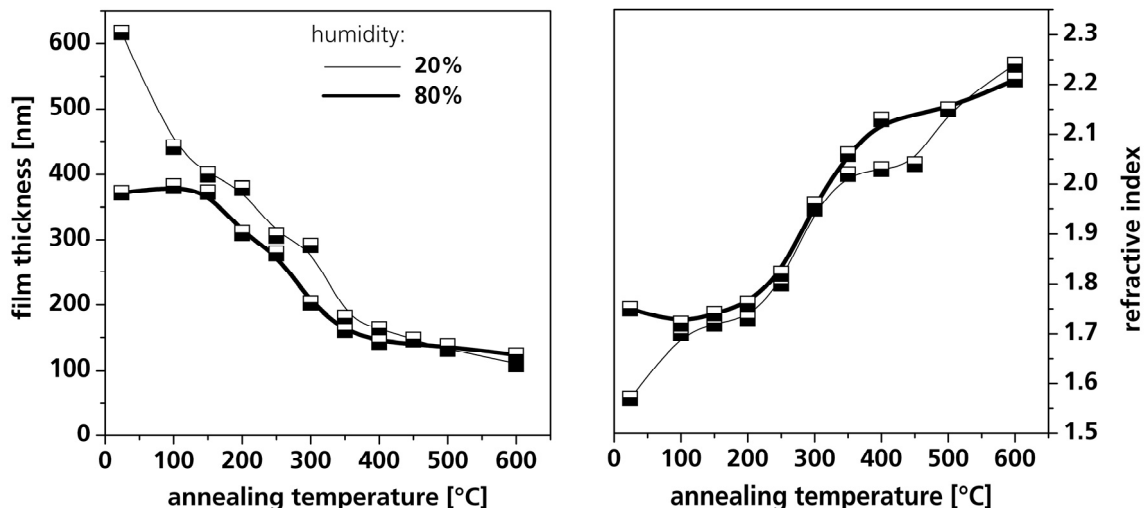


Figure 58. Film thickness (a) and refractive index (b) of TiO_2 films as a function of annealing temperature. The films were obtained from ethanol based coating solutions containing 10 % 1,5-pentanediol prepared at 20 % RH and at 80 % RH. The lines are drawn as guide to the eyes. (Data taken from [BOC07a])

However, while analyzing the defect density of these sample series, especially for the coatings from the pure ethanol based sol, it is obvious that the thickness-to-area ratio of the undamaged

film section separated by cracks varies significantly. This shows the limits of the defect counting method, because the number of defects counted does not necessarily correlate with the area of defects. For any quantitative evaluation of defects as a function of experimental parameters it must be ensured that there are no qualitative changes in the structure of the defects. [BOC07a]

SUMMARY OF 5.2.5 "RESIDUAL STRESS AND CRACKING OF THIN FILMS"

The residual tensile stress in thin films prepared by dip-coating was determined by the deflection method and is a sum of thermal stress and intrinsic stress. For all coating systems investigated the residual stress generally increases by raising the annealing temperature.

Coatings which undergo less hydrolysis and condensation reactions during drying and aging present a lower residual stress at low annealing temperatures. Nevertheless structural changes such as crack formation also influence the degree of residual tensile stress.

An automated method for the quantitative analysis of thin film defects was established. As long as certain methodic boundary conditions are taken into account, the defect density per millimeter can be determined with high reproducibility.

Using this method the defect densities of various experimental series can be assessed. Formation and quantity of defects are directly referred to the development of tensile stress due to structural modification during the drying and densification process. By adding 1,5-pentanediol to the sol thin film cracking can be reduced significantly or even avoided because a higher degree of network flexibility is preserved.

Furthermore a strong dependence of crack formation on the atmospheric humidity was observed. In summary the RH is proposed to determine the ratio of drying/condensation during thin film formation. With increasing RH from 20 % to 40/60 % hydrolysis and condensation reactions are promoted, which lead to further network stiffening and increasing defect density. When the RH is raised up to 80 % the ratio of drying and condensation further increases. However at 80 % the high condensation to drying rate leads to the formation of a huge surface roughness and decrease of defects density.

5.3 WATER BASED COATING SYSTEMS

5.3.1 SOLUBILITY AND STABILITY

With the precursor powder synthesis route described in Paragraph 5.1 also precursor powders, which are soluble and stable in water as solvent, can be synthesized [LOE05]. The solubility of the powders also depends on the synthesis conditions and therefore on the chemical composition of the powders. However, the results of the solubility experiments in water differ from the observations made with ethanol as solvent (Table 10). In this Table the term “insoluble” describes also precursors, which are directly hydrolyzed and therefore immediately form a precipitate.

Powders, which are soluble in water have to be prepared with a higher content of water and acetylacetone as necessary for the ethanol-based solutions. It seems quite logical that the stability of the precursors is determined by the content of hydrolytically unstable -OEt groups. When higher ratios of water were used for the precursor powder synthesis, the powders became insoluble again in water (Table 10) as well as in ethanol (Paragraph 5.2.1, Table 4).

Table 10. Solubility of TiO₂ precursors in water prepared with different molar ratios of Ti/AcAc/water [LOE05].

	water Y					
	1 mol	3 mol	5 mol	7 mol	10 mol	20 mol
AcAcH X						
0.5 mol		insoluble	insoluble			
1.0 mol	(liquid)	insoluble	soluble	soluble	insoluble	insoluble
1.5 mol		insoluble	insoluble	soluble	soluble	insoluble

A high demand of water soluble TiO₂ precursor for large area spray coating experiments led to an increase in batch size of precursor powders. It turned out that especially the reproducibility of water soluble precursor powders is insufficient. Apparently the relatively high water content and the synthesis conditions at the rotational evaporator are difficult to control and led to the high diversity observed.

In general it is known that the hydrolysis and condensation reaction during the synthesis process determine the chemical composition of the xerogel and so the solubility of the powders [LOE03,LOE05]. Therefore the precursor powders were additionally placed in a vented oven at 125 °C after the standard synthesis, because thermal energy in combination with air moisture can also induce hydrolysis and condensation reactions.

Table 11. Stability and solubility of TiO₂ precursors in water. For the preparation the ratio of Ti/AcAc was kept constant (1/1), whereas the molar ratios of Ti/water was varied. The exposure time for the precursor powders at 125 °C was varied between 0 h and 15 h.

exposure time	water Y		
	3 mol	5 mol	7 mol
0 h	insoluble	1 day	3 days
1 h	2 days	~ 1 month	6 days
5 h	12 days	> 6 month	insoluble
15 h	insoluble	insoluble	insoluble

In Table 11 the dependency of exposure time at 125 °C of different precursor powders on their solubility in water is displayed. It is obvious that the exposure procedure significantly improves the long-term stability of all three powders investigated. Even the precursor powder normally insoluble prepared with a ratio Ti/AcAc/H₂O of 1/1/3 becomes soluble in water. Though, it turns out if a long exposure time i.e. 15 h is used, a precursor powder that previously was soluble is also becoming insoluble at all. The best improvement regarding its long term stability presented the powder prepared with a ratio Ti/AcAc/H₂O of 1/1/5.

The oxide yield of this powder increases with increasing duration of exposure procedure (Figure 59). The skeletal density presents a similar behavior and also increases because of the lower content of residual organics (Figure 59). Further investigation on the chemical environment of these powders are done by thermogravimetric analysis (Figure 60 (left)) and differential thermal analysis (Figure 60 (right)).

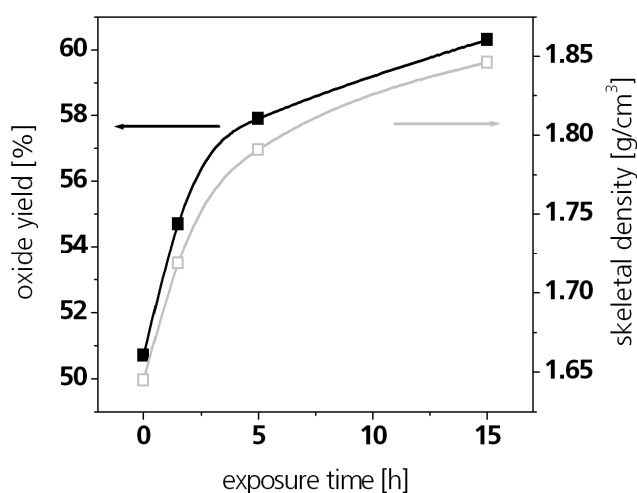


Figure 59. Oxide yield (■) and skeletal density (□) of a precursor powder (ratio Ti/AcAc/H₂O of 1/1/5) as function of exposure time at 125 °C.

According to the oxide yield the final mass loss observed in the TG (Figure 60 (left)) decreases with increasing duration of exposure. This can be attributed to both a decreasing mass loss below 200 °C and as well above temperatures of 400 °C. In the DTA (Figure 60 (right)) the first mass loss below temperatures of 200 °C is linked to an endothermic signal ① and indicates an

evaporation of residual water or physisorbed organic residues. At temperatures above 400 °C a reduction of the exothermic signal ③, which is accompanied with a decreasing content of -OEt groups in the xerogel is visible. This can be explained by thermally induced hydrolysis and thus removal of -OEt groups. In contrast to this the signal of the hydrolytically more stable acetylacetonate groups ② is nearly unaffected by the drying procedure.

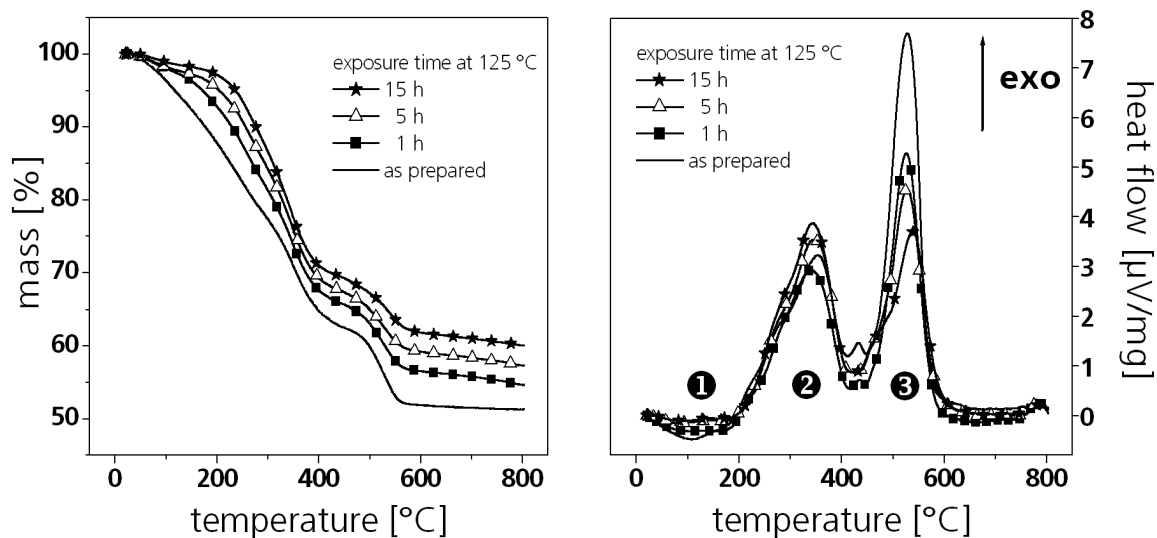


Figure 60. Thermogravimetric analysis (left) and differential thermal analysis (right) of soluble TiO_2 precursor powder synthesized using $\text{Ti}(\text{OEt})_4$, acetylacetonate and water in the molar ratio of 1/1/5. The powders were obtained after differentially long exposure time at 125 °C. All experiments were performed simultaneously under dry air atmosphere with a heating rate of 10 K/min.

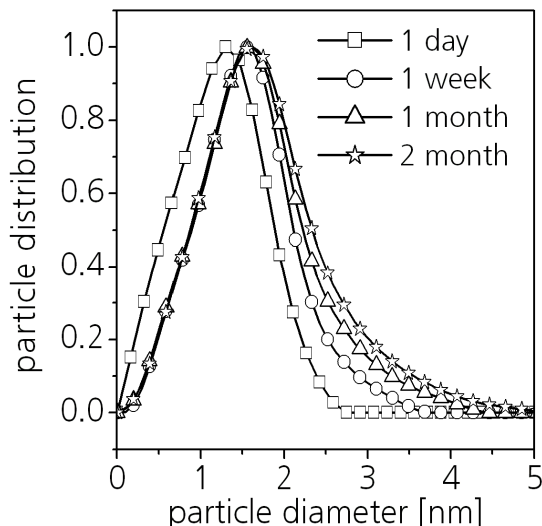


Figure 61. Measurements of particle size distribution by Analytical Ultracentrifugation (AUC) of a sol prepared with a precursor powder (ratio $\text{Ti}/\text{AcAc}/\text{H}_2\text{O}$ of 1/1/5, 5 h exposure time) dissolved in water.

The particle size distributions of a sol prepared from a precursor powder (ratio $\text{Ti}/\text{AcAc}/\text{H}_2\text{O}$ of 1/1/5), which was kept at 125 °C for 5 h is displayed in Figure 61. Shortly after dissolution in water the maximum of the particle size distribution is ~1.3 nm (1 day), increases immediately up to ~1.6 nm (1 week) and remains constant up to 2 month. However with increasing aging time a small portion of bigger particles seems to be formed continuously, but a Tyndall effect or a precipitate have never been observed up to 2 month of aging time.

SUMMARY OF 5.3.1 "SOLUBILITY AND STABILITY"

Using the standard precursor powder route water soluble precursor powders can be synthesized, which yield long-term stable coating solutions. Their solubility critically depends on the chemical composition.

These results agree with the earlier investigations on the structure of soluble precursor powders (Chapter 5.2.1) [LOE05]. In detail, the content of -OEt groups in the xerogel network is the factor determining the solubility and stability. However when the content of -OEt groups is lowered too much the resulting powders are hydrolytic stable, but do not dissolve anymore.

It has been demonstrated that the hydrolysis and condensations can also be very sensitively tuned by thermal treatment at 125 °C. Therefore this thermal procedure is very advantageous as additional step to exactly adjust the chemical composition of the water-soluble precursor powder. When this additional treatment is used the reproducibility of the powder synthesis concerning the long term stability is significantly improved compared to previous synthesis conditions.

Beside the usage of standard coating technique like dip coating, this water-based coating solutions now can be easily applied were alcohol based systems are to dangerous for i.e. spray coating experiments [LOE03b].

5.3.2 GENERAL CONSEQUENCE OF WATER AS SOLVENT

The evaporation of the solvent from a sol under reduced pressure yields the so called sol powder according to Figure 12 (Paragraph 5.2.2). This sol powder is very well suited to study the influence of the solvent on the structure and densification of the precursor powders as seen in Paragraph 5.2.2. When the precursor powders are dissolved in pure ethanol as solvent, no differences between the sol powders and the corresponding precursor powders have been noticed. However previous investigations in Paragraph 5.2.3 revealed that water, i.e. air moisture during thin film drying, significantly contributes to the structure of the precursor material.

If a precursor powder with ratio Ti/AcAc/H₂O of 1/1/5 and 5 h drying time is dissolved in water, a long term stable coating solution is obtained. Thermoanalytic investigations were done to investigate the influence of water as solvent on the structure of the precursor. In Figure 62 the thermogravimetric analysis and differential thermal analysis of the sol powder are displayed. Additionally the data of the respective original precursor powder from Figure 60 are given.

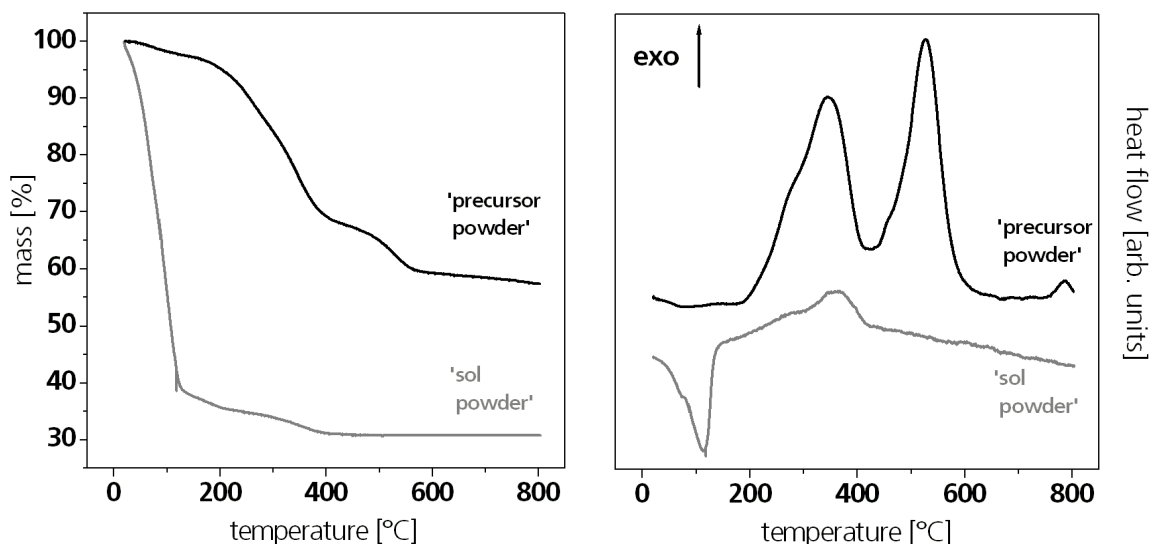


Figure 62. Thermogravimetric analysis (left) and differential thermal analysis (right) of sol powder obtained from a purely water based sol (grey lines). Additionally the data of the respective precursor powder (ratio Ti/AcAc/H₂O of 1/1/5, 5 h exposure time) from Figure 60 is given (black lines). All experiments were performed under dry air atmosphere with a heating rate of 10 K/min.

The total oxide yield of the sol powder is significantly decreased from 58 mass % to 31 mass % compared to the precursor powder. An additional large weight loss at around 100 °C is mainly responsible for this observation. A broad endothermal signal in the DTA is simultaneously accompanied by this observation and can be referred to the evaporation of incorporated water. This can be attributed to the gel like appearance of the sol powder. Obviously the vacuum conditions on the rotating evaporator were not sufficient enough to remove all of the solvent.

However, for the sol powder the mass loss, associated with the degradation of organic moieties, is in sum only around 10 mass %. No indication for any ethanolate group is noticeable and the only very stable acetylacetonate groups remain.

Though, it has to be noted that the conditions on the rotational evaporator i.e. the high temperature combined with an excess of water favors a hydrolytic separation of -OEt groups. For that reason based on the existing data, it can not be totally clarified, if the determined chemical composition of the sol powder is equivalent to the real composition of the precursor particle in a water based solution.

Furthermore an exothermal signal in the DTA of the precursor powder appears around an annealing temperature of 800 °C. Simultaneously no weight change occurs. In that case, this is a typical indication for a phase transformation of anatase to rutile. The sol powder gives no indication for a phase transformation and therefore points out a different crystallization and densification behavior of the sol powder compared to the precursor powder.

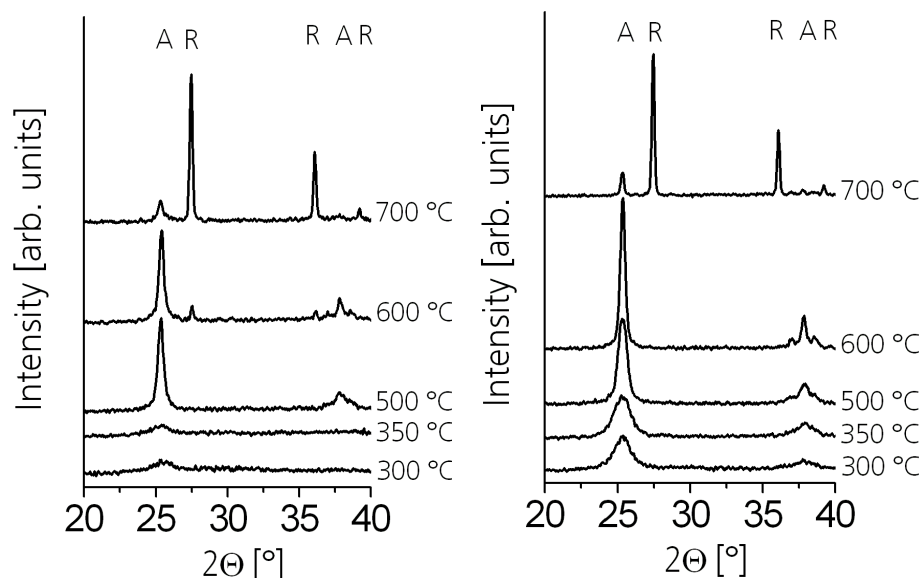


Figure 63. X-ray diffraction patterns of precursor powders (left) and sol powders (right) prepared from purely water based sol. The samples were annealed at temperatures between 300 °C and 700 °C as indicated. Peaks assigned to anatase (A) and rutile (R) are marked individually.

Nevertheless the x-ray diffraction patterns of the isothermally annealed samples can not clearly confirm this observation (Figure 63). Both types of powder present similar diffraction patterns at 700 °C with a major rutile phase. However, the precursor powder sample annealed at 600 °C shows a small reflection, which can be referred to a minor portion of rutile, whereas the sol powder reveals at 600 °C only anatase.

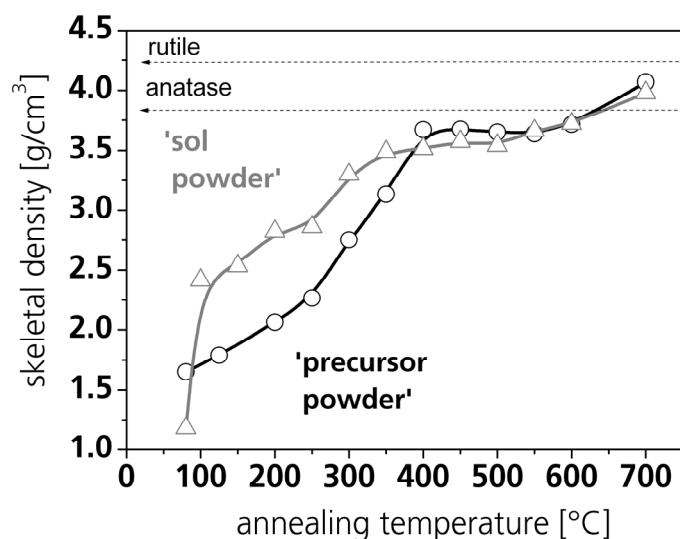


Figure 64. Skeletal density of sol powders prepared from a purely water based sol as a function of annealing temperature (Δ). For comparison the data of the respective precursor (O) are given. The theoretical densities of rutile and anatase are given as references [CRC94].

The skeletal densification (Figure 65) of the water soluble precursor powder is quite similar to the performance of the precursor powder used for the preparation of ethanol based coating solutions (Paragraph 5.2.2, Figure 15). The powders present a typical continuous densification up to ~ 3.6 g/cm³ at 400 °C. Until this temperature the degradation of organic moieties is assumed to be finished under the chosen RTA conditions and the formation of anatase clearly starts (Figure 63).

The slightly lowered skeletal density compared to the theoretical density of anatase might be mostly explained by the existence of residual carbon due to incomplete degradation of organic moieties. The grayish color of the annealed samples confirms that assumption, too. A further increase of density up to 700 °C can be explained by the phase transformation of anatase to rutile (Figure 63).

In contrast to the precursor powder the initial sol powder has a very low density ($\sim 1.2 \text{ g/cm}^3$), because of the high water content. When the water is vaporized at 100 °C the skeletal density rapidly increases, because of the low content of organics. The further skeletal densification has reached a local maximum at 350 °C. That is, because the xerogel consists only of acetylacetonate, which is known to decompose at lower temperatures than -OEt groups, at 200 – 350 °C (Paragraph 5.1). This even might facilitate the early formation of anatase compared to the precursor powder.

However, above 350 °C the skeletal density of the sol powder is lower than the density of the respective precursor powder. The skeletal density of anatase is only reached at temperatures above 600 °C. The powder samples were colorless above 350 °C, which almost rules out the reduction of skeletal density by residual elementary carbon. Nevertheless the existence of closed pores was also excluded by IR-spectroscopy (data not shown).

Therefore additional information about the microstructure of these samples is required. The respective isotherms of the N_2 -sorption experiments are shown in Figure 65. The water soluble precursor powder in general exhibits a quite similar pore structure as seen before in the case of the precursor powder used for ethanol based coating solutions (Paragraph 5.2.2, 5.2.3.1). At first Type I isotherms, caused by micropores with a pore diameter lower than 2 nm, are visible at an annealing temperature of 350 °C. These pores transform by formation of anatase at 400 °C to mesopores (Type IV isotherm) with a medium pore diameter of 4 nm. Upon further annealing to 600 °C a quite dense microstructure is generated. The mesoporosity and surface area as functions of annealing temperature illustrate that behavior as well (Figure 66). They present their respective maximum at 400 °C and afterward decrease significantly up on densification.

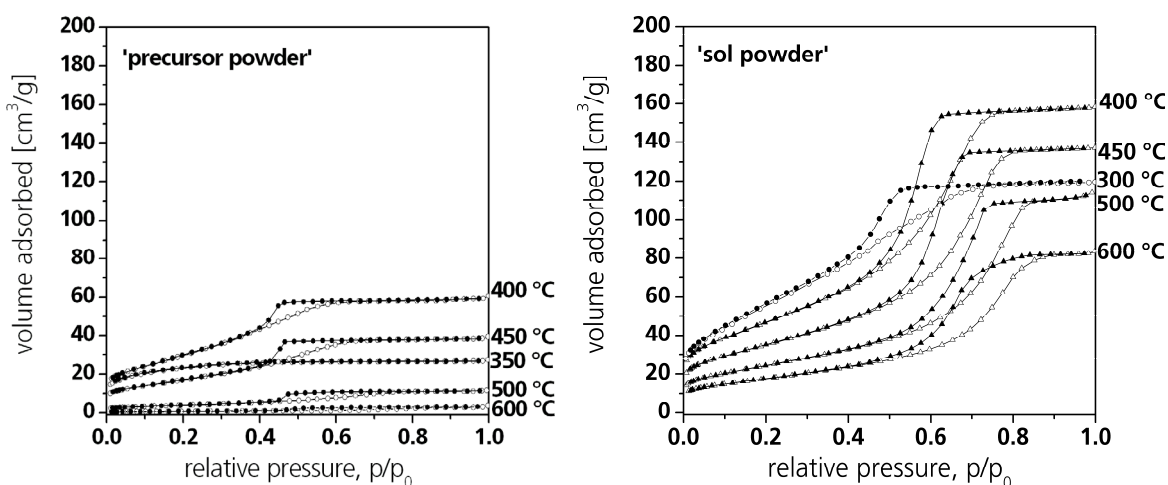


Figure 65. N_2 -adsorption isotherms for precursor powders (left) and purely water based sol powders (right) that had been isothermally annealed for 1 hour at the temperatures indicated.

This situation changes when the sol powder is considered. Simultaneous to the early crystallization of anatase, the sol powder already forms mesopores (Type IV isotherm) at 300 °C annealing temperature. These mesopores with a medium pore diameter of 4 nm increase continuously up on annealing to a pore diameter of 7 nm at 600 °C.

The pore structure just as well is reflected by the evolution of surface area and porosity of the sol powder (Figure 66). In general the sol powders have a significant higher surface area and porosity than the appropriate precursor powder. The relatively high porosity at 600 °C (33 %) is remarkable. Such a densification behavior has up to now never been noticed for any materials obtained from soluble precursor powders based on acetylacetonate. In the literature when in powders at 600 °C such high amount of porosity is mentioned, mostly surfactant assistant synthesis routes were used [GRO03,YAN99]. Upon annealing to 700 °C even in the sol powder these mesopores merge together by sintering and the surface area decreases (Figure 66).

It seems apparent that due to the high water content during the sol powder synthesis and the low amount of residual organic a wide meshed gel network is formed. Up on the vaporization of water and the decomposition of residual organic moieties this transforms to a highly porous ceramic powder.

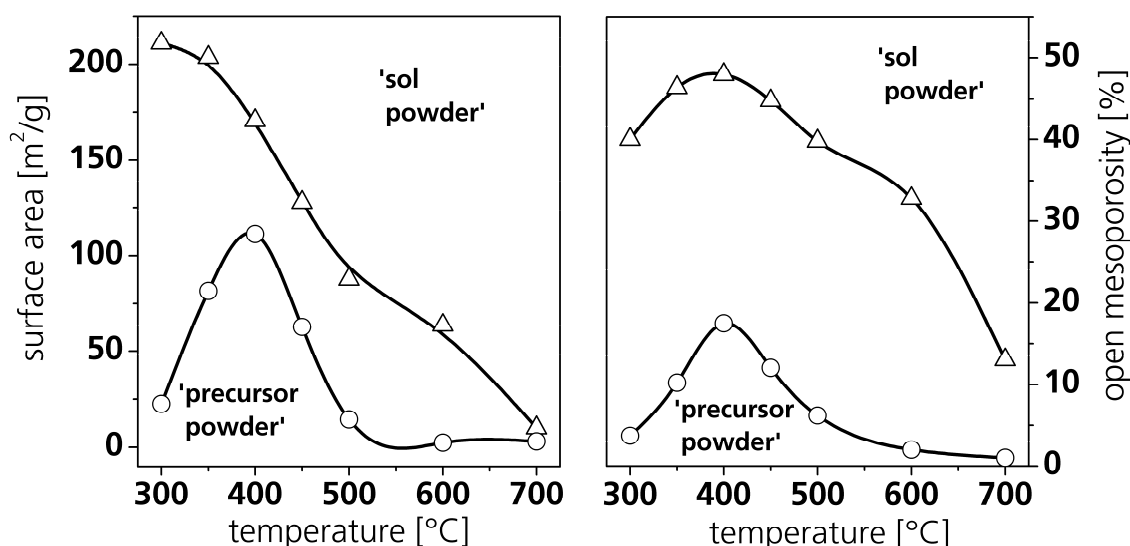


Figure 66. Surface area (left) and open mesoporosity (right) as a function of annealing temperature precursor powders (○) and sol powders (△) prepared from purely water based sol.

SUMMARY OF 5.3.2 "GENERAL CONSEQUENCE OF WATER AS SOLVENT"

When a precursor powder is dissolved in ethanol no difference between the precursor powder and the sol powder was noticed. However, if water is used as solvent the chemical composition is influenced significantly. Due to hydrolysis reactions only a large amount of water in addition to acetylacetonate residues is still present in the sol powder.

Therefore the densification of precursor powder and the corresponding water based sol powder completely differ. By annealing of the sol powder a highly porous microstructure is generated, which up to 600 °C exhibits relatively porous microstructure.

5.3.3 CHANGES INDUCED BY THE SOLVENT COMPOSITION

The addition of 1,5-pentanediol to ethanol based coating solutions prevents hydrolysis and condensation reactions induced by air moisture (Paragraph 5.2.3) [BOC06]. When pure water is used as solvent even the so called water stable precursor undergoes partially hydrolysis reactions (Paragraph 5.3.2). Now it is highly interesting if the addition of 1,5-pentanediol can prevent hydrolysis of the precursor, even when this water stable precursor is dissolved in water.

Therefore in Figure 67 the thermal analysis of sol powders obtained from water based coating solutions containing 0 % (Δ), 10 % (\blacktriangle) and 20 % (\blacktriangle) 1,5-pentanediol is compared. All three type of sol powders present a large overall mass loss up to 800 °C, which increases with increasing content of 1,5-pentanediol. This can directly be referred to the high content of water in the 1,5-pentanediol free sol powder, which is ~60 mass % compared to ~40 mass % in the other two water based sol powders.

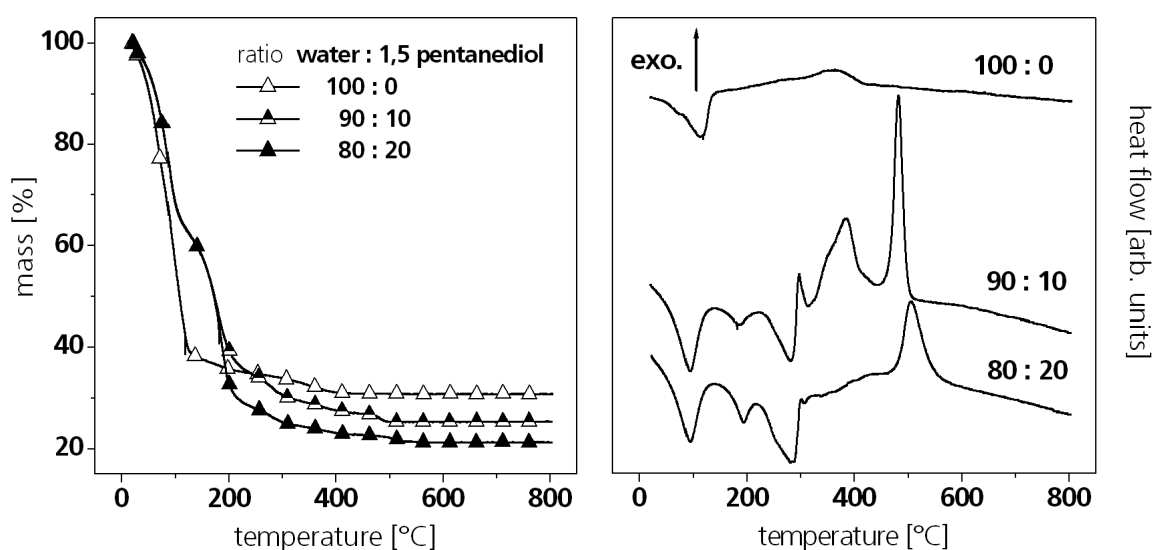


Figure 67. Thermogravimetric analysis (left) and differential thermal analysis (right) of sol powders obtained from water based coating solutions containing 0 % (Δ), 10 % (\blacktriangle) and 20 % (\blacktriangle) 1,5-pentanediol (compositions 100:0, 90:10 and 80:20 respectively). The experiments were performed under dry air atmosphere with a heating rate of 10 K/min.

Beside the first large mass loss, which is associated with an endothermic signal (~100 °C), the sol powders prepared with the addition of 1,5-pentanediol present two additional endothermic signals at higher temperature regimes of ~150-210 °C and ~220-300 °C, respectively. Since the third endothermic signal (~220-300 °C) is attributed to the evaporation of 1,5-pentanediol (bp.: 242 °C), the second signal (~150-210 °C) can be explained by the partial evaporation of free acetylacetone (bp.: 139 °C).

The extreme hydrolytic conditions during the sol powder synthesis probably lead to a generation of uncoordinated acetylacetone. Thus, when 10 mass % of 1,5-pentanediol is used for the sol powder preparation a broad exothermic signal (maximum: 400 °C) is still visible for the decomposition of acetylacetone. Whereas, when the content of 1,5-pentanediol is further increased up to 20 mass % no clear signal is still noticeable for the pyrolysis of acetylacetone.

When aqueous solutions contain 1,5-pentanediol they present a exothermal signal, which is normally assigned to the decomposition of -OEt groups. However, as discussed before in Paragraph 5.2.2, it can not clearly distinguished whether these peaks originate from diol groups in a different chemical environment as those vaporize around $\sim 220\text{--}300\text{ }^{\circ}\text{C}$ or if the 1,5-pentanediolate has a protective function for -OEt moieties during sol powder synthesis.

The respective backbone densification of the sol powders is displayed in Figure 68. The skeletal densities of all freshly prepared water based sol powders are quite similar around 1.1 g/cm^3 . That is, because all powders contain a large amount of water, due to the insufficient vacuum condition on the rotational evaporator. Though, the water is vaporized ($100\text{ }^{\circ}\text{C} - 150\text{ }^{\circ}\text{C}$) the powders prepared with the addition of the diol present a still very low density due to the relative high content of organics in the xerogel. Compared to this behavior, the density of the 1,5-pentanediol free sol powder significantly increase in this temperature regime.

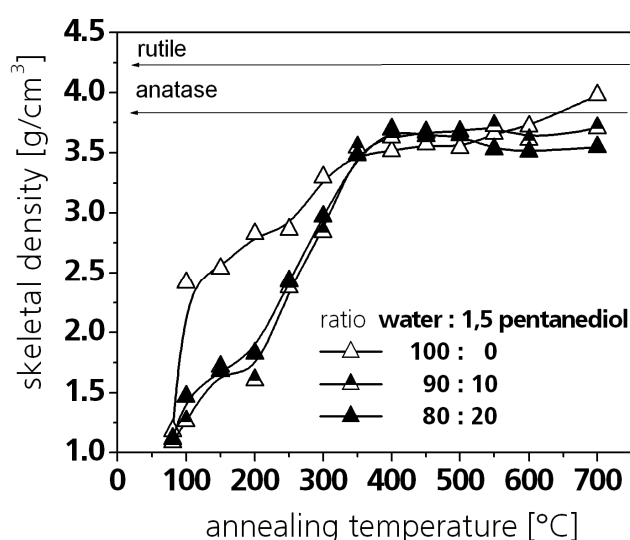


Figure 68. Skeletal densities of sol powders prepared from water based sols containing 0 % (Δ), 10 % (\blacktriangle) and 20 % (\blacktriangle) 1,5-pentanediol as a function of annealing temperature. The theoretical densities of anatase and rutile are given as references.

Under RTA conditions at around $350\text{ }^{\circ}\text{C}$ the vaporization and decomposition of organic residues is nearly finished and the skeletal density has already reached its maximum level ($3.5 - 3.6\text{ g/cm}^3$). The crystallization of anatase (Figure 69) has been simultaneously started at $\sim 300\text{ }^{\circ}\text{C} - 350\text{ }^{\circ}\text{C}$. When the annealing temperature is further increased the crystallite size is increasing (data not shown) and at $700\text{ }^{\circ}\text{C}$ the powders partially transform to rutile. The sol powders prepared with 1,5-pentanediol present a retarded formation of rutile (Figure 69 (right)) and therefore a lower density than the purely water based sol powder (Figure 69 (left, middle)) at $700\text{ }^{\circ}\text{C}$.

Both, a reduced density relative to the theoretical density and a suppressed phase transformation with increasing content of diol, have already been observed in the case of ethanol based sol powders (Paragraph 5.2.2). At that time a high densification rate under RTA annealing conditions led to an incomplete decomposition of organic moieties and therefore an incorporation of residual carbon. This residual carbon lowered the skeletal density and hindered the phase transformation of anatase to rutile.

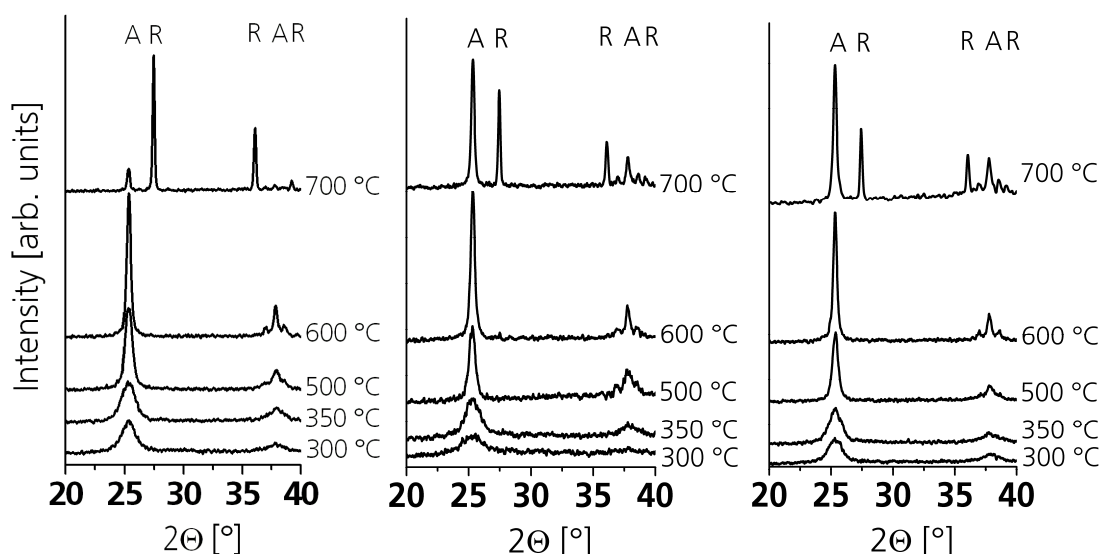


Figure 69. X-ray diffraction patterns of sol powders prepared from water based sols containing 0 % (left), 10 % (middle) and 20 % (right) 1,5-pentanediol respectively. The samples were annealed at temperatures between 300 °C and 700 °C as indicated at the right side of the figure. Peaks assigned to anatase (A) and rutile (R) are marked individually.

In the case considered here, the grayish to black coloring of the samples at 600 and 700 °C is also indicating a high content of incorporated carbon for the samples containing 10 and 20 mass % of 1,5-pentanediol. Nevertheless for a better understanding of the presented behavior further information about the microstructure are required.

For 1,5-pentanediol containing sol powders N_2 -sorption experiments (Figure 70) reveal a pore structure quite similar to the precursor powder (Figure 65 (left)). At temperature above 300 °C a microporous network (Type I isotherm) with an average pore diameter of 2 nm is observed, which transforms up on annealing to a mesoporous network (Type IV isotherm) with medium pore radius of 4 nm. Then above 500 °C only minor amounts of N_2 are adsorbed as it is typical for a quite dense material. As already discussed in the previous Paragraph 5.3.2, up to 600 °C the sol powder without the addition of 1,5-pentanediol presents a porous microstructure.

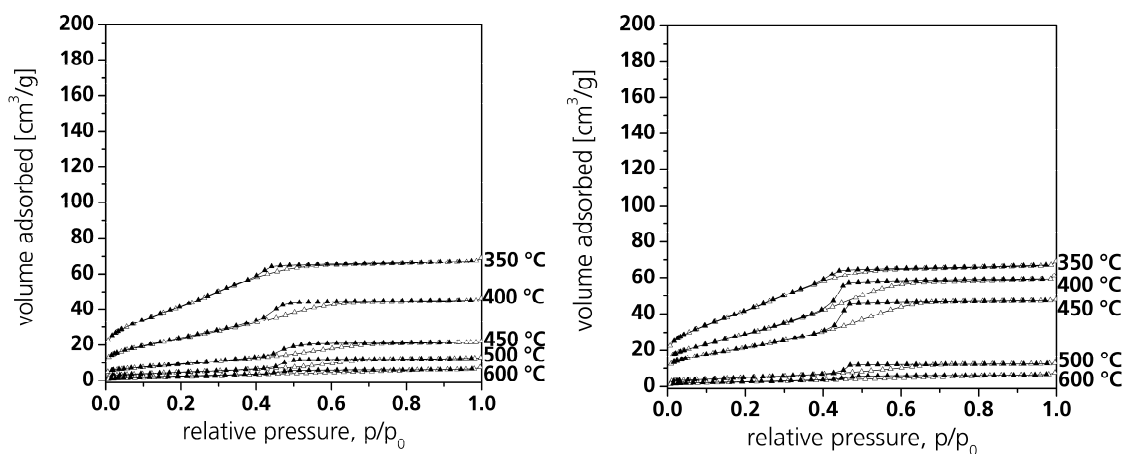


Figure 70. N_2 -adsorption isotherms for sol powders precursor powders prepared from water based sols containing 10 % (left) and 20 % (right) 1,5-pentanediol respectively.

The surface area and mesoporosity of the sol powder (Figure 71) behave in agreement with the evolution of pore structure. The sol powders prepared from 1,5-pentanediol containing solutions have at the corresponding temperatures always a significant lower surface area and mesoporosity than the purely water based sol powder. Similar behavior has been seen before in the case of ethanol based sol powders (Paragraph 5.2.2)

The higher content of organic in the 1,5-pentanediol containing sol powders seems to promote a better densification and formation of a dense ceramic powder. Though, this results in an incomplete decomposition of organic residues and therefore the inclusion of residual carbon. This residual carbon can reduce the skeletal density and retards phase transformation of anatase to rutile.

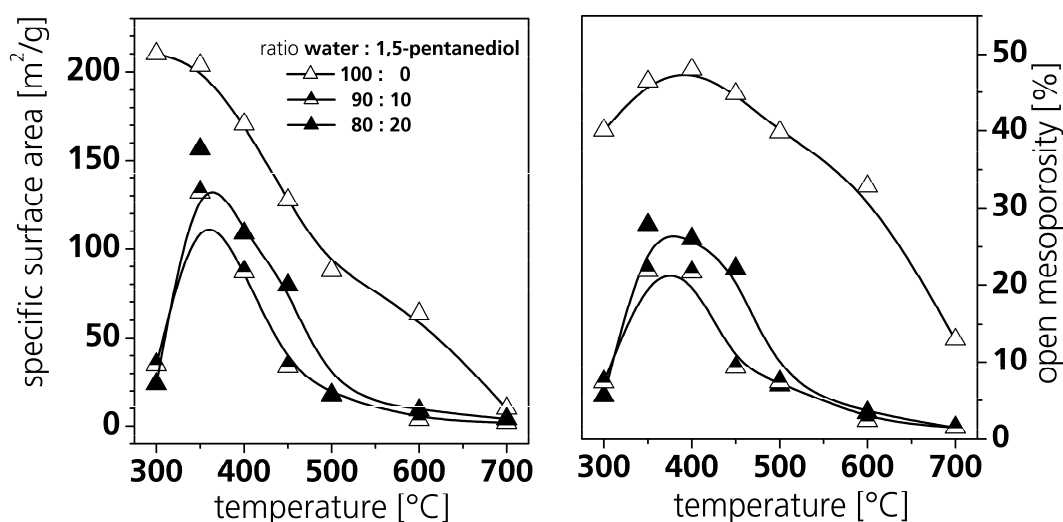


Figure 71. Specific surface area (left) and open mesoporosity (right) as a function of annealing temperature of sol powders prepared from water based sols containing 0 % (Δ), 10 % (\blacktriangle) and 20 % (\blacktriangle) 1,5-pentanediol respectively.

SUMMARY OF 5.3.3 "CHANGES INDUCED BY THE SOLVENT COMPOSITION"

Sol powders synthesized from aqueous solutions with the addition of 1,5-pentanediol still contain a high content of organics. These results suggest a protective function of the diol to the hydrolytic sensible -OEt groups.

The differences in the chemical composition significantly contribute to the skeletal densification at low temperatures (< 300 °C), but in the higher temperature regime no general differences are visible. The skeletal densities of the sol powders seem to be reduced by inclusions of residual carbon.

However, the addition of 1,5-pentanediol retards the phase transformation of anatase to rutile as seen also before in the case of the ethanol based sol powders. Furthermore the addition of 1,5-pentanediol influences the porosity and pore structure of the powders investigated. Even at a temperature of 600 °C without the addition of 1,5-pentanediol, still a mesoporous material is obtained. At this elevated temperature all other sol powders synthesized with the addition of 1,5-pentanediol result in dense ceramic powders.

5.3.4 DENSIFICATION OF WATER BASED FILM POWDERS

5.3.4.1 GENERAL CONSEQUENCE OF LARGE SURFACE-TO-VOLUME RATIO AND AIR MOISTURE DURING FILM FORMATION

When ethanol based coating solution were dried as a thin film, without the addition of 1,5-pentanediol, the high surface-to-volume ratio and air moisture during the thin film formation led to the hydrolysis of -OEt moieties. Therefore the chemical composition and microstructure of thin sol-gel films prepared from pure ethanol based coating solutions differs significantly from the structure of the corresponding sol powders. Though, when water based coating solutions are used, the presence of air moisture during the dip coating procedure may be negligible, but the influence of large surface-to-volume ratio on thin film structure is still unknown.

In Figure 72 the thermoanalysis of a sol powder and the corresponding film powder obtained from a purely water based sol are shown. On the first view the powders differ significantly in their total mass loss, because of the large differences regarding their water content. The sol powder has a residual water content of ~60 mass % compared to ~10 mass % for the film powder. In conclusion, the high surface-to-volume ratio of a film powder during drying seems to cause a better evaporation of the solvent, yielding a dry film powder instead of a wet gel (sol powder).

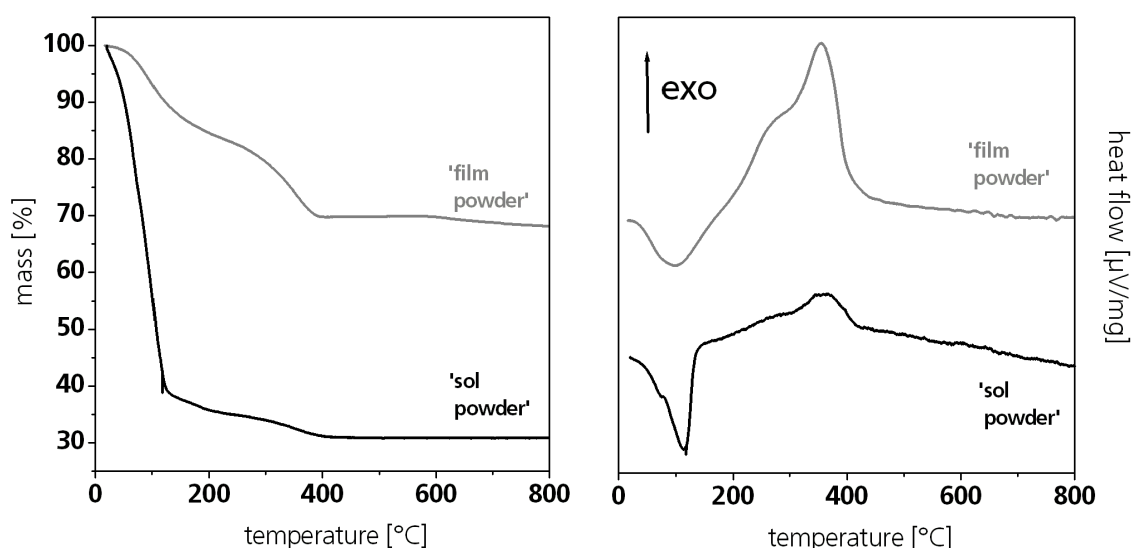


Figure 72. Thermogravimetric analysis (left) and differential thermal analysis (right) of film powder obtained from a purely water based sol (grey lines). Additionally the data of the respective sol powder from Figure 62 is given (black lines). All experiments were performed under dry air atmosphere with a heating rate of 10 K/min.

The chemical decomposition of both powders, investigated by differential thermal analysis, seems quite similar: neither the sol powder nor the film powder present any indications for the presence of -OEt groups in the xerogels. In general the content of acetylaceton and the decomposition behavior of the water based film powder correspond very well to the ethanol based film powder in Paragraph 5.2.3.1. However, it can not be totally clarified, if the hydrolysis of -OEt groups happened during thin film drying or already in the sol, because of the unclear influence of the conditions used during the rotational evaporation on the chemical structure of the sol powder.

The different content of water in the sol powder and film powder xerogels also causes that the starting values for the skeletal density significantly differ (Figure 73). After the evaporation of water both sorts of powders exhibit a quite similar densification behavior, as seen before in the case of sol-gel materials that contain a low amount of organic residues. At higher annealing temperatures the skeletal densification is even quite similar. This agrees with the phase composition of these samples (data not shown).

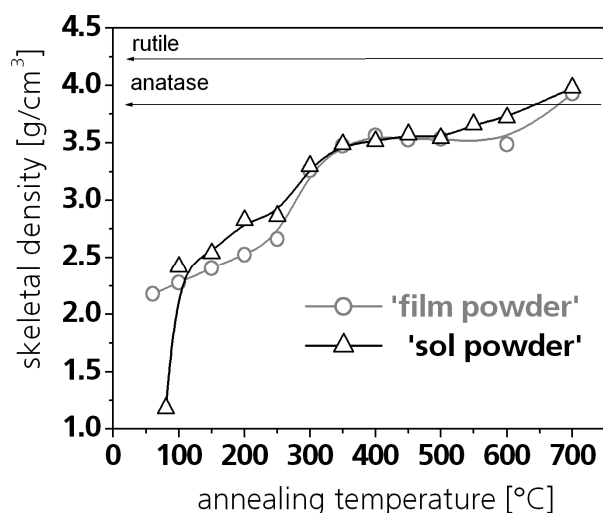


Figure 73. Skeletal density of film powders prepared from a purely water based sol as a function of annealing temperature (○). For comparison the data of the respective sol powder from Figure 64 are shown (△). The theoretical densities of rutile and anatase are given as references [CRC94].

However the N_2 -sorption measurements reveal that the film powders have a denser microstructure than the comparable sol powders. Only the sample annealed at 300 °C – 450 °C exhibit Type-I isotherms (Figure 74 (right)) that result from micropores with a pore diameter below 2 nm. After annealing at 450 °C no open porosity is detected, but IR-measurements still indicate the presence of closed pores filled with CO_2 (data not shown). As considered in the previous paragraphs up to 600 °C the corresponding sol powder presents an open mesoporous microstructure with a residual porosity of ~33 %.

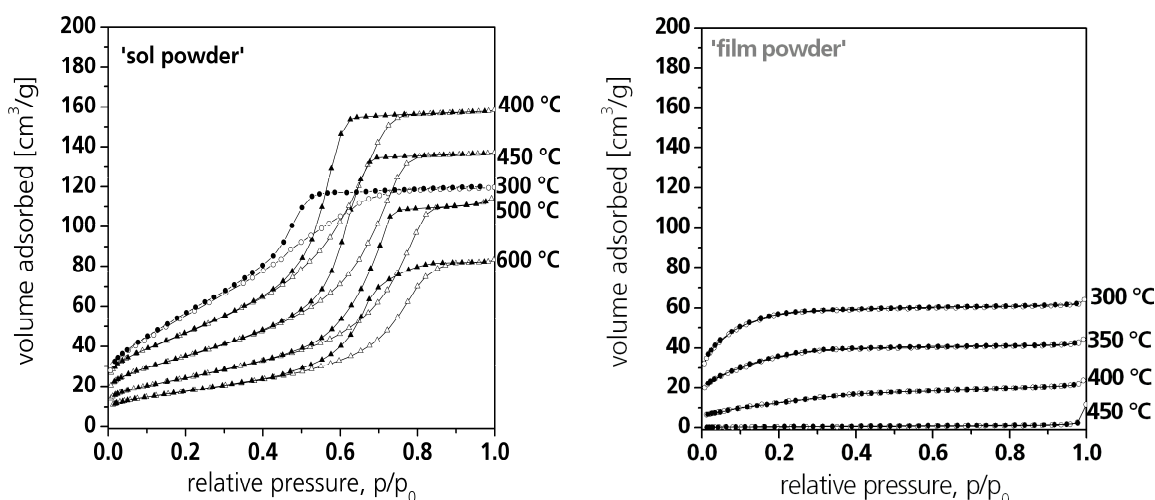


Figure 74. N_2 -adsorption isotherms for purely water based sol powders (left) and the corresponding film powders (right) that had been isothermally annealed for 1 hour at the temperatures indicated.

In the case of the sol powder the high water content leads to the formation of a wide meshed gel network. Upon thermal annealing of this gel a porous ceramic powder is obtained. In contrast to this the water content in the film powder is significantly lower, resulting in better network densification.

5.3.4.2 CHANGES INDUCED BY 1,5-PENTANEDIOL IN THE SOLVENT

The addition of 1,5-pentanediol strongly affects the densification behavior of water based sol powder. Nevertheless it must be considered that the investigation of sol powder does not take in account the large surface-to-volume ratio during practical film drying.

The thermal analysis of film powders obtained from water based coating solutions containing 0 % (○), 10 % (◐) and 20 % (●) 1,5-pentanediol are displayed in Figure 75. With raising content of 1,5-pentanediol the total weight loss increases from ~30 mass % up to ~65 mass %. Especially the weight loss around 200 – 300 °C, which is directly attributed to the exothermal decomposition of 1,5-pentanediol, significantly increases. The DTA of the film powder prepared from the sol which contains 10 % 1,5-pentanediol presents, beside a broad signal from the decomposition of acetylaceton, an additional sharp signal due to the exothermal degradation of 1,5-pentanediol. No signal for –OEt moieties can be identified.

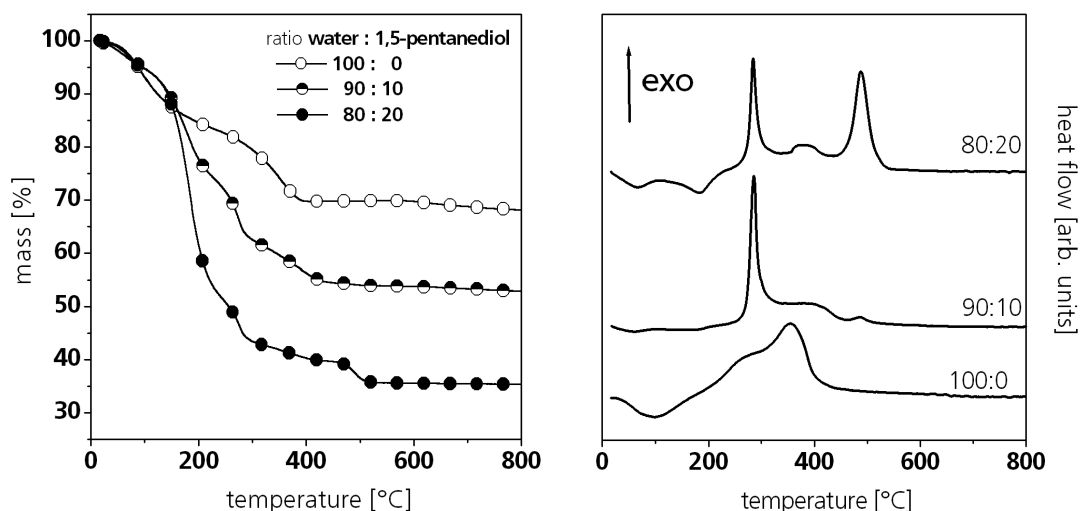


Figure 75. Thermogravimetric analysis (left) and differential thermal analysis (right) of film powders obtained from water based coating solutions containing 0 % (○), 10 % (◐) and 20 % (●) 1,5-pentanediol (compositions 100:0, 90:10 and 80:20 respectively). The experiments were performed under dry air atmosphere with a heating rate of 10 K/min.

However, when the fraction of 1,5-pentanediol is raised up to 20 %, two additional small endothermic bands attributed to the evaporation of water (100 °C) and acetylaceton (150 °C), are noticed. Furthermore one additional exothermic signal around 500 °C appears, which usually belongs to the decomposition of –OEt groups (Paragraph 5.1) [LOE03].

From this observation it can be concluded that without 1,5-pentanediol all –OEt groups are removed by hydrolysis and condensation reactions, which generates a rigid network as seen before in Paragraph 5.2.3.1.

The addition of 10 % 1,5-pentanediol to water based coating solutions is obviously not sufficient to prevent the hydrolytic separation of the –OEt groups during thin film drying. The network should be highly linked, but still maintain some more plasticity due to the presence of the 1,5-pentanediol. In the case of the corresponding sol powder a high content of –OEt was still noticed. This observation can be directly attributed to the large surface-to-volume ratio, which prevails during thin film drying.

When an addition of 20 % of 1,5-pentanediol is used even under this extreme hydrolytic conditions –OEt groups are still present in the xerogel. Therefore an addition of 20 % 1,5-pentanediol should preserve the highest degree of network plasticity.

The skeletal densification of the three water based film powders (Figure 76) is in agreement with the DTA/TG observation. The large difference of the skeletal densities at low temperatures is the consequence of the different content of organic residues in the film powders. A quite similar behavior has already been seen in the case of the ethanol based film powders in Paragraph 5.2.3.2. At an annealing temperature of 250 °C the skeletal density of the film powders coincide. Afterwards up to 450 °C with increasing 1,5-pentanediol content a lowered densities increase is noticed. This might be explained by the corresponding concentration of residual organics, which reduces the skeletal densities.

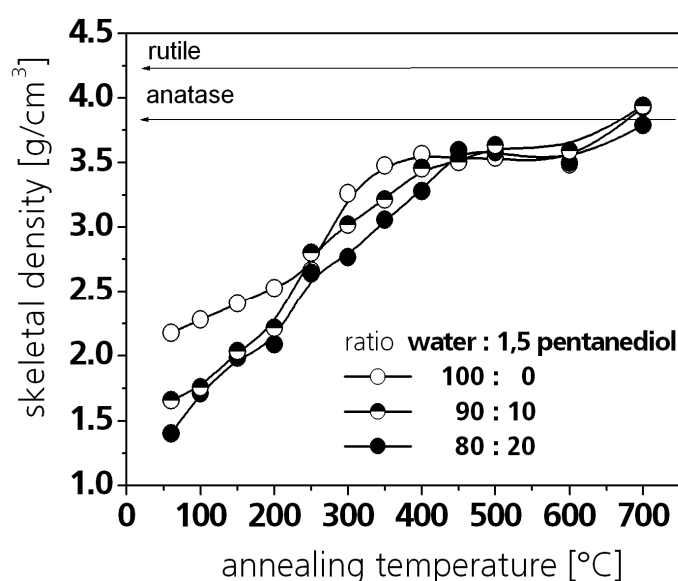


Figure 76. Skeletal densities of film powders prepared from water based sols containing 0 % (○), 10 % (◐) and 20 % (●) 1,5-pentanediol as a function of annealing temperature. The theoretical densities of anatase and rutile are given as references.

At higher annealing temperatures the skeletal densification and even the phase evolution of all three film powders is quite similar. It is obvious that up to 600 °C the theoretical density of anatase is never reached (no rutile detectable), which can be explained by the presence of residual carbon or/and the presence of closed pores as well. According to this observation in N₂-sorption experiments all powders were not accessible to the measurement gas after annealing at 450 °C (data not shown). A related observation has already been discussed before in detail (Paragraph 5.2.3.2) in a comparable case for ethanol based film powders.

SUMMARY OF 5.3.4 "DENSIFICATION OF WATER BASED FILM POWDERS"

The high surface-to-volume ratio of film powders compared to sol powders enhances film drying significantly. Therefore after the evaporation step the film powders have a crumbly appearance, whereas the sol powders have still a gelly consistency with a high content of residual water. Upon annealing the sol powder generates a mesoporous microstructure, whereas film powders were rather dense.

Film powders prepared from pure water based coating solutions immediately form a rigid network during drying and aging. The addition of 1,5-pentanediol significantly contributes to the drying and aging behavior of the water based film powders. The addition of 1,5-pentanediol enhances the stability towards hydrolysis and condensation reactions and preserves more network flexibility. However, a content of 10 % 1,5-pentanediol is not large enough to prevent the hydrolysis of the -OEt groups.

In summary, despite of the different drying and aging behavior of the film powders at higher temperatures the densification behavior is quite similar. In general, the water based film powders showed a comparable densification behavior as ethanol based film powders.

5.3.5 MICROSTRUCTURE AND CRACKING OF THIN FILMS

When thin films are to be compared concerning their crack formation, they must have undergone a comparable densification, i.e. they should reach the same ceramic end film thickness [BOC06]. Nevertheless thin films prepared by dip-coating method, using sols based on solvents with a low vapor pressure, mostly present an inhomogeneous film thickness [OHY03]. Here in the case the film thickness normally increases in the vertical direction from the top of the plate to the bottom, but on the horizontal line no major variations occur. That is, because water vaporizes slower than ethanol, which results in later gelation and causes a longer vertical movement of the wet film. Therefore reproducibility of results is only ensured, when investigations on cracking and microstructure are always performed on the same horizontal position of the film, typically in the middle of the substrate.

Coating series were prepared with a final ceramic end film thickness of around 120 nm at 600 °C annealing temperature. The corresponding film shrinkage as a function of annealing temperature is displayed in Figure 77. The films were obtained from water based coating solutions containing 0 % (○), 10 % (◐) and 20 % (●) 1,5-pentanediol. At low temperatures (100 – 200 °C) films prepared from the pure water based sol show the smallest thickness as one would expect from organic content (Figure 75) and skeletal density (Figure 76). Both films including 1,5-pentanediol present a nearly similar densification starting from a higher thickness level. Since at ~ 400 °C the burn out of the organic is finished the film thickness of all coatings coincide and continues nearly analogous up to 600 °C.

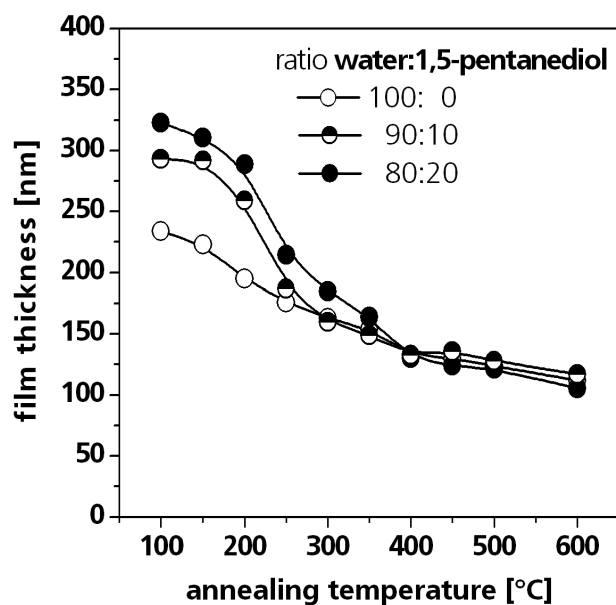


Figure 77. Film thickness of TiO_2 films as a function of annealing temperature. The films were obtained from water based coating solutions containing 0 % (○), 10 % (◐) and 20 % (●) 1,5-pentandiol.

The phase evolution of the coatings (data not shown) is quite similar. At an annealing temperature of 400 °C all coatings start to form anatase that is stable up to 700 °C. No transformation to rutile is noticeable. Similar results were obtained in the case of the ethanol based coatings and are discussed in Paragraph 5.2.3 in detail.

Exemplarily for the investigated water based films, TEM images of a thin film prepared from a pure water based coating solution and annealed at 600 °C are displayed in Figure 78. The measured film thickness of ~130 nm agrees well with the results from UV-Vis, reminding the usual variation in film thickness in films prepared from water based sols. Furthermore no clear indications for pores were given in the images. The observed crystallite size of 20 – 25 nm coincides very well with the value obtained from the integral breath of the GIXRD pattern by the Debye – Scherrer equation. The indicated net planes are originated from anatase crystallites in (101) reflections.

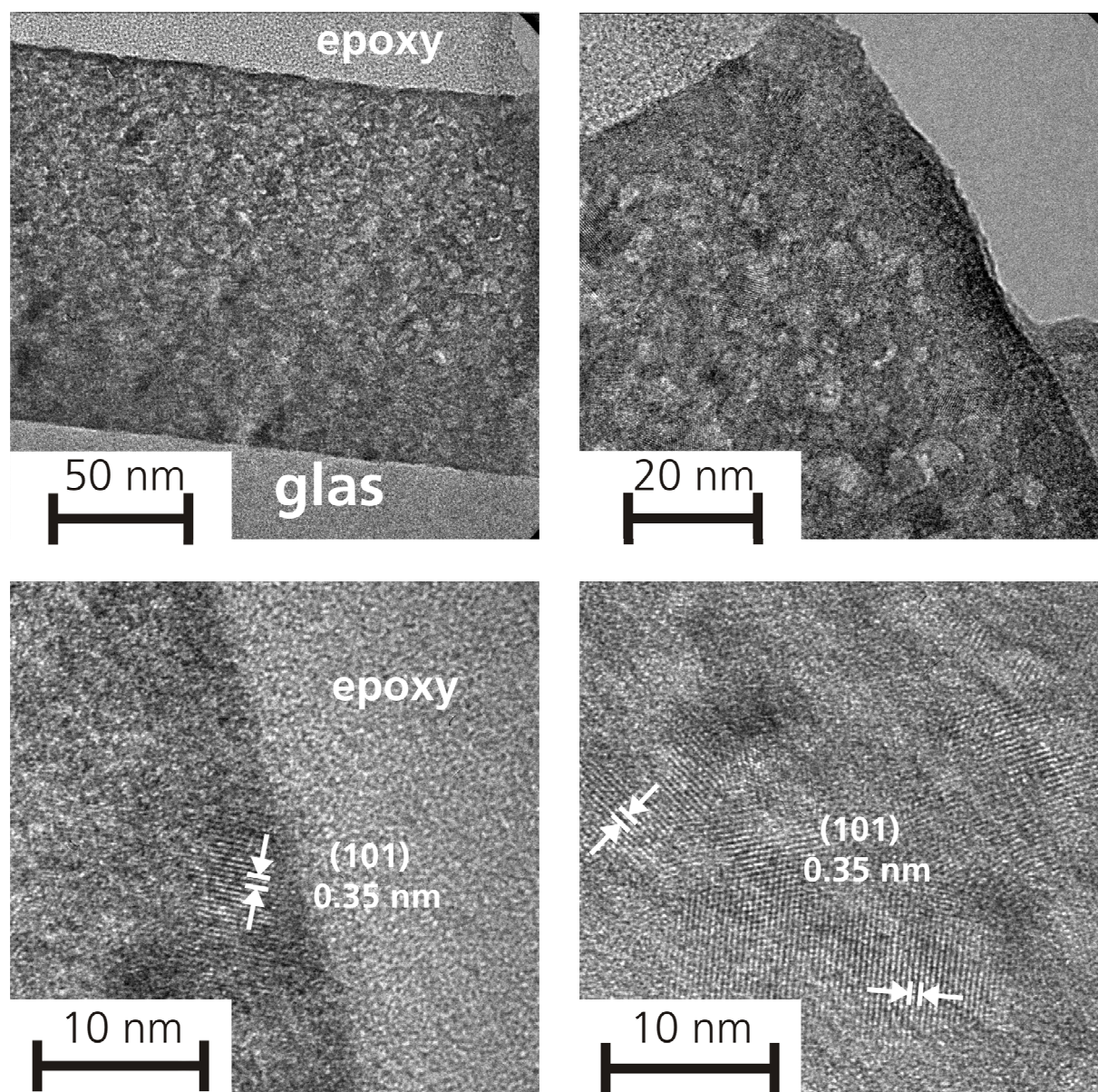


Figure 78. TEM bright field images of thin TiO_2 film on glass. The film was prepared from a coating solution based on pure water (100:0) and was annealed at 600 °C.

Shrinkage of a thin film constraint by the substrate and mismatch of the thermal expansion coefficients induces tensile stress in the film (Paragraph 5.2.5.1) [BRI92]. Cracking of the film occurs when the stress i.e. tensile stress exceeds the cohesive strength of the film. Therefore in the case here one would expect that the coatings comprising 1,5-pentanediol exhibit a higher ratio of cracks than the pure water based films. However, the display of defect density as a function of annealing temperature (Figure 79) brings out something contrary. Without addition of 1,5-pentanediol films show always a closed cracking pattern. Films with 1,5-pentanediol were totally defect free (80:20) or have only star like defects on a minor level. The defect density of all investigated types of films was independent of the used annealing temperature.

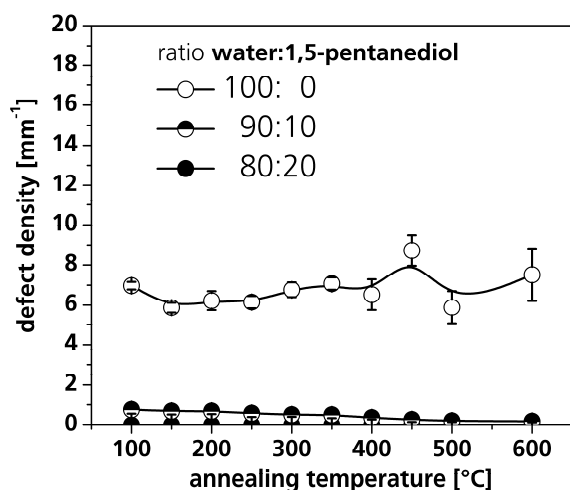


Figure 79. Defect densities for TiO_2 coatings based on different solvent compositions water:1,5-pentanediol as a function of annealing temperature. Thin films were prepared with a withdrawal rate that results at 600 °C in an end film thickness of 120 nm.

From this results it can be excluded that the cracks arise from tensile stress, which is generated neither from the uniaxial film shrinkage during decomposition of organic residues nor from thermal mismatch of substrate and film. In fact it can be concluded that the cracks result from tensile stress generated during drying and aging ≤ 100 °C. The plasticity of films prepared from the diol free solution is not high enough to reduce tensile forces during thin film drying and therefore cracking occurs. Films prepared with 1,5-pentanediol stay crack free, because they have maintained some plasticity during thin film drying.

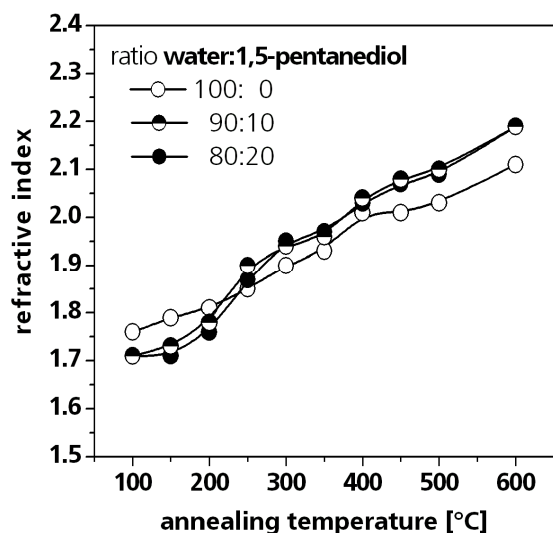


Figure 80. Refractive index of TiO_2 films as a function of annealing temperature. The films were obtained from water based coating solutions containing 0 % (○), 10 % (◐) and 20 % (●) 1,5-pentanediol.

The refractive index as function of annealing temperature of these films (Figure 80) corroborates with this results. Films prepared with the addition of 1,5-pentanediol have at low temperatures (100-150 °C) a reduced refractive index compared to films prepared without the use of the diol. As the temperature is increasing the refractive index of films obtained from 1,5-pentanediol free sol falls behind the other. Cracks lead to an uncovered glass surface that might reduce the overall measured refractive index (Paragraph 5.2.3.2) [MAL07]. Since films prepared without the use of

1,5-pentanediol exhibit a closed cracking pattern the reduction of the refractive index can be mainly attributed to the presence of cracks and not to differences in microstructure i.e. porosity.

Generally when water based and ethanol based coatings are compared many similarities are noticeable: (1) the phase evolution and microstructure at temperatures above 400 °C is almost identical. (2) In both cases the crack formation is attributed to tensile stresses formed during drying and aging at low temperatures. (3) The addition of 1,5-pentanediol to the sols results in a reduction/prevention of crack formation. That is, because 1,5-pentanediol acts as plastification agent, which preserves some network plasticity at low temperatures and reduces tensile stresses.

Nevertheless some distinctions are still visible: (1) the critical single coating film thickness (~160 nm), reachable with water based coatings is significantly lower than obtained from ethanol based coating solutions (~280 nm). This can be explained, by the higher surface tension of water (72.3 N/m²) compared to ethanol (22.4 N/m²), which during thin film drying emerges higher capillary forces in the pores [CRC94]. From this it follows that higher tensile forces in water based coatings are build up, which causes that the critical film thickness is lowered (compare Paragraph 2.5).

(2) At low annealing temperatures ethanol based coatings can never be obtained without defects, even when a comparable final film thickness of 120 nm is reached at 600 °C (Figure 81). This was attributed to hydrolysis and condensation reactions, which occur at low annealing temperatures and increase with time. At higher annealing temperatures these processes are superimposed by the pyrolysis of organic residues, which even can lead to stress release and increase of inner coherence of the thin film (compare Paragraph 2.4). However, water based coatings present no dependency of defect density on annealing temperature. That is, because the amorphous sol-gel particles in the water based coating solutions are relatively insensitive towards hydrolysis and condensation reactions and therefore in the water-based films no additional tensile stress is build up with aging time. Thus the film cracking only depends on the plasticity of the sol-gel film, which can be directed by the addition of 1,5-pentanediol.

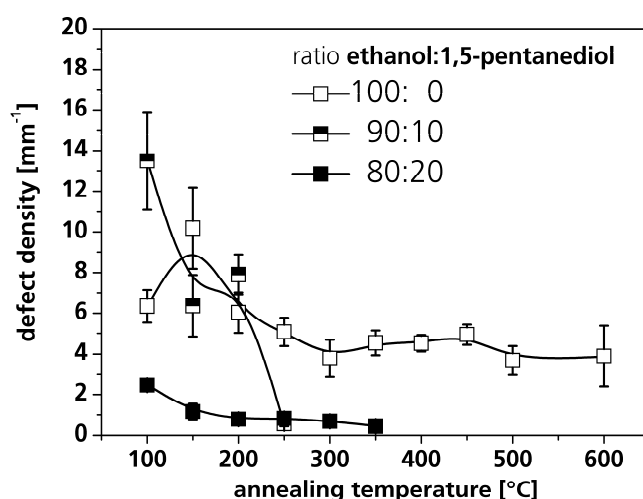


Figure 81. Defect densities for TiO₂ coatings based on different solvent compositions ethanol:1,5-pentanediol as a function of annealing temperature. Thin films were prepared with a withdrawal rate that results at 600 °C in an end film thickness of 120 nm.

SUMMARY OF 5.3.5 "MICROSTRUCTURE AND CRACKING OF THIN FILMS"

Films prepared by dip coating using water based coating solutions always present a vertical gradient in film thickness, because of the low vapor pressure of water.

The microstructure of the investigated ceramic films is quite similar except crack density. Coatings prepared without the addition of 1,5-pentanediol already form cracks during drying and aging at low temperatures, because of tensile stresses. The addition of 1,5-pentanediol to the sols preserves some network plasticity, which results in a reduction/prevention of crack formation.

Generally concerning their densification, phase evolution and microstructure the water based and ethanol based coatings have a lot in common. Nevertheless the critical film thickness of water based coatings is significantly lower than of ethanol based coatings. This was explained by the different surface tensions of the basis solvents, which causes in water based coatings higher capillary forces and tensile stresses during thin film drying.

Furthermore in contrast to the ethanol based coatings the defect density in the case of the water based coatings was independent of annealing temperature. The high stability of the amorphous water stable precursors against hydrolysis and condensation reactions is made responsible for this observation.

5.4 TRIETHANOLAMINE BASED PRECURSOR POWDERS

In previous paragraphs all investigations attended to films prepared from coating solution based on soluble precursor powders using acetylacetonate as chelate ligand. The respective solutions become gradually more stable towards hydrolysis by air moisture during the coating process and even aqueous coating solutions can be obtained [LOE05].

In order to prepare defect-free films from the precursor powders based on acetylacetonate it was necessary to use solvent mixtures that contain some 1,5-pentanediol in addition to the main solvent component. It was shown that the diol partially remains incorporated in the film during drying which provides sufficient intermediate network flexibility [BOC06] and thus cracking can be avoided [BOC07a].

Even though it is obviously feasible to optimize the TiO₂-films by adjusting the solvent mixture, it is attractive to combine a sufficient hydrolytic stability of the Ti-precursor with a satisfactory film densification characteristic. In this paragraph the synthesis of soluble precursor powders based on triethanolamine, which also allows the preparation of TiO₂ films from purely ethanol based coating solutions, is compared to previous results.

5.4.1 CHARACTERIZATION OF POWDERS ISOLATED FROM COATING SOLUTIONS

The chemical composition of the precursor powders based on triethanolamine is almost identical to the sol powders prepared from solutions that used pure ethanol as solvent. The sol-powders prepared from this precursors powder (data not shown) just as well do not significantly differ from the respective film powder that were prepared by dip-coating and drying under ambient conditions (Figure 82): In both cases the total mass loss is up to around 65 mass % and occurs in two steps at temperature from 250-350 °C and 500-550 °C (Figure 82 (left)). The mass loss of each step is comparable around 25-30 mass %. However, in the DTA the first mass loss at 250-350 °C is only associated by a small endothermal signal (340 °C), whereas at 500-550 °C major exothermal decomposition reactions takes place.

In contrast to this behavior film powders based acetylacetonate as chelate ligand (Figure 82) show different properties: The mass loss essentially is completed up to 400 °C. The reactions in this temperature region are attributed to the decomposition of acetylacetonate groups. Most -OEt functionalities, which are expected to decompose between 450 °C and 600 °C, are separated by hydrolysis and condensation reactions induced by air moisture during the drying process.

It is well known that TEA acts a tridentate ligand [YEŞ06] and the resulting cluster are hydrolytically more stable than compounds based on acetylacetonate [PON90,TAK00,TRA05]. It can be concluded that the TEA based films contain a significant larger amount of residual organics after drying than their AcAc-counterparts. Since the films scraped off rather have a "pasty" consistency than a crumbly appearance, the incorporated triethanolamine-groups obviously provide some film plasticity even after drying in the presence of air moisture.

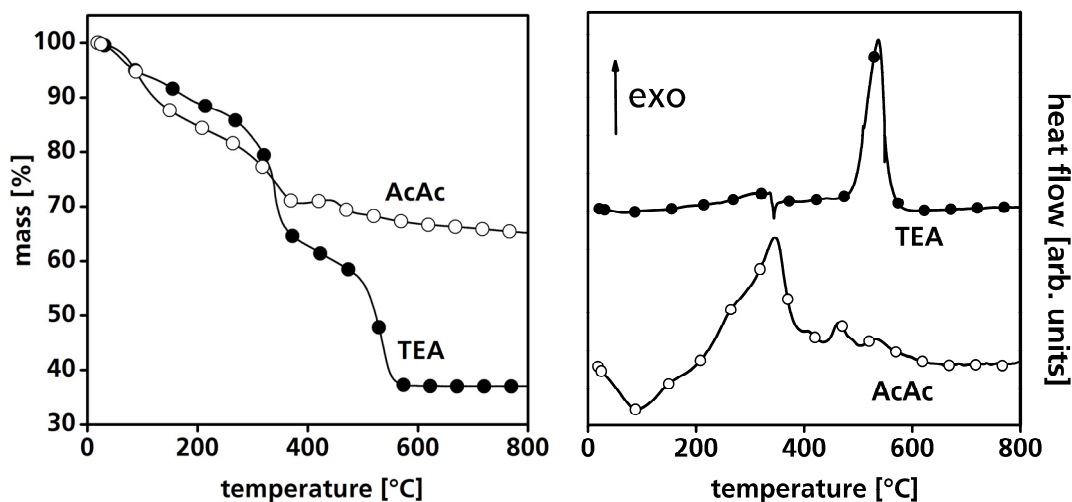


Figure 82. Thermogravimetric analysis (left) and differential thermal analysis (right) of film powders scraped of glass substrates prepared using triethanolamine (TEA, ●) and acetylaceton (AcAc, ○) based precursor powders. The respective sols were prepared with ethanol as a solvent. The experiments were performed with a heating rate of 10 K/min under dry air atmosphere.

The properties of TEA based films are also reflected by measurements of the skeletal density (Figure 83): Initially they exhibit a relatively low skeletal density compared to the corresponding samples obtained from AcAc based precursor, because of their high content of residual organics. Up to 300 °C isothermal annealing temperature no significant skeletal densification is observed, which is in agreement with a higher thermal and hydrolytic stability of the material. At temperatures above 300 °C film powders based on TEA-precursor undergo a steady and strong densification, but first at 500 °C they reach the same level as the film powders from AcAc based precursors. After annealing at 700 °C the skeletal density (4.12 g/cm³) is far above the theoretical density of pure anatase. The X-ray diffraction patterns (Figure 84 (left)) confirm that TEA based film material already start the formation anatase at 400 °C and contains rutile after annealing at 600 °C, which becomes the exclusive phase at 700 °C.

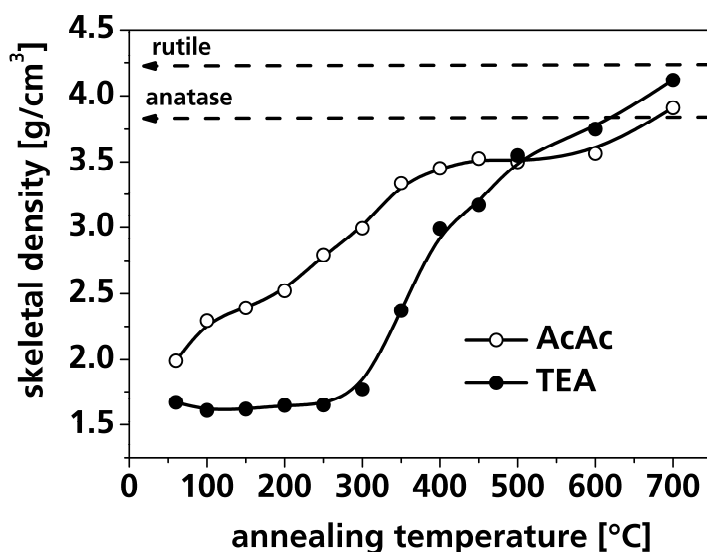


Figure 83. Skeletal densities of film powders using triethanolamine (TEA, ●) and acetylaceton (AcAc, ○) based precursor powders. The coating solutions were prepared with ethanol as solvent. Samples were annealed for 1 hour in air atmosphere at the temperature indicated.

Film powders originating from AcAc-precursors have a higher initial skeletal density. Their structural solidification already starts at 60 °C and continuously keeps on until a plateau is reached at around 400 °C. At low temperatures this observation can be ascribed to the evaporation of water and afterwards to the decomposition reactions of acetylacetone, which are known to start at around 200 °C and persist up to 350 °C (Paragraph 5.1). However, after sintering at 700 °C only a backbone density of 3.92 g/cm³ is measured, even though the coexistence of rutile and anatase (Figure 84 (right)).

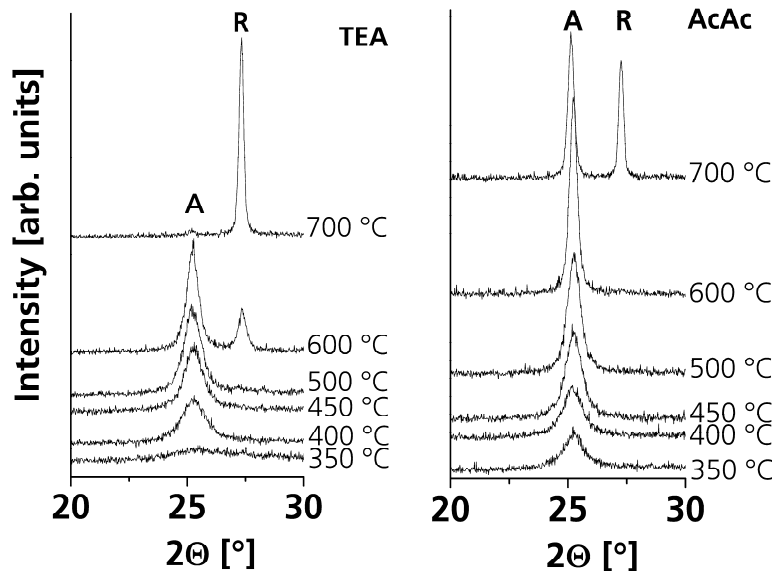


Figure 84. X-ray diffraction patterns of film powders isothermally annealed at the temperatures indicated. The films were prepared using precursors based on triethanolamine (TEA, left) and acetylacetone (AcAc, right). Peaks are marked individually assigned to anatase (A) and (R) rutile.

In the case of the AcAc based film powders the reduced skeletal density at temperature of 350-600 °C was partly explained by the existence of closed pores (Paragraph 5.2.3.2). Furthermore incorporated residual carbon (Figure 85), due to incomplete decomposition reactions of residual organics, reduces the skeletal density of the film powders.

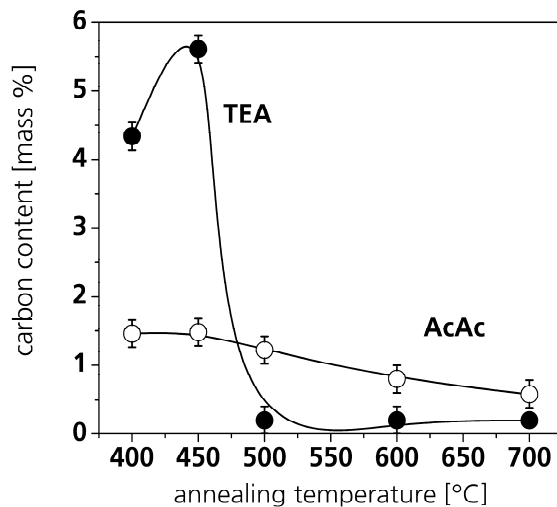


Figure 85. Residual carbon content as a function of annealing temperature of film powders using triethanolamine (TEA, ●) and acetylacetone (AcAc, ○) based precursor powders.

IR measurements of film powders prepared from TEA based precursor powder give no indication for the existence of closed pores (data not shown). However, at annealing temperatures of 400 °C and 450 °C the residual carbon content of film powders using TEA as ligand (Figure 85) is significantly higher than of the respective AcAc based film powders. Apparently, the thermal decomposition of the TEA based film powders leads to insufficient oxidative decomposition reactions below 500 °C [TRA05]. Thereby large amounts of residual carbon are formed, which reduce the skeletal density.

No significant amount of residual carbon is detectable in TEA based film powders at temperatures above 450 °C. In the DTA simultaneously a strong exothermal signal was noticed (Figure 82), indicating the oxidative decomposition reaction of residual carbon species. Simultaneously the skeletal density increases, but is still below the theoretical density of anatase (Figure 83).

Thus N₂-sorption experiments were also performed on film-powders obtained by using precursor powders synthesized with TEA. In Figure 86 (left) the adsorption isotherms show that mesopores are formed by annealing the samples above 300 °C. A level of approximately 45 % mesoporosity is maintained up to 500 °C (Figure 87 (left)), while the specific surface area steadily decreases above 350 °C (Figure 87 (right)). Therefore it can be concluded that in this temperature region small pores merge together to form larger cavities, while the surface area is reduced in the course of this process.

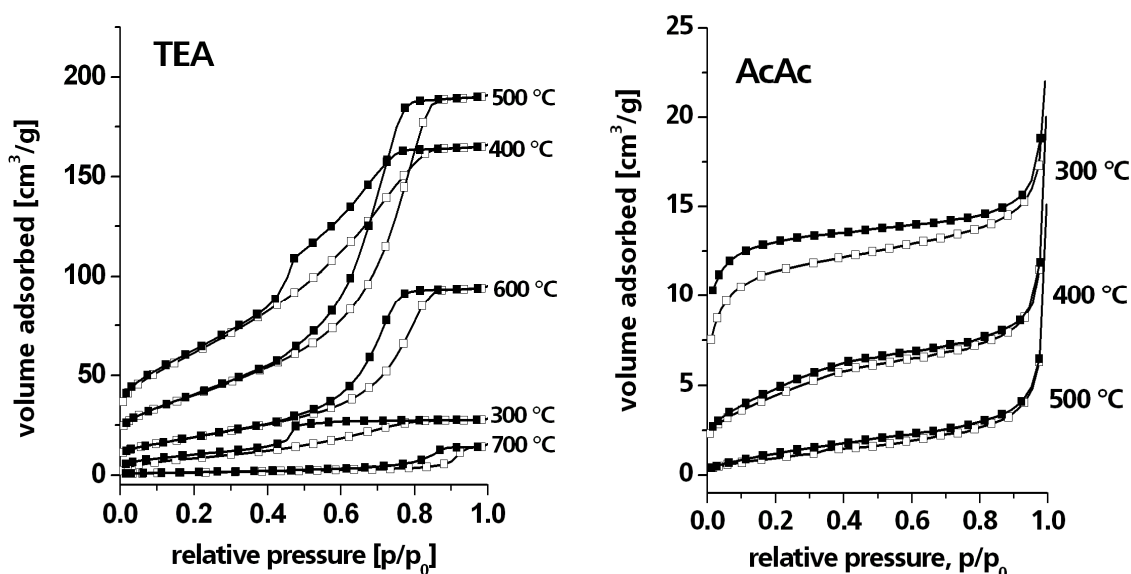


Figure 86. Nitrogen adsorption- (■) and desorption (□) isotherms for film powders prepared from TEA (left) and AcAc (right) based precursors. The samples were isothermally annealed at the temperatures indicated.

The intermediate formation of mesopores obviously goes along with a low initial density, subsequent strong backbone solidification and preferential formation of rutile in both TEA based film powders and sol powders. It seems reasonable to assume that in the presence of pores the decomposition reaction of residual carbon is promoted, leading to a carbon free microstructure. This microstructure easily transforms to the thermodynamically more stable rutile, because no residual carbon hinders the phase transformation, as seen before in the case of sol powders prepared from AcAc based precursors (Paragraph 5.2.2).

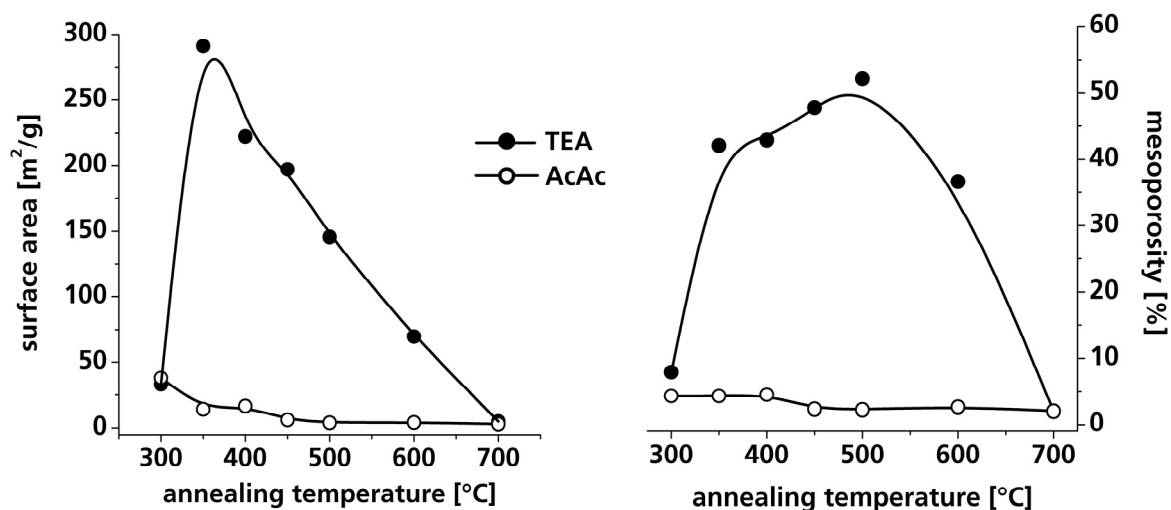


Figure 87. Surface area (left) and mesoporosity (right) of film powders prepared from TEA (●) and AcAc (○) based precursors as derived from measurements shown in Figure 86. The mesoporosity was calculated from the BJH-pore volume and the backbone densities (He-pyknometry, Figure 83).

SUMMARY OF 5.4.1 "CHARACTERIZATION OF POWDERS ISOLATED FROM COATING SOLUTIONS"

The replacement of AcAc by TEA as chelate ligand for Titanium also results in a redissolvable precursor powder. The respective TEA based film powders are distinguished by its high hydrolytic stability and network plasticity during thin film densification. Whereas, the structure of film powders obtained from AcAc based precursor powder dissolved in pure ethanol is strongly affected by the large surface-to-volume ratio and presence of air moisture during thin film drying. Therefore during thin film formation a rigid network was formed, because most of the –OEt groups are separated by hydrolysis and condensation reactions.

In contrast to the previous investigated AcAc based film powders the thermal decomposition of TEA based film powders result in the formation of large amounts of residual incorporated carbon.

Since the scraped off thin films tend to form a highly mesoporous network up to 600 °C the decomposition of residual carbon above 450 °C is relieved. Therefore a preferred phase transformation to rutile is observed in contrast to the AcAc based film powders.

5.4.2 DENSIFICATION OF THIN FILMS

In Figure 88 the thickness of the different films prepared by using ethanol as solvent are given as a function of annealing temperature. It should be noted, that different withdrawal rates were chosen for both experimental series, resulting in considerable discrepancies at lower temperatures. Nevertheless the samples reach similar thicknesses at 600 °C. Therefore both sample series have undergone a comparable densification with respect to the purely inorganic film material, irrespective different initial or transient film structures.

The films based on TEA-precursors have a thickness of approximately 650 nm after drying. The first and major densification step is observed for annealing temperatures between 200 °C and 300 °C. This can be correlated to the first mass loss in the TGA (Figure 82; 250-350 °C), because the changes detected by TGA under constant heating rate conditions will have reached an ad-

vanced state in the films isothermally annealed at the same temperature [BOC06]. It was also shown by He-pykometry (Figure 83) that in this temperature region the skeletal densification of the respective film powders is initiated.

A second minor decrease of film thickness is observed between 450 °C and 600 °C. Simultaneously in this temperature regime the appearance of the coatings changes from dark brown to colorless, which is accompanied by a significant improvement in coating transparency. This indicates the presence of large amounts of residue carbon in the coatings at intermediate temperatures, which decompose up to 600 °C, as already has been noticed in the case of the comparable film powders. Based on the mass loss and increase in skeletal density measured for the film powders a stronger shrinkage would have been expected here for the films. This observation may point at a limited comparability of film powders and the actual films at least in this temperature region.

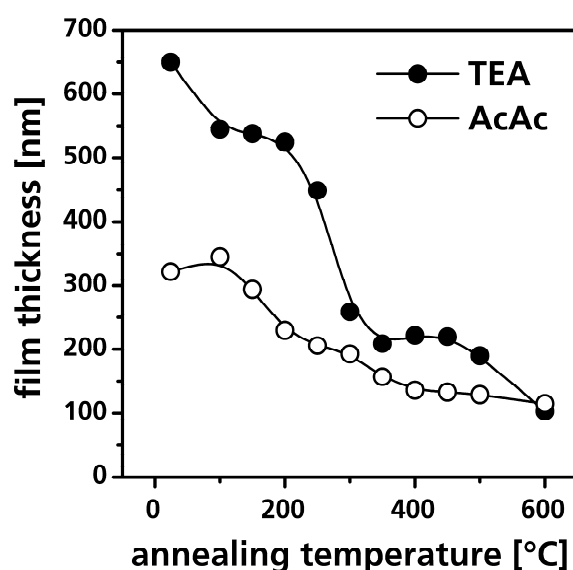


Figure 88. Thickness of films prepared by dip-coating from ethanol based solutions using TEA (●) and AcAc (○) based precursor powders as a function of isothermal annealing temperature.

In general, the measurements of the refractive indices (Figure 89) also reflect the observed differences concerning the densification behavior of the two precursors. Though, some structural differences of film powders and films for higher treatment temperatures are also implied. Up to annealing temperatures of 500 °C the TEA based films generally show smaller refractive indices as expected for a material with a higher content of organic residues. Films that have been annealed at 500 °C have a refractive index of almost 2.0, even though the films yet do not contain any crystalline TiO₂ (Figure 91 (left)). If a porosity of 45 % is assumed, as the N₂-sorption experiments on film powders suggest (Figure 87 (right)), the “backbone” film material should have a refractive index of around 6. Since this assumption is somewhat unrealistic, the films must have a lower porosity than the respective film powders.

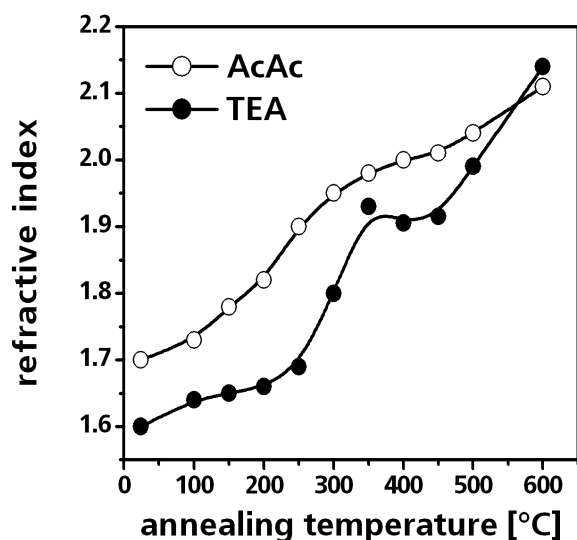


Figure 89. Refractive index of films prepared by dip-coating from ethanol based solutions using TEA (●) and AcAc (○) based precursor powders as a function of isothermal annealing temperature.

It is well known that sol-gel films have to sustain considerable tensile stresses in-plane, since their densification is basically limited to the direction perpendicular to the substrate [CAI97]. As a consequence, cracking may occur [ROE99,KOZ03]. The data in Figure 88 and 90 clearly demonstrate, that the films prepared from TEA based precursors have to suffer a high degree of densification after drying, nevertheless no defects are observed. In contrast to this, all corresponding films originating from the AcAc-route develop cracks.

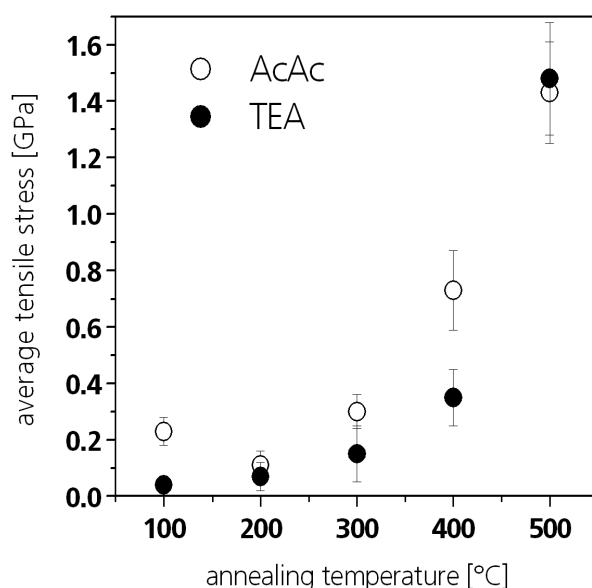


Figure 90. Residual tensile stress of TiO_2 coatings using TEA (●) and AcAc (○) based precursor powders as a function of isothermal annealing temperature.

Nevertheless both sorts of coatings exhibit at 500 °C a similar average tensile stress of around 1.4 GPa (Figure 90). In principle the residual stress strongly increases with temperature no direct connection to the quantity of defects is noticeable. Though, at an annealing temperature of 100 °C in films based on AcAc-precursors a significant degree of tensile arises, whereas TEA based films present no tensile stress. Therefore the formation of defects may be attributed to

tensile stresses build up directly after thin film formation at low temperatures (compare Paragraph 5.2.5.1). Obviously the high hydrolytic stability and the “sticky” consistency as observed for the TEA based precursor powders provides sufficient network flexibility during drying and aging to compensate the tensile stresses without cracking.

Grazing incidence X-ray diffraction (GIXRD) was used to characterize the crystallization of TiO_2 for the different film systems (Figure 91). At 400 °C films based on AcAc-precursors precursor start the formation of anatase, whereas in TEA based films crystalline TiO_2 can be first detected after annealing at 600 °C. Both time the phase transformation amorphous to crystalline coincide with a distinct rise in coating transparency, i.e. the decomposition of residual carbon. Obviously crystallization of TiO_2 is retarded by residual carbon as reported before [OHY03,TAK00,KED94] and therefore the crystallization onset temperature of TEA based films is raised up to 600 °C, compared to AcAc based films.

However, in the TEA based film powders the crystallization of anatase (Figure 83) still occurs, though a high content of residual carbon (Figure 85) is present. At 400 °C, when the crystallization occurs, the film powders are highly porous. When is assumed that the corresponding films consist of anatase than the refractive index of the films also indicates an overall porosity of ~20-25 % in the films. However ellipsometric porosimetry measurements give no indication of open porosity for films annealed at 400 or 500 °C. This can be explained by the formation of a dense crust on top of the films resulting in exclusively closed porosity. Similar behavior has been seen before for several sol-gel films. This sort of cover film structure might cause in this films quasi reductive conditions compared to the film powders. When a quite large content of residual carbon is incorporated in the amorphous network, i.e. substituted some oxygen, it can be assumed that under oxidative conditions this disturbing carbon is easier replaced and crystallization is induced at lower annealing temperatures despite of an additional carbon phase.

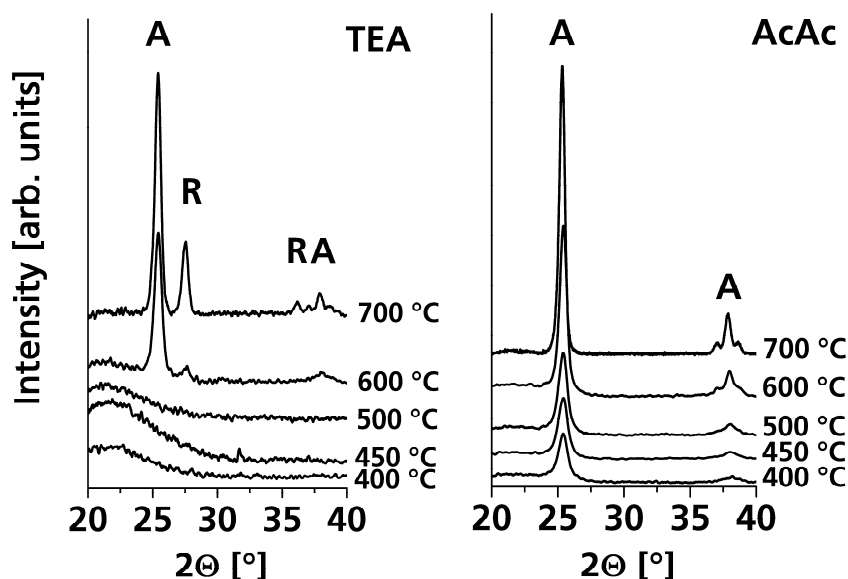


Figure 91. GIXRD pattern of TiO_2 films prepared from coating solutions using TEA (left) and AcAc (right) based precursor powders. The films were isothermally annealed (1 h) at the temperatures indicated.

TEM images of a TEA based TiO_2 film annealed at 600 °C exemplary are displayed in Figure 92. The film microstructure exhibit a granular morphology with a medium crystallite size of around 20-30 nm. Obviously no clear indication for pores is given, as already has been observed in previous investigations on films prepared from AcAc based precursors. In the TEM investigation no rutile was found, even though the TEA-based precursor presented minor reflections of rutile at this elevated temperature. In summary, though the AcAc- and TEA- based film powders and films differ concerning their chemical composition, densification and phase evolution, the microstructure of the observed thin films (compare Paragraph 5.2.4.2 Figure 42) after calcination at 600 °C is quite similar.

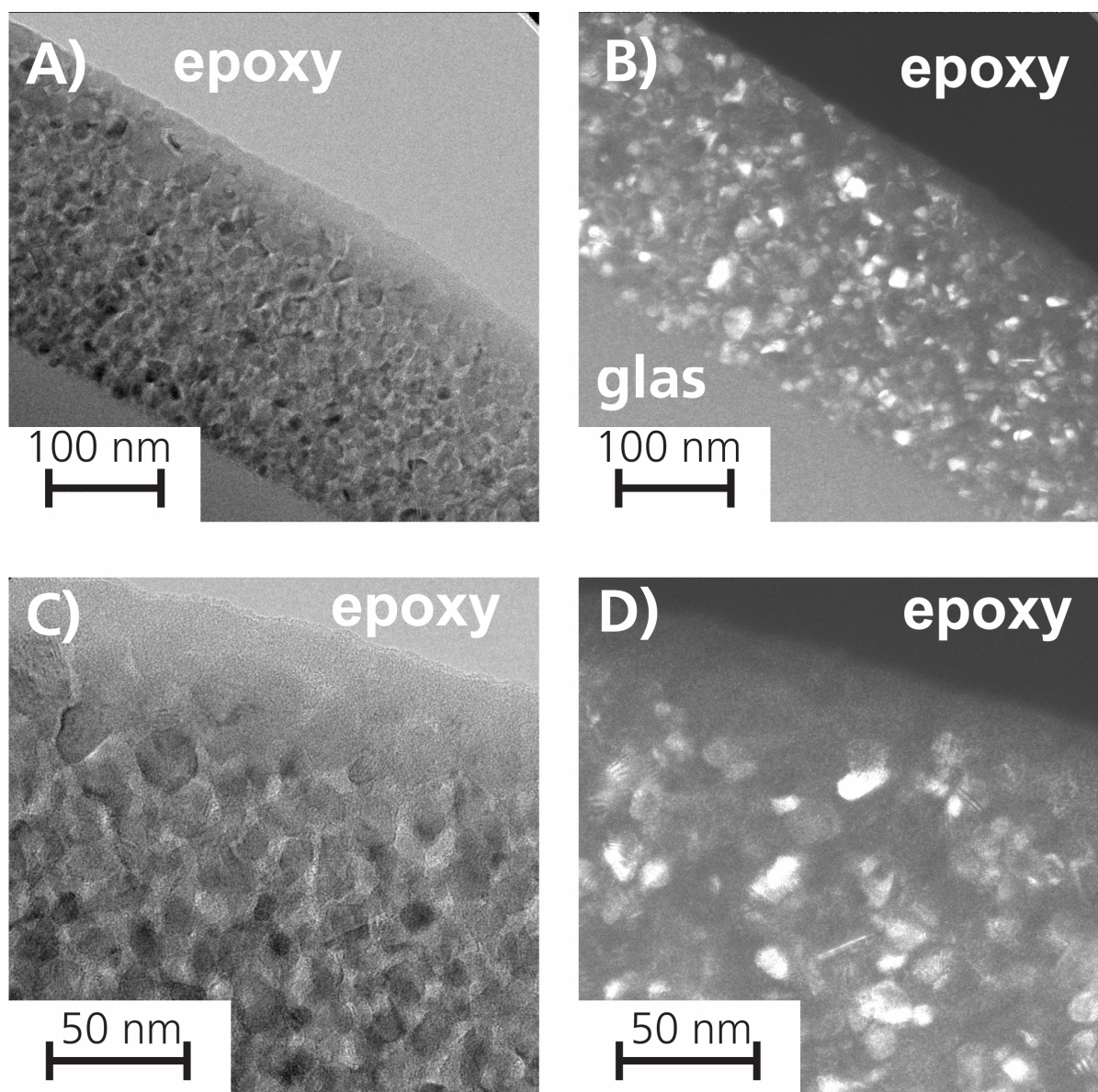


Figure 92. TEM bright (left) and dark (right) filed images of thin TiO_2 film on glass. The film was prepared from an ethanol based coating solution using a TEA based precursor powder and was annealed at 600 °C.

Up on further annealing no crystallization of rutile is found in thin AcAc based films even after treatment at 700 °C, whereas in TEA based films at 700 °C beside anatase a clear fraction of rutile is build up. In general similar tendencies are already observed for the respective film pow-

ders (Figure 84). In both films or powders from TEA-precursors the phase transformation of anatase to rutile seems to be more promoted compared to the respective films or powders prepared from AcAc-precursors. This was attributed to the different decomposition behavior of TEA and AcAc, resulting in more or less residual carbon, which affects the phase transformation.

However, it seems to be a feature of both systems that the formation of the thermodynamically more stable phase is hindered in the films rather than in powder samples, as already has been discussed in a comparable case before (see Paragraph 5.2.5.1). It has been reported for several systems, that tensile stresses can retard crystallization processes, which is an appropriate explanation for the modified phase formation observed in the films [POP05, LIU05, SCH97b]. More interestingly the uniaxial film densification and the occurrence of tensile stresses obviously lead to some structural changes: Whereas films scraped of the sample surface form pores accessible to N_2 -sorption experiments, in the actual film material a crust is formed in top of the film and therefore the oxidative decomposition of organic residuals is limited.

SUMMARY OF 5.4.2 "DENSIFICATION OF THIN FILMS"

Thin films using ethanol based coating sols were prepared from precursors using either AcAc or TEA as chelate ligand. Both precursors result at 600 °C calcinations temperature in crystalline TiO_2 coatings with almost equal porosity (~15 %). However coatings prepared from TEA-precursor exhibit a higher tendency to form a secondary rutile phase beside anatase.

The residual stress in these two types of coatings is at 500 °C comparable high, even though the AcAc based films present at every annealing temperature a closed cracking pattern, whereas TEA based films never show any defects. This was explained by the high hydrolytic stability and plasticity during thin film drying and shrinkage of the TEA based films compared to the AcAc based films.

In principle, in this study it was confirmed again that the film powders are probably the best match to the microstructure of the thin films and are even a valuable tool, when the formation of defects in thin films has to be interpreted. However at annealing temperatures >300 °C the comparability of films and film powders is limited, which mostly can be attributed to the tensile forces, which are only active in thin films and not in film powders.

5.5 VALIDITY FOR OTHER SOL-GEL SYSTEMS (8YSZ)

Previous investigations revealed a distinctive influence of chemical composition of sol-gel precursors on the structure of the resulting TiO_2 thin films. Precursors prepared from soluble precursor powders, which ensured sufficient hydrolytic stability and network flexibility during thin film formation and densification, allowed the preparation of crack free ceramic thin films with low residual porosity of around 10 %.

Now the question arises how far the observations made with these TiO_2 sol-gel coatings are in general also valid for other sol-gel coatings. Therefore 8YSZ (8 mol % Y_2O_3 stabilized ZrO_2) was chosen as appropriate object for comparison, since re-dissolvable sol-gel precursor powders are also available for this comparison. Their preparation is quite similar to the TiO_2 precursor powders [LOE00,KRU06]. Basically this amorphous precursor powders are based on Zr-n-propylate stabilized with acetylacetonate or triethanolamine as chelate ligand.

When these precursor powders were dissolved in ethanol as solvent and the solvent is stripped off again, the structure of the resulting sol powder is similar to the precursor structure. In general the thermal degradation behavior and the skeletal densification of these precursor or sol powders are analogous to the observed decomposition of the respective TiO_2 powders (compare Figure 14 and 93).

In the case of AcAc based sol powder prepared from pure ethanol based sol, typical signals for the decomposition of acetylacetonate are visible at 200-400 °C, followed by the pyrolysis of alkoxide groups above 400 °C (Figure 93). For thin film synthesis with AcAc based precursor powders of 8YSZ, the powders were dissolved in various solvent mixtures of ethanol and 1,5-pentane-diol.

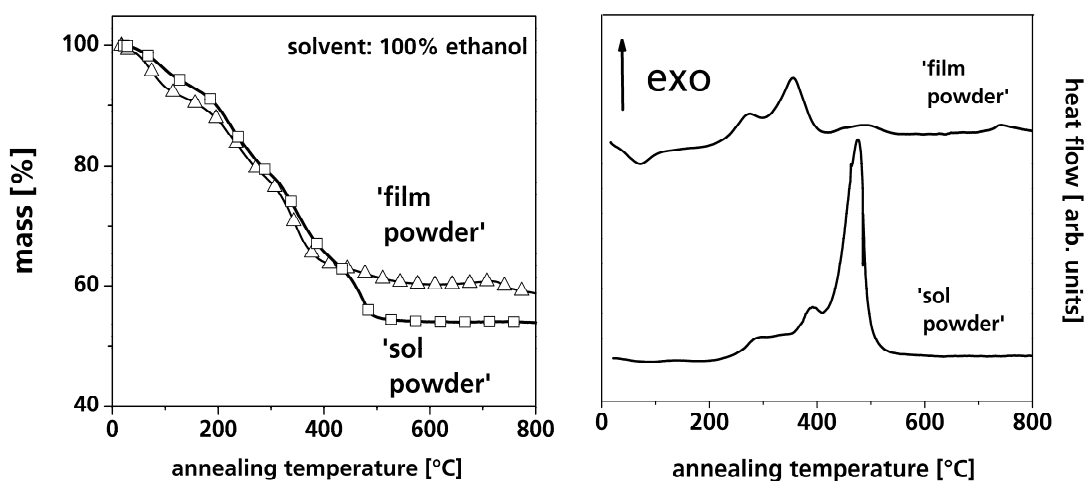


Figure 93. Thermogravimetric analysis (left) and differential thermal analysis (right) of AcAc based 8YSZ sol powder and film powder obtained from a purely ethanol based coating solution. All experiments were performed under dry air atmosphere with a heating rate of 10 K/min.

Similar to TiO_2 when pure ethanol is used as solvent the chemical composition of thin films is highly affected by the high surface-to-volume ratio and air moisture during the thin film formation. The thermogravimetric analysis in Figure 93 (left) for instance clearly shows that the total weight loss of this film powder compared to the sol powder is significantly lower. Along with the

corresponding differential thermal analysis it can be concluded that, because of hydrolysis and condensation reactions during thin film drying in the film powders, no alkoxide moieties are present anymore. As already pointed out for TiO_2 this leads to the formation of a rigid network.

This situation changes when the solvent mixture contains 1,5-pentanediol. Now as like in the TiO_2 case (compare Paragraph 5.2.3.2, Figure 28) the 1,5-pentanediol partly prevents hydrolysis and condensation reactions (DTA/TG data not shown), which preserves some network flexibility. As a consequence of the higher content of organics, due to presence of the diol, the film powders prepared from sols containing 1,5-pentanediol show below 250 °C significantly lower skeletal densities than the respective material from purely ethanol based sols (Figure 94 (left)).

As like for titania the replacement of AcAc by TEA as chelate ligand for zircon results in re-dissolvable precursor powders, too. The respective TEA based film powders are distinguished by its high hydrolytic stability and network plasticity during thin film densification. Whereas the structure of film powders obtained from AcAc based precursor powder dissolved in pure ethanol is strongly affected by the large surface-to-volume ratio and presence of air moisture during thin film drying. These differences concerning the hydrolytic stability directly influence the content of residual organics and thus the network plasticity and densification behavior. The skeletal densification (Figure 94 (right)) of the respective film powders prepared either from TEA based precursor powders or AcAc based precursor powder corresponds with the different hydrolytic stability of the used precursors: As higher the hydrolytic stability of the precursors as lower is the skeletal density at low annealing temperatures (RT- 300 °C).

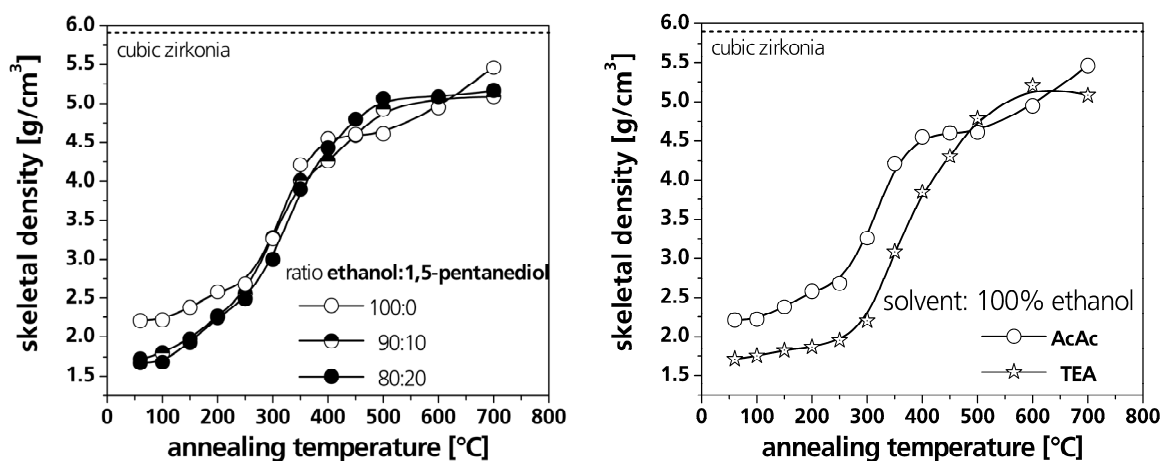


Figure 93. Skeletal densities of film powder prepared from ethanol based sols as a function of annealing temperature. Sols were prepared either from AcAc based precursor powder containing 0 % (○), 10 % (●) and 20 % (●) 1,5-pentanediol or TEA based precursor powder (☆) dissolved in pure ethanol. The theoretical densities of anatase and rutile are given as references [CRC94].

The thin film densification in principle proves the results made on the TiO_2 thin films. As already mentioned in the TiO_2 case, at intermediate temperatures the TEA based films present a significant higher amount of residual carbon, than the AcAc based films. This residue carbon delays crystallization as already has been reported for anatase (data not shown, [PIE06]).

As pointed out for the TiO_2 systems the crack formation of thin films is directly linked to the chemical composition of the precursor and its densification. Crack free films were obtained when

precursors were used, which assure a high hydrolytic stability and plasticity during thin film drying and film shrinkage. (compare Paragraph 5.2.5.3 and 5.4.2)

The investigations concerning crack formation of 8YSZ coatings seem to confirm these results. In Figure 95 the defect densities of the analogous 8YSZ coatings annealed at 600 °C as function of single film thickness are displayed. From pure ethanol based AcAc precursors crack free films never can be obtained even at relatively low film thicknesses. Whereas when this AcAc precursor is dissolved in mixtures of ethanol and 1,5-pentanediol (90:10 or 80:20) the critical film thickness, which can be reached by one single dip coating step before cracking occurs, increases to around 80 nm. However, this critical film thickness can be extended further to 180 nm by the use of sols, based on TEA precursor powders that exhibit the highest observed degree of hydrolytic stability and plasticity.

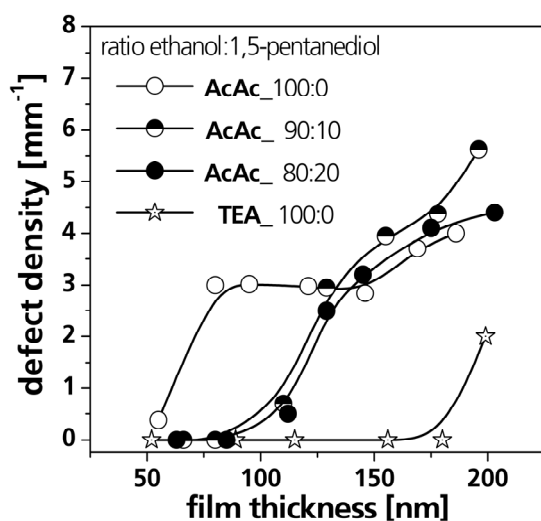


Figure 95. Defect density of ethanol based thin TiO_2 films annealed at 600 °C as function of film thickness. Films were prepared either from AcAc based precursor powder containing 0 % (○), 10 % (◐) and 20 % (●) 1,5-pentanediol or TEA based precursor powder (☆) dissolved in pure ethanol.

Nevertheless a clear distinction between TiO_2 and 8YSZ coatings concerning the reachable critical film thickness also is visible. As pointed out in the previous paragraphs, with most ethanol based sols defect-free dense TiO_2 single coatings can be easily prepared up to film thickness of 220 nm (600 °C). However, the highest reachable film thickness of 8YSZ without any defects by a single coating step is 180 nm (600 °C).

Though, when the thin film densification of 8YSZ is compared to TiO_2 it must be noted that indeed the thin sol-gel films start from comparable skeletal densities, but their theoretical ceramic densities significantly differ: i.e. 3.84 g/cm³ for TiO_2 (anatase) and 5.9 g/cm³ for 8YSZ. As consequence the theoretical degree of shrinkage of 8YSZ is higher than for TiO_2 . Therefore when comparable microstructures and ceramic film thicknesses for the thin films are assumed the uniaxial shrinkage induces in 8YSZ coatings a higher degree of tensile stress than in TiO_2 coatings.

SUMMARY OF 5.5 "VALIDITY FOR OTHER SOL-GEL SYSTEMS (8YSZ)"

The general validity of the conclusion made on the sol-gel synthesis of TiO₂ thin films for other sol-gel coatings was proven on the basis of 8YSZ coatings. 8YSZ was selected, because for 8YSZ comparable re-dissolvable sol-gel precursor powders were available, too.

In principle all investigations made on the interconnection of precursor chemistry, thin film shrinkage and structure of the thin films was also valid in the case of 8YSZ sol-gel coatings.

Therefore the shrinkage and defect structure in thin sol-gel gel films prepared from soluble precursor powders is directly linked to the hydrolytic stability and plasticity of the sol-gel precursor during thin film drying and densification.

5.6 FURTHER CONSEQUENCES OF THIN FILM DENSIFICATION

In the previous paragraph it has been shown, that the conclusions drawn from the understanding of structural and chemical sol-gel processes happening during thin film formation and densification are the basis to understand and avoid defects on a microscopic level. However, the densification of thin sol-gel films is not only related to defects, but also to several further characteristics of sol-coatings.

Thus the presented results were also the basis for better understanding of the mechanical properties of thin films [LOE99]. Results indicate that the mechanical properties of sol-gel coatings are improved during annealing due to solidification of the inorganic backbone, crystallization and further densification.

For example upon annealing of TiO_2 sol-gel coatings on glass a significant increase of adhesion and pencil hardness was noticed, which was correlated to stiffening of the inorganic backbone [MAL07,PIE06]. In Figure 96 the pencil hardness of TiO_2 thin films prepared from AcAc or TEA based precursors is compared. As one would expect, according to their skeletal densification, the pencil hardness of TEA based thin films below 300 °C is significantly lower than the hardness of AcAc based thin films. That is because below 300 °C the TEA based films exhibit a higher plasticity than AcAc based films and therefore a lower mechanical stability and scratch resistance (compare Paragraph 5.4).

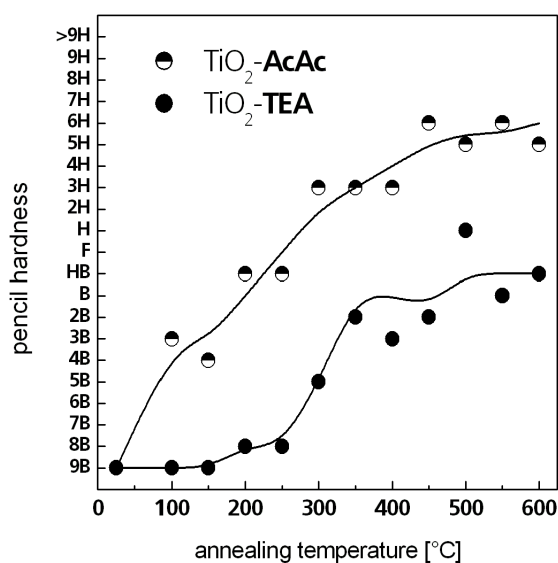


Figure 96. Pencil hardness of ethanol based thin TiO_2 films as function of annealing temperature (200 nm final film thickness at 600 °C). Films were prepared either from AcAc based precursor powder containing 10 % (○) 1,5-pentanediol or TEA based precursor powder (●) dissolved in pure ethanol.

Though, at higher annealing temperatures, above 300 °C the films prepared from TEA based films never reach the pencil hardness of the AcAc based films, which also seems to be a cause of the different densification behavior of the precursors used. However, parameters determining the pencil hardness yet are not fully understood, but further investigations will focus on his specific topic in detail.

Furthermore a typical stiffening phenomenon of fiber bundles coated with 8YSZ sol-gel precursors was quantified by three point bending test (Figure 97). For higher calcinations temperatures an increasing stiffness (indicated by the increasing slopes) was measured and was correlated to structural investigations happened during transformation of amorphous sol-gel film to a ceramic thin film [KRU06].

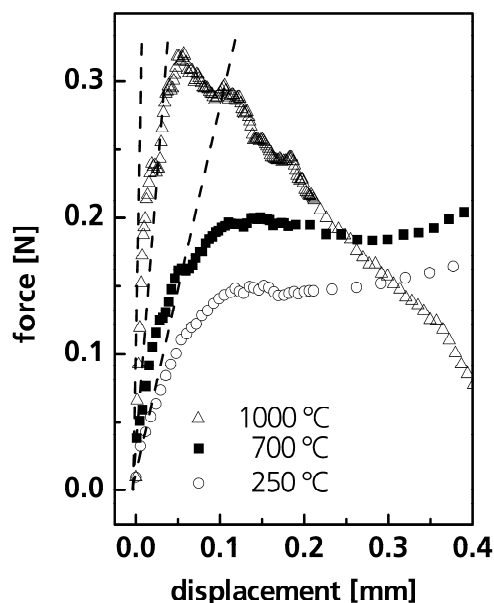


Figure 97. 3-point bending test of Nextel™ 610 fiber bundles coated with 2 mass % 8YSZ solutions with different calcinations temperature (250 °C, 700 °C, 1000 °C). Stiffness indicating slopes: 250 °C: 2.0 +/- 0.4 N/mm, 700 °C: 3.6 +/- 0.8 N/mm, 1000 °C: 23 +/- 7.9 N/mm. (Data taken from [KRU06])

Additionally the fiber strength degradation of 8YSZ coated fibers was in good correlation with the individual densification behavior of the various coatings [BOC07b]. When coatings densify large tensile stresses are present by thermal expansion mismatch and the shrinking process constrained by the fiber. Stress concentration arising from inhomogeneous film thickness was identified as the cause of fiber degradation. Degradation can be avoided for coatings that scarcely densify, have weak adhesion to the fiber or can relax stresses by e.g. phase transformation (data not shown, [BOC07b]).

SUMMARY OF 5.6 "FURTHER CONSEQUENCES OF THIN FILM DENSIFICATION"

The conclusions drawn from the understanding of structural and chemical sol-gel processes happening during thin film formation and densification can be associated to several further phenomenons of thin films beside crack formation.

The mechanical properties of thin films, i.e. pencil hardness or stiffening, are directly related to the densification behavior of thin films. Furthermore the fiber strength degradation of 8YSZ coated fibers correlates with the densification of the coatings.

6 SUMMARY

The main focus of this work was to get a deeper understanding of the relationship between the structure of sol-gel films, their densification and their macroscopic cracking. First of all titania was chosen as model system.

Therefore a synthesis route starting from the preparation of long-term stable amorphous re-dissoluble precursor powders based on acetylacetonate as chelate ligand was utilized. The solubility and stability of the powders in various solvents can be determined by chemical synthesis and technological parameters. When dissolved in a solvent mixture of ethanol and 1,5-pentanediol, thin films can be easily prepared by dip-coating technique. Thereby the quality of the titania films enormously depends on the calcinations temperature and the solvent mixture is used.

In order to investigate the influence of different solvents and solvent mixtures on the microstructure and densification of the precursors, the coating solutions were stripped off (sol powder) and analyzed as function of annealing temperature. It was pointed out that a high densification rate caused by the addition of 1,5-pentanediol, results in dense microstructure with trapped residual carbon. These impurities can retard the phase transformation of anatase to rutile.

The analysis of so-called "film powders" scraped off multiple dip-coated substrates provides valuable information on the effect of air moisture and unidirectional densification during drying and aging on the structure of thin films. The high surface-to-volume ratio and access to air moisture determine the chemical composition of the as-prepared film, which controls shrinkage, crystallization and defect structure of the coatings. Further it was shown, that drying as a thin film results in the formation of closed pores and much denser microstructure than the respective sol powder. Without the addition of 1,5-pentanediol all -OEt moieties undergo hydrolysis reactions, which causes the formation of a rigid network. The presence of 1,5-pentanediol retards this hydrolysis reactions and provides some network plasticity.

Generally the microstructure of thin films is comparatively close to the microstructure of the film powders. The addition of 1,5-pentanediol prevents hydrolysis and condensation reactions as like in the film powders. However even at 700 °C, thin films never transform to rutile, which was attributed to the tensile stresses in thin films.

In thin films and in film powders as well a comparable amount of closed pores are formed during annealing. Further it was shown that most of the thin sol-gel films investigated form a dense crust on their tops during annealing. This explains why crack free films exhibit only closed pores. However, when cracks appear during thin film shrinkage in the coating, this crust is burst, which generates open porosity.

The defect density in the coatings was determined by an automated analysis of surface images. The crack formation and quantity can be directly referred to tensile stresses in the coatings, which arise from hydrolysis and condensation during thin film drying and aging. Therefore when 1,5-pentanediol is added to the sol, thin film cracking was avoided, because hydrolysis and

condensation reactions are retarded, which preserves a higher network flexibility. Furthermore the crack formation was significantly influenced by the atmospheric humidity that was used during the coating process, which was explained by different drying and condensation rates.

Under certain chemical starting conditions water soluble precursor powders can be also obtained. In general the observations made with the water based coating solutions are mostly in agreement with the former results based on ethanol based coating solutions.

For example the high surface-to-volume ratio of film powders compared to sol powders also significantly enhances film drying and densification. The addition of 1,5-pentanediol also clearly contributes to their densification behavior and phase evolution. As seen before in the case of ethanol based coatings, 1,5-pentanediol enhances the stability towards hydrolysis and condensation reactions and preserves some network plasticity. Therefore coatings prepared without the addition of 1,5-pentanediol already form cracks during film drying and aging because of tensile stresses. Thus, the addition of 1,5-pentanediol results in a reduction/prevention of crack formation.

Nevertheless some differences were observed, i.e. the critical single coating film thickness of ethanol based coatings is nearly twice that of water based coatings. This was explained by the different surface tensions of the basis solvents, which during thin film drying causes significantly higher capillary forces and tensile stresses in water based coatings.

When acetylacetonone is replaced by triethanolamine as chelating ligand for titanium also re-dissolvable precursor powders can be synthesized. The film powders combine a high hydrolytic stability of the precursor with sufficient intermediate network flexibility. The different type of organics changes the drying and densification behavior: i.e. in contrast to film powders obtained from acetylacetonone based precursor powders the structure of triethanolamine based film powders is unaffected by the thin film drying process. This high hydrolytic stability and plasticity of this precursor allows the preparation of defect free coatings up to single film thickness of 300 nm. However triethanolamine based thin films present at intermediary annealing temperatures a distinctively different microstructure compared to acetylacetonone based films.

The general validity of the conclusions was proved on the basis of zirconia coatings that were also prepared by the use of re-dissolvable precursor powders. In principle all conclusions concerning the interconnection of precursor chemistry, film formation, densification and structure were transferable to the respective zirconia coatings. Differences mainly arise only from differential material properties i.e. bulk density.

Finally, it has been pointed out that the findings obtained on the densification behavior of thin sol-gel films are also a valuable tool for improved explanations of other important scientific questions concerning sol-gel films, i.e. scratch resistance of sol-gel coatings, fiber -bridging and -degradation of sol-gel coated fibers.

7 ZUSAMMENFASSUNG

Grundsätzlich war es Ziel der vorliegenden Arbeit, die Zusammenhänge zwischen Struktur von Sol-Gel Schichten, ihrer Verdichtung und der Entstehung von makroskopischen Rissen besser verstehen zu können. Als Modellsystem wurde hierfür Titanoxid ausgewählt.

Hierzu wurde von einer Syntheseroute basierend auf der Verwendung von langzeitstabilen amorphen re-dispergierbaren Vorstufenpulvern mit Acetylaceton als Chelatligand ausgegangen. Die Löslichkeit und Stabilität der Pulver in verschiedenen Lösungsmitteln lässt sich über die chemische Synthese bzw. technologischen Parameter einstellen. Wenn die Pulver in einem Lösungsmittelgemisch aus Ethanol und 1,5-Pentandiol gelöst werden, lassen sich mittels Tauchbeschichtungsverfahren einfach dünne Schichten herstellen. Die Qualität der Titanoxidschichten hängt dabei entscheidend von der verwendeten Pyrolysetemperatur und der Menge an verwendetem 1,5-Pentandiol ab.

Um den Einfluss von verschiedenen Lösungsmitteln und Lösungsmittelgemischen auf die Mikrostruktur und Verdichtung der Vorstufen zu untersuchen, wurden die Sole am Rotationsverdampfer eingeeengt (Sol-Pulver) und in Abhängigkeit von der Behandlungstemperatur analysiert. Dabei stellte sich heraus, dass eine hohe Verdichtungsrate verursacht durch den Zusatz von 1,5-Pentandiol, in einer dichten Mikrostruktur mit eingeschlossenem Rest-Kohlenstoff resultiert. Diese Kohlenstoff-Rückstände können die Phasenumwandlung von Anatas zu Rutil hemmen.

Die Analyse der so genannten „Film-Pulver“, welche von mehrfach tauchbeschichteten Substraten abgekratzt worden sind, ermöglicht den Zugang zu entscheidenden Informationen über den Einfluss der Luftfeuchtigkeit und der unidirektionalen Verdichtung, während der Film-Trocknung und –Alterung, auf die Struktur der dünnen Schichten. Es zeigte sich, dass das große Oberfläche zu Volumen Verhältnis und der Kontakt mit Luftfeuchtigkeit die chemische Zusammensetzung der frisch hergestellten Schichten bestimmen. Diese wiederum steuert die Schichtschumpfung, Kristallisation und Defektstruktur der Schichten. Ferner konnte dargestellt werden, dass die Trocknung als dünner Film zu der Entstehung von geschlossenen Poren und zu einer deutlich dichteren Mikrostruktur als die der entsprechenden Sol-Pulver führt. Ohne den Zusatz an 1,5-Pentandiol kommt es zur Hydrolyse der –OEt Gruppen, was die Bildung eines rigiden Netzwerkes bewirkt. 1,5-Pentandiol als Zusatz hemmt diese Hydrolysereaktionen und bedingt damit eine gewisse Plastizität des Netzwerkes.

Im Großen und Ganzen ist die Mikrostruktur der dünnen Schichten mit der Struktur der Film-Pulver gut vergleichbar. Durch den Zusatz an 1,5-Pentandiol werden in den Schichten die Hydrolyse und Kondensationsreaktionen ebenso gehemmt wie in den entsprechenden Film-Pulvern. Allerdings bei den dünnen Schichten ist auch bei 700 °C keine Phasenumwandlung zu beobachten, was auf Zugspannung in den dünnen Filmen zurückzuführen ist.

Während der Calcinierung kommt es sowohl in dünne Schichten wie als auch in den Film-Pulvern zur Ausbildung von geschlossenen Poren. Ferner wurde gezeigt, dass die meisten untersuchten dünnen Schichten während der Pyrolyse auf ihrer Oberfläche eine dichte Kruste ausbilden. Dies erklärt warum rissfreie Schichten nur geschlossene Poren aufweisen. Allerdings wenn Risse

während der Schichtschumpfung in der Schicht auftreten, wird diese Kruste durchbrochen, was zur Bildung von offener Porosität führt.

Die Defektdichte in den Schichten wurde mittels einer automatisierten Bildanalyse der Oberfläche bestimmt. Die Riss-Bildung und Riss-Häufigkeit kann dabei direkt mit der Entstehung von Zugspannung, durch Hydrolyse und Kondensation während der Schicht-Trocknung und –Alterung, in Zusammenhang gebracht werden. Durch die Zugabe von 1,5-Pentandiol konnte die Rissentstehung verhindert werden, da Hydrolyse und Kondensations-Reaktionen gehemmt werden, was eine höhere Flexibilität des Netzwerkes erhält. Weiterhin wurde die Rissentstehung signifikant durch die herrschende Luftfeuchtigkeit während des Beschichtungsprozesses beeinflusst, was mit unterschiedlichen Hydrolyse- und Kondensations-Raten zu erklären ist.

Unter Verwendung bestimmter chemischer Syntheseparameter, können ebenso wasserlösliche Vorstufenpulver erhalten werden. Grundsätzlich sind die Untersuchungen an den hieraus resultierenden wässrigen Solen und Schichten in guter Übereinstimmung mit den vorherigen Untersuchungen an ethanolischen Beschichtungssystemen.

So zum Beispiel, beschleunigt ebenso das große Oberfläche zu Volumen Verhältnis der Film-Pulver deutlich die Film-Trocknung und –Verdichtung, im Vergleich zu den Sol-Pulvern. Auch beeinflusst ein Zusatz an 1,5-Pentandiol eindeutig das Verdichtungsverhalten und die Phasenentwicklung. Wie schon bereits im Fall der Ethanol basierenden Beschichtungen festgestellt worden ist, erhöht 1,5-Pentandiol die Beständigkeit hinsichtlich Hydrolyse und Kondensationsreaktionen und erhält hiermit eine gewisse Netzwerkplastizität. Deshalb bilden Filme die ohne einen Zusatz an 1,5-Pentandiol hergestellt worden sind, aufgrund von Zugspannung, schon während der Film-Trocknung und -Alterung Risse aus. Durch einen Zusatz von 1,5-Pentandiol kann dagegen die Entstehung von Rissen vermindert bzw. vermieden werden.

Allerdings zeigten sich auch einige Unterschiede: So ist zum Beispiel die erreichbare Einzelschichtdicke der ethanolischen Beschichtungssystemen nahezu doppelt so groß wie die der wässrigen Beschichtungssysteme. Dies wurde mit der unterschiedlichen Oberflächenspannung des Basislösungsmittels erklärt, welche während der Schichttrocknung deutlich höhere Kapillarkräfte und Zugspannung in wässrigen Filmen erzeugt.

Wird Acetylaceton gegen Triethanolamin als Chelatligand für Titan ausgetauscht, so können ebenso re-dispergierbare Vorstufenpulver hergestellt werden. Die Film-Pulver kombinieren hohe hydrolytische Stabilität der Vorstufe mit einer ausreichenden intermediären Netzwerkflexibilität. Der andere Komplexbildner verändert entscheidend das Trocknungs- und Verdichtungsverhalten: so z.B. wird die die Struktur von Film-Pulvern basierend auf Triethanolamin nicht entscheidend durch die Trocknung als dünne Schicht beeinflusst, im Gegensatz zu Film-Pulvern hergestellt von Vorstufenpulvern mit Acetylaceton als Chelatligand. Diese hohe hydrolytische Stabilität und Plastizität der Vorstufe ermöglicht die Herstellung von defektfreien Beschichtungen bis hin zu einer Einzelschichtdicke von 300 nm. Dennoch unterscheidet sich bei intermediären Pyrolysetemperaturen die Mikrostruktur der Triethanolamin basierenden Schichten deutlich von der auf Acetylaceton basierenden Schichtsystemen.

Die Allgemeingültigkeit der Schlussfolgerungen wurde anhand Zirkonoxidbeschichtungen, welche ebenfalls unter Verwendung von löslichen Vorstufenpulvern hergestellt worden sind, überprüft. Grundsätzlich zeigte sich hierbei, dass alle Schlüsse hinsichtlich der Zusammenhänge der Vorstufenchemie, Film-Bildung, -Verdichtung und -Struktur auf die entsprechenden Zirkonoxidbeschichtungen übertragbar sind. Unterschiede ergeben sich nur aus unterschiedlichen Materialeigenschaften wie z.B. der makroskopischen Dichte.

Letztlich wurde dargestellt, dass die Erkenntnisse hinsichtlich des Verdichtungsverhalten der Sol-Gel Schichten die Grundlage für die Aufklärung vieler anderer wichtiger wissenschaftlich Fragestellungen hinsichtlich Sol-Gel Beschichtungen bilden, wie z.B. der Kratzfestigkeit von Sol-Gel Schichten, Faser-Verbrückung und -Schädigung von Sol-Gel beschichteten Fasern.

8 LITERATURE

- [AND04] O. Anderson, K. Bange, B. Germain, P. Lehuédé, M. Farnworth, *Glass Sci. Technol.* 77 [2] (2004) 58.
- [AQU66] E. N. Aqua, *Acta Cryst.* 20 (1966) 560.
- [ATA99] G. Atanassov, J. Turlo, J. K. Fu, Y. S. Dai, *Thin Solid Films* 342 (1999) 83.
- [AYT03] T. Aytug, M. P. Paranthaman, B. W. Kang, D. B. Beach, S. Sathyamurthy, E. D. Specht, D. F. Lee, R. Feenstra, A. Goyal, D. M. Kroeger, K. J. Leonard, P. M. Martin, D. K. Christen, *J. Am. Ceram. Soc.* 86 [2] (2003) 257.
- [BAN97] K. Bange, *Glastech. Ber. Glass Sci. Technol.* 70 [8] (1997) 238.
- [BAK00] M. R. Baklanov, K. P. Mogilnikov, *Optica Applicata* 30 [4] (2000) 491.
- [BAK02] M. R. Baklanov, K. P. Mogilnikov, *Microelectron. Eng.* 64 (2002) 335.
- [BOC06] M. Bockmeyer, P. Löbmann, *Chem. Mater.* 18 [18] (2006) 4478.
- [BOC07a] M. Bockmeyer, P. Löbmann, *Thin Solid Films* 515 (2007) 5212.
- [BOC07b] M. Bockmeyer, R. Krüger, *J. Am. Ceram. Soc.*, submitted 2007.
- [BOG75] M. P. Bogaard, B.J. Orr, Electric Dipole Polarisabilities of Atoms and Molecules, in International Review of Science, Series 2, ed. A.D. Buckingham (Butterworths, London, 1975), vol. 2, p. 149.
- [BOI05] C. Boissiere, D. Grosso, S. Lepoutre, L. Nicole, A. B. Bruneau, C. Sanchez, *Langmuir* 21 [26] (2005) 12362.
- [BOS04] F. Bosc, A. Ayril, P.-A. Albouy, L. Datas, C. Guizard, *Chem. Mater.* 16 (2004) 2208.
- [BRE99] R. Brenier, C. Urlacher, J. Mugnier, M. Brunel, *Thin Solid Films* 392 (2001) 142.
- [BRE01] R. Brenier, A. Gagnaire, R. Brenier, C. Urlacher, J. Mugnier, M. Brunel, *Thin Solid Films* 338 (1999) 136.
- [BRI85] C. J. Brinker, G. W. Scherer, *J. Non-Cryst. Solids* 70 (1985) 301.
- [BRI90] C. J. Brinker and G. W. Scherer, *Sol-Gel Science: The Physics and Chemistry of the Sol-Gel Processing*, Academic Press Limited, Boston, 1990.
- [BRI91] C. Brinker, A. Hurd, G. Frye, P. Shunk, C. Ashley, *J. Ceram. Soc. Jap.* 99 (1991) 862.
- [BRI92] C. J. Brinker, A. J. Hurd, P. R. Schunk, G. C. Frye, C. S. Ashley, *J. Non-Cryst. Solids* 147&148 (1992) 424.
- [BRI95] C. Brinker, S. Wallace, N. Raman, R. Sehgal, J. Samuel, S. Contakes, In: T. Pinnavaia, M. Thorpe (Eds.), *Access in Nanoporous Materials*, Plenum Press, New York, USA, 1995, p. 123.
- [BU04] S. Bu, Z. Jin, X. Liu, H. Du, Z. Cheng, *J. Sol-Gel Sci. Technol.* 30 (2004) 239.
- [BUR99] M. Burgos, M. Langlet, *J. Sol-Gel Sci. Technol.* 16 (1999) 267.
- [BUR04] A. Burns, G. Hayes, W. Li, J. Hirvonen, J. D. Demaree, S. I. Shah, *Mater. Sci. Eng. B* 111 (2004) 150.
- [BRU00] Bruker advanced X-ray solutions: DIFFRACplus REFSIM Version 2.0, Bruker AXS, Karlsruhe, Germany (2000).
- [CAI97] R. Caincross, S. Chen, P. Schunk, C. Brinker, A. Hurd, *Ceram. Trans.* 69 (1997) 153.
- [CHA95] J. Chaibi, M. Henry, H. Zarrouk, N. Gharbi, J. Livage, *J. Sol-Gel Sci. Technol.* 4 (1995) 217.
- [CHE92] R. W. Cheary, A. Coelho, *J. Appl. Cryst.* 25 (1992) 109.
- [CHR98] P. Chrysicopoulou, D. Davazoglou, C. Trapalis, G. Kordas, *Thin Solid Films* 323 (1998) 188.
- [COE04] H. Cölfen, A. Völkel, *Progr. Colloid & Polym. Sci.* 127 (2004) 31.

- [COL92] P. Colomban, E. Bruneton, *J. Non-Cryst. Solids* 147&148 (1992) 201.
- [CHO00] L. A. Chow, B. Dunn, K. N. Tu, C. Chiang, *J. Appl. Phys.* 87 (2000) 7788.
- [CHO04a] H. Choi, D. Dionysiou, Prepr. Ext. Abstr. ACS Natl. Meet., Am. Chem. Soc., *Div. Environ. Chem.* 44 (2004) 197.
- [CHO04b] S. Y. Choi, M. Mamak, N. Coombs, N. Chopra, G. A. Ozin, *Adv. Funct. Mater.* 14 (2004) 335.
- [CRC94] D. Lide, H. Frederikse, CRC Handbook of Chemistry and Physics, CRC Press, Inc., Boca Raton (1993-1994).
- [CRE02] E. L. Crepaldi, D. Grosso, G. J. de A. A. Soler-Illia, P.-A. Albouy, H. Amenitsch, C. Sanchez, *Chem. Mater.* 14 (2002) 3316.
- [DIA04] A. Diaz-Parralejo, R. Caruso, A. Ortiz, F. Guiberteau, *Thin Solid Films* 458 (2004) 92.
- [DJA02b] Y. Djauoued, R. Taj, R. Brüning, S. Badilescu, P. V. Ashrit, G. Bader, T. Von-Van, *J. Non-Cryst. Solids* 297 (2002) 55.
- [DIE03] U. Diebold, *Surf. Sci. Reports* 48 (2003) 53.
- [DOE87] S. Doeuff, M. Henry, C. Sanchez, J. Livage, *J. Non Cryst. Solids* 89 (1987) 206.
- [EGG04] P. Egger, G. D. Sorarù, S. Diré, *J. Eur. Ceram. Soc.* 24 (2004) 1371.
- [EVA88] A. G. Evans, M. D. Drory, M. S. Hu, *J. Mater. Res.* 3 [5] (1988) 1043.
- [EXA92] G. J. Exarhos, N. J. Hess, *Thin Solid Films* 220 (192) 254.
- [EXN94] H. Exner, IN: E.Lifshin (Ed.), *Materials Science and Technology: A Comprehensive Treatment, Volume 2B Characterisation of materials Part II*, VCH, Weinheim, Germany, 1994, p. 351.
- [FAN02] C.-L. Fan, D. Ciardullo, J. Paladino, W. Huebner, *J. Mater. Res.* 17 [6] (2002) 1520.
- [FID03] A. Fidalgo, I. M. Ilharco, *J. Sol-Gel Sci. Technol.* 26 (2003) 357.
- [FIS96] K. Fischer, H. Oettel, *Mater. Sci. Forum* 228-231 (1996) 301.
- [FLI87] P. A. Flinn, D. S. Gardner, W. D. Nix, *IEEE Trans. Electron. Dev.* ED-34 (1987) 689.
- [FUJ99] Fujishima, A.; Hashimoto, K.; Watanabe, T. *TiO₂ Photocatalysis – Fundamentals and Applications*; BKC Inc.: Tokyo, 1999.
- [GEI98] S. Geis, P. Löbmann, J. Fricke, *J. Non-Cryst. Solids* 225 (1996) 226.
- [GOE99] C. Goebbert, M. A. Aegerter, D. Burgard, R. Nass, H. Schmidt, *J. Mater. Chem.* 9 (1999) 253.
- [GOE07] S. Götzendorfer, Diplom's Thesis, University Würzburg, 2007.
- [GOM98] A. Gombert, W. Glaubitt, K. Rose, J. Dreibholz, C. Zanke, B. Bläsi, A. Heinzl, W. Horbelt, D. Sporn, W. Döll, V. Wittwer, J. Luther, *Sol Energy* 62 [3] (1998) 177.
- [GOM99] A. Gombert, W. Glaubitt, K. Rose, J. Dreibholz, B. Bläsi, A. Heinzl, D. Sporn, W. Döll, V. Wittwer, *Thin Solid Films* 351 [4] (1999) 73.
- [GOM00] A. Gombert, W. Glaubitt, K. Rose, J. Dreibholz, B. Bläsi, D. Sporn, W. Döll, V. Wittwer, J. Luther, *Sol Energy* 68 [4] (2000) 357.
- [GRI03] A. Grill, V. Patel, K.P. Rodbell, E. Huang, M.R. Baklanov, K.P. Mogilnikov, M. Toney, H.-C. Kim, *J. Appl. Phys.* 94 [5] (2003) 3427.
- [GRO06] D. Grosso, G. J. de A. A. Soler-Illia, E. L. Crepaldi, F. Cagnol, C. Sinturel, A. Bourgeois, A. Brunet-Bruneau, H. Amenitsch, P. A. Albouy, Clément Sanchez, *Chem. Mater.* 15 (2003) 4562.
- [GRO06] D. Grosso, C. Boissière, Lionel Nicole, Clément Sanchez, *J. Sol-Gel Sci. Technol.* 40 (2006) 141.
- [HAL53] W. Hall, G. K. Williamson, *Acta Metall* 1 (1953) 22.
- [HEI00] O. Heintz, D. Robert, J. V. Weber, *J. Photochem. Photobiol. A: Chem.* 135 (2000) 77.
- [HER04] B. Herbig, P. Löbmann, *J. Photochem. Photobiol. A: Chem.* 163 (2004) 359.

- [HER06] B. Herbig, intern information, Fraunhofer ISC (2006).
- [HIR97] S.-I. Hirano, *Glastech. Ber. Glass Sci. Technol.* 70 C (1997) 224.
- [HIR05] M. Hirano, K. Ota, T. Ito, *J. Am. Ceram. Soc.* 88 (2005) 3303.
- [HOL07] E. Holbig, M. Bockmeyer, L. Dubrovinsky, P. Löbmann, *J. Alloys Compd.* in Press 2007.
- [HON02] Y. J. Hong, M. P. Brungs, R. P. Chaplin, E. Sizgek, *J. Aust. Ceram. Soc.* 1 [38] (2002) 74.
- [HOR72] M. Horn, C. F. Schwerdtfeger, E. P. Meagher, *Z. Kristallogr.* 136 (1972) 273.
- [HOI95] A. F. Hollemann, E. Wiberg, N. Wiberg, *Lehrbuch der anorganischen Chemie*, de Gruyter, Berlin, 1995.
- [HUA06] F. Huang, M. Zhou, Y.-B. Cheng, R. A. Caruso, *Chem. Mater.* 18 [25] (2006) 5835.
- [HYE81] M. W. Hyer, *J. Comp. Materials* 15 (1981) 296.
- [IMA97] IMAGE CTM User's Manual, IMTRONIC GmbH, Berlin, Germany (1997).
- [JOL00] J.-P. Jolivet, *Metal Oxide Chemistry and Synthesis: From Solution to Solid State*, John Wiley & Sons Ltd., Chichester, 2000.
- [JUV04] H. Juvonen, Master's Thesis, University of Joensuu, 2004.
- [KER02] R. J. Kerans, R. S. Hay, T. A. Parathasarathy, M. K. Cinibulk, *J. Am. Ceram. Soc.* 85 [11] (2002) 2599.
- [KHA02] S. U. M. Khan, M. Al-Shahry, W. B. Ingler Jr., *Science* 297 (2002) 2243.
- [KAJ98] K. Kajihara, K. Nakanishi, K. Tanaka, K. Hirao, N. Soga, *J. Am. Ceram. Soc.* 81 (1998) 2670.
- [KAJ00a] K. Kajihara, T. Yao, *J. Sol-Gel Sci. Technol.* 17 (2000) 173.
- [KAJ00b] K. Kajihara, T. Yao, *J. Sol-Gel Sci. Technol.* 17 (2000) 239.
- [KAL92] M. Kallala, C. Sanchez, B. Cabane, *J. Non-Cryst. Solids* 147&148 (1992) 189.
- [KED91] J. L. Keddie, E. P. Giannelis, *J. Am. Ceram. Soc.* 74 [10] (1991) 2669.
- [KED94] J. L. Keddie, P. V. Braun, E. P. Giannelis, *J. Am. Ceram. Soc.* 77 [6] (1994) 1592.
- [KEM00] T. Kemmitt, N. I. Al-Salim, G. J. Gainsford, *Inorg. Chem.* 39 (2000) 6067.
- [KHO03] I. N. Kholmanov, E. Barborini, S. Vinati, P. Piseri, A. Podestà, C. Ducati, C. Lenardi, P. Milani, *Nanotechnology* 14 (2003) 1168.
- [KLE90] W. Keber: *Einführung in die Kristallographie*. 17., stark bearb. Aufl./von H.-J. Bausch-Berlin: Verlag. Technik, 1990.
- [KLU02] A. Klukowska, U. Posset, G. Schottner, M. L. Wis, C. Salemi-Delvaux, V. Malatesta, *Mater. Sci.* 20 (2002) 95.
- [KOZ00a] H. Kozuka, M. Kajimura, T. Hirano, K. Katayama, *J. Sol-Gel Sci. Technol.* 19 (2000) 205.
- [KOZ00b] H. Kozuka, M. Kajimura, *J. Am. Ceram. Soc.* 83 [5] (2000) 1056.
- [KOZ02] H. Kozuka, S. Takenaka, *J. Am. Ceram. Soc.* 85 [1] (2002) 2696.
- [KOZ03] H. Kozuka, S. Takenaka, H. Tokita, T. Hirano, Y. Higashi, T. Hamatani, *J. Sol-Gel Sci. Technol.* 26 (2003) 681.
- [KOZ06] H. Kozuka, *J. Sol-Gel Sci. Technol.* 40 (2006) 287.
- [KRU02] R. Krüger, W. Glaubitt, P. Löbmann, *J. Am. Ceram. Soc.* 85 (2002) 2827.
- [KRU05] M. Krunks, I. Oja, K. Tõnsuaadu, M. Es-Souni, M. Gruselle, L. Niinistö, *J. Therm. Anal. Cal.* 80 (2005) 483.
- [KRU06] R. Krüger, M. J. Bockmeyer, A. Dutschke, P. C. Löbmann, *J. Am. Ceram. Soc.* 89 (2006) 2080.
- [JUN99] M. W. Jung, H. J. Oh, J. C. Yang, Y. G. Shul, *Bull. Korean Chem. Soc.* 20 [12] (1999) 1394.

- [LAN06] U. Lange, intern information, Julius-Maximilians-Universität Würzburg (2006).
- [LANb] M. Langenbacher, P. Löbmann, J. Hall, U. Demisch, 5thInternat. Symp. on Humidity and Moisture – ISHM 2006 Brazil
- [LAU96] M. Laube, F. Rauch, C. Ottermann, O. Anderson, K. Bange, *Nucl. Instr. and Meth. B* 113 (1996) 288.
- [LI05] Y. Li, D.-S. Hwang, N. H. Lee, S.-J. Kim, *Chem. Phys. Lett.* 404 (2005) 25.
- [LIN05] L. Lin, W. Lin, Y. X. Zhu, B. Y. Zhao, Y. C. Xie, Y. He, Y. F. Zhu, *J. mol. Catal. A* 236 (2005) 46.
- [LIU05] L. Xiaoxin, J. Zhengguo, B. Shaojing, T. Yin, *J. Sol-Gel Sci. Technol.* 36 (2005) 103.
- [LIV89] J. Livage, C. Sanchez, M. Henry, S. Doeuff, *Solid State Ionics* 32/33 (1989) 633.
- [LOE96] P. Löbmann, J. Groß, W. Glaubitt, J. Fricke, *J. Non-Cryst. Solids* 201 (1996) 66.
- [LOE99] F. Löffler, *Thin Solid Films* 339 (1999) 181.
- [LOE00] P. C. Löbmann, R. Jahn, S. Seifert, D. Sporn, *J. Sol-Gel Sci. Technol.* 19 473 (2000) 473.
- [LOE01] P. C. Löbmann, W. Glaubitt, and D. Sporn, "Verfahren zur Abscheidung von Zirkonoxid-Schichten unter Verwendung von löslichen Pulvern" European Patent EP 1 084 992 A1.
- [LOE02] P. C. Löbmann, W. Glaubitt, and D. Sporn, "Verfahren zur Abscheidung von Titandioxid-Schichten unter Verwendung von löslichen Pulvern" European Patent EP 1 084 992 A1.
- [LOE03] P. C. Löbmann, P. Röhlen, *Glass Sci. Techn.* 76 [3] (2003) 1.
- [LOE03b] P. Löbmann, *Oberflächenveredlung von Glas HVG* (2003) 37.
- [LOE05] P. C. Löbmann, *J. Sol-Gel Sci. Techn.* 33 [3] (2005) 175.
- [MA02] H. Ma, A. K.-Y. Jen, L. R. Dalton, *Adv. Mater.* 14 [19] (2002) 1339.
- [MAC00] J. MacKenzie, E. Bescher, *J. Sol-Gel Sci. Techn.* 19 (2000) 23.
- [MAE03] K. Maex, M. R. Baklanov, D. Shamiryan, F. Iacopi, S. H. Brongersma, Z. S. Yanovitskaya, *J. Appl. Phys.* 93 [11] (2003) 8793.
- [MAL97] S. G. Malhotra, Z. U. Rek, S. M. Yalisove, J. C. Bilello, *J. Vac. Sci. Technol. A.* 15 [2] (1997) 345.
- [MAR03] C. Martos, F. Rubio, J. Rubio, J. L. Oteo, *J. Sol-Gel Sci. Techn.* 26 (2005) 511.
- [MAT04] M. Matsuzawa, M. Abe, S. Horibe, J. Sakai, *Acta Mater.* 52 (2004) 1675.
- [MCI92] P. C. McIntyre, M. J. Cima, J. A. Smith Jr., R. B. Hallock, *J. Appl. Phys.* 71 (1992) 1868.
- [MEH97] A. Mehner, H. Klümper-Westkamp, F. Hoffmann, P. Mayr, *Thin Solid Films* 308&309 (1997) 363.
- [MEH05] A. Mehner, W. Datchary, N. Bleil, H.-W. Zoch, M. J. Klopstein, D. A. Lucca, *J. Sol-Gel Sci. Technol.* 36 (2005) 25.
- [MOG02] K. P. Mogilnikov, M. R. Baklanov, *Electrochem. Solid-State Lett.* 5 [12] (2002) F29.
- [MOU06] M. Mougnot, M. Lejeune, J. F. Baumard, C. Boissiere, F. Ribot, D. Grosso, C. Sanchez, R. Noguera, *J. Am. Ceram. Soc.* 89 [6] (2006) 1876.
- [NAM04] H.-J. Nam, T. Amemiya, M. Murabayashi, K. Itoh, *J. Phys. Chem. B* 108 (2004) 8254.
- [NIE06] M. Niederberger, G. Garnweitner, J. Buha, J. Polleux, J. Ba, N. Pinna, *J. Sol-Gel Sci. Technol.* 40 (2006) 259.
- [OHY99] Y. Ohya, J. Mishina, T. Matsuda, T. Ban, Y. Takahashi, *J. Am. Ceram. Soc.* 82 [10] (1999) 2601.
- [OHY03] T. Ohya, A. Nakayama, Y. Shibata, T. Ban, Y. Ohya, Y. Takahashi, *J. Sol-Gel Sci. Technol.* 26 (2003) 799.
- [OKA01] K. Okada, N. Yamamoto, Y. Kameshima, A. Yasumori, *J. Am. Ceram. Soc.* 84 [7] (2006) 1591.
- [ORE91] B. O'Regan, M. Grätzel, *Nature* 353 (1991) 737.

- [OTT93] C. Ottermann, J. Otto, U. Jeschkowski, O. Anderson, M. Heming, K. Bange, *Mater. Res. Soc. Proc.* 308 (1993) 2431.
- [OTT96] C. R. Ottermann, K. Bange, *Thin Solid Films* 286 (1996) 32.
- [PEL98] J. W. Pell, K. M. Delak, H.-C. zur Loye, *Chem. Mater.* 10 [7] (1998) 1764.
- [PER90] A. J. Perry, *Thin Solid Films* 193/194 (1990) 463.
- [PER96] A. J. Perry, J. A. Sue, P. J. Martin, *Surf. Coat. Technol.* 81 (1996) 17.
- [PIE06] B. Pietschmann, Diplom's Thesis, University Würzburg, 2006.
- [PIT96] W. Pietschke, *Mat. Sci. Forum* 178 (1996) 228.
- [PON90] O. Poncelet, L. Hubert-Pfalzgraf, J.-C. Daran, *Polyhedron* 9 [19] (1990) 1305.
- [POP05] S. Popović, Z. Skoko, A. Gajović, K. Furić, S. Musić, *Fizika A* 14 [1] (2005) 19.
- [PUE04] J. Pütz, M. A. Aegerter, *Glass Sci. Technol.* 77 [5] (2004) 229.
- [ROD97] R. Rodríguez-Talavera, S. Vargas, R. Arroyo-Murillo, R. Montiel-Campos, E. R. Haro-Poniatowski, *J. Mater. Res.* 12 (1997) 439.
- [ROE99] R. K. Roeder, E. B. Slamovich, *J. Mater. Res.* 14 [6] (1999) 2364.
- [ROU99] F. Rouquerol, J. Rouquerol and K. Sing, *Adsorption by Powders and porous Solids: Principles, Methodology and Applications*, Academic Press, London, 1999.
- [PRE96] P. Prevéy in "Developments in Materials Characterization Technologies", eds. G. Vander Voort & J. Friel, ASM International, Materials Park, OH, 1996, 103.
- [RUE05] A. Rüdinger, W. Glaubitt, W. Pritzkow, in Schlimmer, M.: *Verbundwerkstoffe und Werkstoffverbunde 2005: Vortragstexte des 15. Symposiums Verbundwerkstoffe und Werkstoffverbunde*, 6. - 8. April 2005, Kassel. Frankfurt: MAT-INFO Werkstoff-Informationsgesellschaft, 2005, pp. 163.
- [RUP06] J. L. M. Rupp, A. Infortuna, L. J. Gauckler, *Acta. Mat.* 7 (2006) 1721.
- [RYU99] H.-K. Ryu, J.S. Heo, S.-I. Cho, S.H. Moon, *J. Electrochem. Soc.* 146 [3] (1999) 1117.
- [SAK03] S. Sakthivel, H. Kisch, *Angew. Chem. Int. Ed.* 42 (2003) 4908.
- [SAN88] C. Sanchez, J. Livage, M. Henry, F. Babonneau, *J. Non-Cryst. Solids* 100 (1988) 65.
- [SAN89] H. Sankur, W. Gunning, *J. Appl. Phys.* 66 [2] (1989) 807.
- [SCH88a] H. Schmidt, *J. Non-Cryst. Solids* 100 (1988) 51.
- [SCH88b] G. W. Scherer, *J. Non-Cryst. Solids* 99 (1988) 324.
- [SCH88c] G. W. Scherer, *J. Non-Cryst. Solids* 100 (1988) 77.
- [SCH92] G. W. Scherer, *J. Non-Cryst. Solids* 147&148 (1992) 363.
- [SCH97a] P. R. Schunk, A. J. Hurd, C. J. Brinker, In: S. F. Kistler, P. M Schweizer (Eds.), *Liquid Film Coating*, Chapman & Hall, London, UK, 1997, p. 672.
- [SCH97b] G. W. Scherer, *J. Sol-Gel Sci. Technol.* 8 (1997) 353.
- [SCH06] H. Schmidt, *J. Sol-Gel Sci. Technol.* 40 (2006) 115.
- [SCH06b] T. Schuler, T. Krajewski, I. Grobelsek, M.A. Aegerter, *Thin Solid Films* 502 (2006) 67.
- [SEN98] S. S. Sengupta, S. M. Park, D. A. Payne, L. H. Allen, *J. Appl. Phys.* 83 [4] (1998) 2291.
- [SKR00] S. J. Skrzypek, A. Baczmanski, W. Ratuszek, E. Kusior, *J. Appl. Cryst.* 34 (2001) 427.
- [STO09] G. G. Stoney, *Proc. Roy. Soc. London A* 32 (1909) 172.
- [SUR04] T. Suratwala, M. L. Hanna, P. Whitman, *J. Non-Cryst. Solids* 349 (2004) 368.
- [SWA 84] R. Swanepoel, *J. Phys. E.: Sci. Instrum.* 19 (1984) 1214.

- [TAK00] Y. Takahashi, A. Ohsugi, T. Arafuka, T. Ohya, T. Ban, Y. Ohaya, *J. Sol-Gel Sci. Technol.* 17 (2000) 227.
- [TAK06] T. Muromachi, T. Tsujino, K. Kamitani, K. Maeda, *J. Sol-Gel Sci. Technol.* 40 (2006) 267.
- [TH89] J. A. Thornton, D. W. Hoffman, *Thin Solid Films* 171 (1989) 5.
- [TRA05] C. Trakanprapai, V. Esposito, S. Licocchia, E. Traversa, *J. Mater. Res.* 20 [1] (2005) 128.
- [VRE90] P. Vretenar, *Vakuum* 40 [1-2] (1990) 173.
- [XAG99] A. P. Xagas, E. Androulaki, A. Hiskia, P. Falaras, *Thin Solid Films* 357 (1999) 173.
- [XU04] J. Xu, W. Meneskoulou, E. Ivers-Tiffée, *J. Electroceram.* 13 (2004) 229.
- [YAN97] J. Yang, Y. X. Huang, J. M. F. Ferreira, *J. Mater. Sci. Let.* (1997) 1933.
- [YAN99] P. Yang, D. Zhao, D. I. Margolese, B. F. Chmelka, G. D. Stucky, *Chem. Mater.* 11 (1999) 2813.
- [YES06] O. Z. Yeşilel, H. Ölmez, *J. Therm. Anal. Cal.* 86 [1] (2006) 211.
- [YOU95] R. A. Young: Introduction into the Rietveld method. in: Young, R.A. [Pub]: The Rietveld method. Int. Union of Crystallography, Oxford University Press, New York, 1995.
- [YU02] J. C. Yu, H. Y. Tang, J. Yu, H. C. Chan, L. Zhang, Y. Xie, H. Wang, S. P. Wong *J. Photochem. Photobiol.,A* 153 (2002) 211.
- [YU03] J. Yu, J. C. Yu, W. Ho, M. K.-P. Leung, B. Cheng, G. Zhang, X. Zhao, *Appl. Catal. A: General* 255 (2003) 309.
- [VRE90] P. Vretenar, *Vacuum* 40 (1990) 173.
- [WIJ01] J. E. G. J. Wijnhoven, L. Bechger, W. L. Vos, *Chem. Mater.* 13 (2001) 4486.
- [WIN03] J. Winkler, U. Zorll [Pub], Titanoxid, Vincentz Network, Hannover, 2003.
- [ZHO05] F. Zhou, K. Liang, H. Shao, *Mater. Sci. Forum* 475-479 (2005) 1227.
- [ZHU05] K.-R. Zhu, M.-S. Zhang, J.-M. Hong, Z. Yin, *Mater. Sci. Eng. A* 403 (2005) 87.

8YSZ	8 mol % Y_2O_3 doped ZrO_2
AcAcH	Acetylacetone
BET	Brunauer, Emmet and Teller
b.p.	Boiling Point
AUc	Analytical Ultracentrifugation
CHR	Constant Heating Rate
CVD	Chemical Vapor Deposition
DTA	Differential Thermal Analysis
EP	Ellipsometric Porosimetry
FHG	Fraunhofer Gesellschaft
FT	Fourier Transformation
GIXRD	Grating Incidence X-Ray Diffraction
ICP-AES	Inductively Coupled Plasma-Atomic Emission Atom Spectroscopy
IMEC	Interuniversity Microelectronics Centre
ISC	Institut Silicatforschung
IB_i	Instrumental Broadening
IR	Infra-Red
MPI	Max-Planck-Institute
n	Refractive Index
NIST	National Institute of Standards and Technology
-OEt	Ethanolate
PVD	Physical Vapor Deposition
RH	Relative Humidity
RT	Room Temperature
RTA	Rapid Thermal Annealing
SEM	Scanning Electron Microscopy
TEA	Triethanolamine
TEM	Transmission Electron Microscopy
TG	Thermogravimetry
UV	Ultraviolet
Vis	Visible
XRD	X-Ray Diffraction
XRR	X-Ray Reflectometry

The work presented in this thesis was done at the Chair for Chemical Technology of Materials Synthesis in cooperation with the Fraunhofer Institut für Silicatforschung. I would like to express my gratitude to all people who have contributed to it.

Prof. Dr. Gerd Müller and Prof. Dr. Gerhard Sextl are gratefully acknowledged for offering me the unique opportunity to work in the Institute.

I warmly thank my supervisor, PD. Dr. Peer Löbmann for giving me the chance of being involved in one of the most important and challenging problem in the field of sol-gel chemistry. I am deeply indebted for the guidance, support and encouragement that he provided during my years at the Fraunhofer Institute.

I am grateful for the confidence given to in me as a young project manager by Dipl.-Ing. Walther Glaubitt. With his positive spirit towards the endeavour of carrying out applied research, he provided me a vision of future materials and new innovative products.

Dr. Reinhard Krüger and Dr. Uwe Guntow deserve some special thanks, for our long scientific (and not only) discussions, for their positive criticism and rich ideas which helped me to go forward with this work.

I acknowledge Dipl.-Chem. Dieter Sporn for his always sincere expression of opinion and for the opportunity to be in charge of the Nanolonics and SupraNanoSol projects. Thanks also to your secretary Ms. Jocelyne Sauer.

I also like to thank the Chair of Prof. Dr. Ellen Ivers-Tiffée at IWE University of Karlsruhe, especially Dipl.-Ing. Cristoph Peters. I appreciate the valuable discussions and efficient cooperation.

Further the generous support of Prinz Optics (Stromberg) by providing tailor-cut glass substrates is gratefully acknowledged.

Many thanks to Dr. Mikhail Baklanov from IMEC at Leuven (Belgium) for providing several EP measurements free of any charge. Your work decisively improved the scientific use of my work.

I am further grateful for UCI measurements performed at the MPI in Golm by PD. Dr. Helmut Cölfen and Ms. Antje Völkel.

Of course this endeavor would not have been possible without the help of my colleges and friends who provided support and encouragement as well as scientific discussion. In particular, Dr. Uta Helbig (excellent support concerning crystallographic questions), Dipl.- Ing. Bettina Herbig (photocatalyse), Dipl.-Phys. Anke Dutschke (TEM), Ms. Tatjana Shinkar (wonderful cooperation), Ms. Margit Schubertrügmer (SupraNanoSol), Ms. Bärbel Böhm (professional lab management), Dipl.-Ing. Arne Rüdigner (support at XRD and several other technological problems), Dipl.-Phys. Gerhard Domann (laserprofilometrie), Mr. Kurt Henkel (DTA/TG), Mr. Peter Michel (extraordinary N₂ sorption measurements), Dr. Uwe Posset (GI-IR), Dipl.-Phys. Manfred Römer (SEM), Dipl.-Ing. Rainer Jahn (Swanepoel method), Dr. Stefan Holzner, Dipl.-Chem. Matthias Mallack, Mr. Oliver Schüssler (support by coffee and milk) as well all as other members of KF1 (Miranda, Claudia, Martina & Annett).

Futhermore I gratefully acknowledge the enormous support by several Master or Diploma students and trainees: Ms. Helka Juvonen, Mr. Bernd Pietschmann, Mr. Stefan Götzendörfer, Mr. Rémi Lemennais, Mr. Abi-Hanna Joseph, Ms. Ira Biedermann, Ms. Nicole Pfeiffer, Ms. Prisca Eckert, Mr. Dennis Trögel, Mr. Johannes Mederer, Mr. Matthias Kühnle, Mr. Johannes Kostka, Mr. Markus Scholz and Mr. Florian Sommer.

For accommodation and excellent food support in a peaceful atmosphere I deserve very special thanks to my grandma Ellen Bockmeyer in Worms and Eberhard Neidlein and Irene Leitner in Aiglkofen.

Special thanks to all the members of Corps Rhenania Würzburg, *Amico pectus, hosti frontem!*

I am also greatly indebted to Ms. Melanie Beyer.

Finally, I acknowledge the grand help and support of my family.

- Type: Full paper
M. Bockmeyer, P. Löbmann "Densification and Microstructural Evolution of TiO_2 Films ", Chem. Mater. 2006, 18, 4478-4485.
- Type: Full paper
M. Bockmeyer, P. Löbmann "Crack Formation in TiO_2 Films Prepared by Sol-Gel Processing: Quantification and Characterization ", Thin Solid Films, 2007, 515, 5212-5219.
- Type: Full paper
M. Bockmeyer, P. Löbmann, "Use of Triethanoleamine for the Preparation of Soluble TiO_2 -Precursor Powders: Formation, Densification and Properties of Sol-Gel Films", in preparation.
- Type: Full paper
R. Krüger, M. Bockmeyer, A. Dutschke, P. Löbmann "Continuous Sol-Gel Coating of Ceramic Multifilaments: Evaluation of Fiber Bridging by Three Point Bending Test ", J. Am. Ceram. Soc. 2006, 89, (7), 2080-2088.
- Type: Full paper
M. Mallak, M. Bockmeyer, P. Löbmann "Liquid Phase Deposition of TiO_2 on Glass: Systematic Comparison to Films prepared by Sol-Gel Processing", Thin Solid Films, submitted 2006.
- Type: Full paper
E. Holbig, M. Bockmeyer, L. Dubrovinsky, P. Löbmann "Sol-Gel synthesis of amorphous and nanocrystalline ZrO_2 - TiO_2 powders", J. Alloys Compd., submitted 2006.
- Type: Full paper
Christoph Peters, Matthias Bockmeyer, Reinhard Krüger, André Weber, Ellen Ivers-Tiffée: "Processing of Dense Nanocrystalline Zirconia Thin Films by Sol-Gel, in Current and Future Trends of Functional Oxide Films", edited by D. Kumar, V. Craciun, M. Alexe, K.K. Singh (Mater. Res. Soc. Symp. Proc. 928E, Warrendale, PA, 2006), GG16-01.
- Type: Poster
R. Krüger, M. Bockmeyer "Continuous Coating of NextelTM 610 with Zirconia from liquid Precursors: Minimizing Fiber Bridging and Strength Degradation", Hochleistungskeramik-Symposium, Selb, Germany 12./13. October 2005.
- Type: Presentation
M. Bockmeyer, P. Löbmann "Anatasschichten auf Glas über Sol-Gel Verfahren", 12. Keramiktag der BAM, Symposium: Glasig-kristalline Funktionswerkstoffe - Vielfalt und Präzision., 12/13. Mai 2005.
- Type: Patent
M. Bockmeyer, R. Krüger, U. Guntow, P. Löbmann "Stabile Suspensionen von kristallinen ZrO_2 -Partikeln aus hydrothermal behandelten Sol-Gel-Vorstufenpulvern", Patentanmeldung 10 2006 032 759.4.
- Type: Patent
M. Bockmeyer, B. Herbig, P. Löbmann "Stabile Suspensionen von kristallinen TiO_2 -Partikeln aus hydrothermal behandelten Sol-Gel-Vorstufenpulvern", Patentanmeldung 10 2006 032 755.1.

Personal Data:

Mr.

Matthias Johannes-Franz Bockmeyer

Dipl.-Chemiker

Birth Date: 21.06.1977

Nationality: German

**Academic Track Record**

- 01.2004 – 12.2006 (defense approx. 04.2007)
Ph.D. in Chemistry (Material Science) at Fraunhofer ISC, Würzburg, Germany
Title of thesis: Structure and Densification of Thin Films prepared from Soluble Precursor Powders by Sol-Gel Processing.
- 10.1997 - 09.2003
German Diplom thesis in Chemistry at Julius-Maximilians-University Würzburg, Germany
overall grade: 2 ("good")
Title of Diplom thesis: Continuous coating of ceramic fibers with zirconia and gahnite by sol-gel method.
- 03.2001 - 07.2001
undergraduate exchange student at University College Dublin, Dublin, Ireland
inorganic chemistry
Title of research project: Aromatic C-H-bond activation using Lithium atoms.
- 09.1987 - 06.1996
A-levels at Röntgen Gymnasium Würzburg, Germany
- 09.1983 - 07.1987
basic primary school, Ottobrunn, Germany

Teaching experience

- 01.2004 -
Fraunhofer ISC, Würzburg, Germany
Description: Supervised two German Diploma theses, one Finish Master thesis, three French Master theses and several student research projects (in German and English).

Work experience

- 01.2006 -
Fraunhofer ISC, Würzburg, Germany
Job Title: project manager, scientific associate
Scope of Duties: Guidance in research projects focusing on new materials for power engineering (HT Superconductors), Solid Oxid Fuel Cell (SOFC) and antireflective coatings.
- 04.2005 - 01.2006
Fraunhofer ISC, Würzburg, Germany
Job Title: graduate associate
Scope of Duties: Collaboration in industrial or scientific projects.

- 08.1999 - 10.2000
Julius-Maximilians-University Würzburg, Würzburg, Germany
Job Title: scientific assistant
Scope of Duties: Synthesis and characterization of organic hydrogels.
- 09.1998 - 02.2001
Restaurant Auflauf, Würzburg, Germany
Job Title: cook
Scope of Duties: Cooking of soufflés and gratins.
- 09.1996 - 06.1997
German Air Force, Bayreuth and Neuburg an der Donau, Germany
Job Title: air traffic specialist
Scope of Duties: Assistance of air traffic control.

Publications

- Type: Full paper
M. Bockmeyer, P. Löbmann "Densification and Microstructural Evolution of TiO_2 Films", Chem. Mater. 2006, 18, 4478-4485.
- Type: Full paper
M. Bockmeyer, P. Löbmann "Crack Formation in TiO_2 Films Prepared by Sol-Gel Processing: Quantification and Characterization", Thin Solid Films, 2007, 515, 5212-5219.
- Type: Full paper
M. Bockmeyer, R. Krüger, "Influence of Precursor Densification on Strength Retention of Zirconia Coated Nextel™ 610 Fibers", J. Am. Ceram. Soc., submitted 2007.
- Type: Full paper
M. Bockmeyer, P. Löbmann, "Use of Triethanoleamine for the Preparation of Soluble TiO_2 -Precursor Powders: Formation, Densification and Properties of Sol-Gel Films", in preparation.
- Type: Full paper
R. Krüger, M. Bockmeyer, A. Dutschke, P. Löbmann "Continuous Sol-Gel Coating of Ceramic Multifilaments: Evaluation of Fiber Bridging by Three Point Bending Test", J. Am. Ceram. Soc. 2006, 89, (7), 2080-2088.
- Type: Full paper
M. Mallak, M. Bockmeyer, P. Löbmann "Liquid Phase Deposition of TiO_2 on Glass: Systematic Comparison to Films prepared by Sol-Gel Processing", Thin Solid Films, accepted 2006
- Type: Full paper
E. Holbig, M. Bockmeyer, P. Löbmann "Sol-Gel synthesis of amorphous and nanocrystalline ZrO_2 - TiO_2 powders", J. Alloys Compd., submitted 2006.
- Type: Full paper
Christoph Peters, Matthias Bockmeyer, Reinhard Krüger, André Weber, Ellen Ivers-Tiffée: "Processing of Dense Nanocrystalline Zirconia Thin Films by Sol-Gel, in Current and Future Trends of Functional Oxide Films", edited by D. Kumar, V. Craciun, M. Alexe, K.K. Singh (Mater. Res. Soc. Symp. Proc. 928E, Warrendale, PA, 2006), GG16-01.
- Type: Full paper
J.P. Dunne, M. Bockmeyer, M. Tacke "Co-Condensation Reactions of Substituted Aromatic Compounds with Lithium Atoms at 77 K", Eur. J. Inorg. Chem. 2003, 3, 458-466.
- Type: Poster
R. Krüger, M. Bockmeyer "Continuous Coating of Nextel™ 610 with Zirconia from liquid

Precursors: Minimizing Fiber Bridging and Strength Degradation", Hochleistungskeramik-Symposium, Selb, Germany 12./13. October 2005.

- Type: Presentation
M. Bockmeyer, P. Löbmann "*Anatasschichten auf Glas über Sol-Gel Verfahren*", 12. Keramiktag der BAM, Symposium: Glasig-kristalline Funktionswerkstoffe - Vielfalt und Präzision., 12/13. Mai 2005.
- Type: Presentation
M. Bockmeyer "*Struktur von Sol-Gel-Schichten und deren Anwendung*", 2. DEGUSSA Summer School Science to Business Nanotronics, 11.-13. September 2006.
- Type: Presentation
C. Peters, A. Weber, E. Ivers-Tiffée, H. Störmer, D. Gerthsen, M. Bockmeyer, R. Krüger, "*Interaction between grain size and electrical conductivity in YSZ thin films*", MRS Fall Meeting, Boston, November 27th – December 1st 2006.
- Type: Presentation
C. Peters, M. Bockmeyer, R. Krüger, A. Weber, E. Ivers-Tiffée "*Processing of Dense Nanocrystalline Zirconia Thin Films by Sol-Gel, MRS Spring Meeting*", San Francisco, April 17th – 21st 2006.
- Type: Patent
M. Bockmeyer, R. Krüger, U. Guntow, P. Löbmann "*Stabile Suspensionen von kristallinen ZrO₂-Partikeln aus hydrothermal behandelten Sol-Gel-Vorstufenpulvern*", Patentanmeldung 10 2006 032 759.4.
- Type: Patent
M. Bockmeyer, B. Herbig, P. Löbmann "*Stabile Suspensionen von kristallinen TiO₂-Partikeln aus hydrothermal behandelten Sol-Gel-Vorstufenpulvern*", Patentanmeldung 10 2006 032 755.1.

Language skills

- English: Business fluent
- German: Mother tongue

Miscellaneous

- Awards: Participant at the Lindau Nobel Laureates Meetings on Chemistry 2006
- Interests: Equity trading, cooking, tennis, mountain-biking
- Member of Liberal Democratic Party (FDP)
- Kösener Corpsstudent

Hiermit erkläre ich ehrenwörtlich, dass ich die Dissertation "STRUCTURE AND DENSIFICATION OF THIN FILMS PREPARED FROM SOLUBLE PRECURSOR POWDERS BY SOL-GEL PROCESSING" selbständig angefertigt und keine anderen als die von mir angegebenen Quellen und Hilfsmittel benutzt habe. Ich erkläre außerdem, dass diese Dissertation weder in gleicher noch in anderer Form bereits in einem anderen Prüfungsvorhaben vorgelegen hat. Ich habe früher außer den mit dem Zulassungsgesuch urkundlich vorgelegten Graden keine weiteren akademische Grade erworben oder zu erwerben versucht.

Würzburg, den

(Matthias Bockmeyer)